

THESIS ON NATURAL AND EXACT SCIENCES B148

**Application of Remote Sensing Methods for the
Investigation of Spatio-Temporal Variability of
Sea Surface Temperature and
Chlorophyll Fields in the
Gulf of Finland**

RIVO UIBOUPIN

TUT
PRESS

TALLINN UNIVERSITY OF TECHNOLOGY
Marine Systems Institute

Dissertation was accepted for the defence of the degree of Doctor of Philosophy in Earth Sciences on December 13, 2012.

Supervisor: Dr Jaan Laanemets,
Marine Systems Institute at Tallinn University of Technology

Opponents: Dr Jari Haapala, Finnish Meteorological Institute

Dr Tiit Kutser, Estonian Marine Institute, University of Tartu

Defence of the thesis: February 5, 2013 at the Marine Systems Institute at
Tallinn University of Technology,
Akadeemia tee 15a, Tallinn, Estonia

Declaration:

Hereby I declare that this doctoral thesis, my original investigation and achievement, submitted for the doctoral degree at Tallinn University of Technology has not been submitted for any academic degree.

/Rivo Uiboupin/



European Union
European Social Fund



Investing in your future

Copyright: Rivo Uiboupin, 2013
ISSN 1406-4723
ISBN 978-9949-23-425-7 (publication)
ISBN 978-9949-23-426-4 (PDF)

LOODUS- JA TÄPPISTEADUSED B148

**Kaugseire rakendused merepinna
temperatuuri ja klorofülli väljade
ajalis-ruumilise muutlikkuse
uurimiseks Soome lahes**

RIVO UIBOUPIN

CONTENTS

LIST OF ORIGINAL PUBLICATIONS	6
AUTHOR'S CONTRIBUTIONS.....	7
APPROBATION OF THE RESULTS	7
ACKNOWLEDGMENTS.....	8
1 INTRODUCTION	9
1.1 Background.....	9
1.1.1 Description of the Gulf of Finland	9
1.1.2 Wind regime and upwelling	10
1.1.3 Application of remote sensing data	11
1.2 Motivation and objectives.....	13
2 MATERIAL AND METHODS.....	15
2.1 Field data.....	15
2.2 Wind data.....	15
2.3 Remote sensing SST data and processing.....	17
2.3.1 SST imagery.....	17
2.3.2 SST data processing	18
2.3.3 Parameters calculated from SST	18
2.4 Remote sensing Chl <i>a</i> data and processing.....	18
2.5 SAR data	19
3 COMPARISON OF REMOTE SENSING AND IN SITU DATA	20
3.1 Comparison of MODIS and in situ temperature data.....	20
3.2 Evaluation of remote sensing Chl <i>a</i> retrievals	22
4 CHARACTERISTICS OF UPWELLING AND RELATED PHENOMENA.....	25
4.1 Upwelling area.....	25
4.2 Upwelling filaments.....	27
4.3 Manifestation of SST signatures and biogenic slicks on SAR.....	29
5 EFFECT OF UPWELLING EVENTS ON CHL <i>a</i> DISTRIBUTION.....	33
5.1 Upwelling-related temperature variability	33
5.2 Chl <i>a</i> variability caused by upwelling events	34
CONCLUSIONS	38
REFERENCES.....	40
PUBLICATIONS	49
Paper I.....	49
Paper II.....	77
Paper III	87
Paper IV	99
ABSTRACT	105
RESÜMEE	107
ELULOOKIRJELDUS.....	109
CURRICULUM VITAE	113

LIST OF ORIGINAL PUBLICATIONS

- I. Uiboupin, R., Laanemets, J., Sipelgas, L., Raag, L., Lips, I. and Buhhalko, N. 2012. Monitoring the effect of upwelling on the chlorophyll a distribution in the Gulf of Finland (Baltic Sea) using remote sensing and in situ data. *Oceanologia* 54(3), 395–419.
- II. Uiboupin, R. and Laanemets, J. 2009. Upwelling characteristics derived from satellite sea surface temperature data in the Gulf of Finland, Baltic Sea. *Boreal Environment Research* 14(2), 297–304.
- III. Uiboupin, R. and Sipelgas, L. 2007. Comparison of satellite sea surface temperature with in situ surface layer temperature. *Proceedings of the Estonian Academy of Sciences: Biology, Ecology* 56(1), 47–56.
- IV. Uiboupin, R. and Laanemets, J. 2009. Observation of mesoscale eddies by using SAR data complemented with optical remote sensing and in situ measurements. In: *Proceedings of International Geoscience and Remote Sensing Symposium, 2009 IEEE International, Cape Town, 12–17 July 2009. IEEE, 2009 (1), 224–227.*

Some unpublished data are also presented.

AUTHOR'S CONTRIBUTIONS

- I.** The author was responsible for data analysis and writing the manuscript. The author also processed the sea surface temperature imagery and was involved in retrieving chlorophyll *a* concentration from remote sensing data.
- II.** The author was responsible for sea surface temperature data processing and analysis of the data. The author was also responsible for the writing of the manuscript.
- III.** The author was responsible for processing of the remote sensing data and in situ measurements. The author contributed to the writing of the manuscript.
- IV.** The author was responsible for data processing and analysis as well as for writing the manuscript.

APPROBATION OF THE RESULTS

The results have been presented at the following international conferences:

1. Baltic Sea Science Congress on 19–23 March 2007, Rostock, Germany. Upwelling characteristics derived from satellite sea surface temperature data in the Gulf of Finland (Baltic Sea).
2. Fifth Study Conference on BALTEX on 4–8 June 2007, Kuressaare, Saaremaa, Estonia. Upwelling parameters derived from satellite sea surface temperature data in the Gulf of Finland.
3. Baltic Sea Science Congress on 17–21 August 2009, Tallinn, Estonia. Observation of mesoscale eddies by using SAR data complemented with optical remote sensing and in situ measurements.
4. IEEE International Geoscience and Remote Sensing Symposium on 12–17 July 2009, Cape Town, South Africa. Observation of mesoscale eddies by using SAR data complemented with optical remote-sensing and in situ measurements.

ACKNOWLEDGMENTS

I am very grateful to my supervisor, Dr Jaan Laanemets, for his guidance during my studies. I also thank him for his patience and understanding during the periods when I was not focused on my Ph.D. studies.

I am also grateful to Dr Liis Sipelgas for her support and for introducing and explaining remote sensing principles.

I am grateful to Dr Urmas Raudsepp, who has been a great motivator and who has provided me with plenty of opportunities to try new and experimental remote sensing applications.

I would like to express my gratitude to Prof. Urmas Lips and Dr Juss Pavelson for reviewing the thesis and making comments that helped to improve the manuscript.

I would also like to express my gratitude to my coauthors and colleagues at the Marine Systems Institute for their contribution and for kindly providing field data. I also thank the Finnish Meteorological Institute for providing weather station wind data, the Estonian Meteorological and Hydrological Institute for HIRLAM wind data, and the Finnish Environmental Institute for providing Alg@line data.

I would like to thank Uku Kaarel, with whom I have had long and fruitful scientific discussions on marine remote sensing.

This study was financially supported by the Estonian Science Foundation through grant nos. 7467 and 8968, the European Social Fund's Doctoral Studies and International Programme DoRa, Doctoral School of Earth Sciences and Ecology.

1 INTRODUCTION

1.1 Background

1.1.1 Description of the Gulf of Finland

The Gulf of Finland is an elongated basin in the northeastern part of the Baltic Sea. The length of the Gulf is about 400 km, its width varies between 48 and 135 km, its surface area is about 29 600 km², and it has a total volume of 1100 km³.

The Gulf has quite complicated bottom topography with a number of peninsulas and small islands, especially in the northern coastal sea. The southern part is deeper and has a steeper bottom slope compared with the northern Gulf. The along-gulf depth decreases from 80–110 m at the entrance to 20–30 m in the shallow eastern part.

The vertical thermal stratification in the Gulf of Finland has a highly seasonal cycle. The surface temperature starts to rise in April when the ice has melted and incoming solar radiation exceeds the outgoing radiation at the sea surface. The seasonal thermocline in the Gulf of Finland usually forms at the beginning of May and is at its strongest in July–August (e.g. Alenius et al. 1998). Typically, it settles at a depth of 10–15 m. Liblik and Lips (2011) showed that the average seasonal upper mixed layer (UML) depth increased from 11 m in June to 12.1 and 15.1 m in July and August respectively. The larger UML depths (~15 m) were in the western part of the gulf, while in the central part of the gulf the UML was shallower (~13 m). The mean UML temperature during summer was 15.2 °C on average and increased from ~12 °C in June to ~17 °C in July and August, while the surface layer maximum temperature may rise up to ~23 °C. The cold intermediate layer temperature varies in the range of 1.3–3.6 °C (Liblik and Lips 2011). Thus, the temperature difference between the warm surface layer and the cold intermediate layer below the thermocline may be up to 20 °C. Convection and wind-induced vertical mixing cause the seasonal thermocline to vanish by late October–early November.

According to a study by Palmén (1930) the long-term circulation in the Gulf is cyclonic. The relatively poor stability of currents in the Gulf indicates that the mean cyclonic circulation is a statistical property, not a constant phenomenon (Alenius et al. 1998). At shorter time scales the current system is more complicated. The deviations from the long-term scheme are mainly caused by the changes in wind forcing (Alenius et al. 1998 and references therein; Elken et al. 2003).

The annual saline water inflow from the Baltic Proper along the southern coast is on average 480 km³ and the outflow of brackish water along the northern coast is about 600 km³ (Alenius et al. 1998). The annual freshwater runoff is about 110 km³, mainly from River Neva (77.6 km³ annually, Bergström

et al. 2001) in the eastern part of the Gulf. Therefore, the surface salinity at the entrance to the Gulf (6–7) is higher compared to the easternmost part (about 1).

1.1.2 Wind regime and upwelling

Coastal upwelling caused by the alongshore wind forcing is an important process that influences the temperature, salinity, nutrient, and phytoplankton distribution through vertical and cross-shore water exchange.

The dominant wind direction in the Baltic Sea in general (Lehmann et al. 2011) and specifically in the Gulf area (Keevallik 2003; Soomere and Keevallik 2003) is from the southwest. Wind data from Kalbådagrund weather station showed that during the warm period (May–September) the monthly mean wind speed is lower (around 7–8 m s⁻¹) compared to the rest of the year, when it reaches values of over 10 m s⁻¹ (Keevallik and Soomere 2010). However, wind data from Hanko and Helsinki-Kataja weather stations showed that winds from the ENE direction can occur quite often in addition to the typical southwesterly direction (Soomere and Keevallik 2003; Keevallik and Soomere 2009). The secondary frequency peak from the ENE direction is mostly caused by strong winds of over 10 m s⁻¹ (Soomere and Keevallik 2003). Moreover, Keevallik and Soomere (2009) found that the peak from the ENE direction occurs only during the warm period of the year.

Owing to the prevailing southwesterly winds, the Gulf of Finland, especially its northern coastal sea, is an active upwelling area in the Baltic Sea in summer (Kahru et al. 1995; Myrberg and Andrejev 2003; Lehmann and Myrberg 2008; Myrberg et al. 2008). Due to the strong thermal stratification, large sea surface temperature contrasts could be expected in the upwelling regions. Numerical simulations by Zhurbas et al. (2008) and field measurements by Lips et al. (2009) have shown that, in the narrow and elongated Gulf of Finland, upwelling along one coast is accompanied by downwelling along the opposite coast; that is, two longshore baroclinic jets and their related thermohaline fronts develop simultaneously. Field measurements (Haapala 1994; Vahtera et al. 2005; Lips et al. 2009) and model simulations (Zhurbas et al. 2008; Laanemets et al. 2009) showed that summer upwelling events transport nutrients with a clear excess of phosphate to the surface layer of the Gulf.

Kahru et al. (1995) found two highly significant upwelling centers where filaments emerge from the upwelling front off the Hanko and Porkkala peninsulas and move south towards the Estonian coast. The model simulation by Zhurbas et al. (2004, 2008) also showed that the development of filaments and eddies due to the instability of longshore baroclinic jets can be attributed to topographic irregularities. Upwelling-related filaments and eddies are important factors for the offshore transport of upwelled nutrients (e.g. Laanemets et al. 2011).

Coastal upwelling events also influence the phytoplankton distribution and community structure. Field measurements showed that during upwelling the surface phytoplankton community is transported offshore and replaced by

species that are normally resident in the upper part of the thermocline (Kanoshina et al. 2003; Vahtera et al. 2005; Lips and Lips 2010).

1.1.3 Application of remote sensing data

Remote-sensing data have been widely used for monitoring the ecological and physical state of the Baltic Sea. A wide range of sensors with different measuring methods have been used for sea surface temperature (SST) monitoring, for example MODIS (Moderate Resolution Imaging Spectroradiometer), AVHRR (Advanced Very High Resolution Radiometer), AATSR (Advanced Along-Track Scanning Radiometer), and so on. The SST estimates from different space-borne sensors have accuracies of ± 0.3 – 0.5 °C (e.g. Brown and Minnett 1999; Llewellyn-Jones et al. 2001; Karagali et al. 2012). In addition to measurement technology a number of factors contribute to the SST errors: heat flux conditions, the time of day when the measurement is obtained (diurnal warming), regional peculiarities (atmospheric conditions), and wind conditions (e.g. Donlon et al. 2002; Corlett et al. 2006). Donlon et al. (2002) showed that the variability between skin layer SST measured by radiometer within a thin layer (~ 500 μm) and SST at 5 m depth measured by the flow-through (FT) system is diminished and a mean bias of 0.14 °C exists when the wind speed is over 6 m s^{-1} ; thus the satellite SST and FT measurements are comparable in the case of moderate and high wind speeds.

Studies of upwelling parameters in the Baltic Sea using remote sensing data started in the 1980s with the exploitation of the AVHRR instrument. Satellite imagery has been used for detecting inter-annual, seasonal, and mesoscale variability of the SST and for determining upwelling parameters for the period of thermal stratification of the sea by a number of authors (Horstmann 1983; Gidhagen 1987; Siegel et al. 1994; Kahru et al. 1995; Krężel et al. 2005a; Siegel et al. 2006; Bradtke et al. 2010). They have found that the typical temperature difference between the upwelled and surrounding waters varies within 2 – 10 °C, the alongshore extent is of the order of hundreds of kilometers, and the offshore scale is tens of kilometers. The lifetime of an upwelling event is from a few days to one month. Lehmann et al. (2012) also found that the frequency of upwelling events (May–September) in the Gulf of Finland estimated from 443 weekly AVHRR composite SST maps over a 20-year period can be up to 25% (depending on the region and month).

The spatio-temporal variability of biological-chemical parameters can be monitored using different in situ measurements (Rantajärvi et al. 1998; Lips and Lips 2008; Petersen et al. 2008). However, for obtaining information about the chlorophyll and consequently phytoplankton biomass surface distribution over large sea areas, remote-sensing imagery is invaluable. Satellite imagery for monitoring water quality parameters with sufficient temporal resolution has been

regularly available from SeaWiFS (Sea-viewing Wide Field-of-view Sensor), MERIS (Medium Resolution Imaging Spectrometer), and MODIS for the Baltic Sea region. A study by Darecki and Stramski (2004) showed that MODIS standard algorithms for optically complex Case 2 waters are characterized by systematic and large overestimation of chlorophyll *a* (Chl *a*) concentration. Also, Reinart and Kutser (2006) showed that MODIS/Aqua and SeaWiFS standard algorithms overestimate the Chl *a* concentration (especially in heavy bloom conditions) compared to the MERIS Chl *a* concentration estimates, due to the unsuitable set of spectral bands. MERIS was designed to monitor coastal waters (Doerffer et al. 1999), and therefore it has sufficient spectral resolution in the range of wavelengths above 555 nm for routine monitoring of turbid waters like the Baltic Sea (Reinart and Kutser 2006; Gitelson et al. 2009). An overview of various algorithms (from band ratios to bio-optical modeling) developed for different satellite sensors to determine Chl *a* concentration in phytoplankton (including cyanobacterial) blooms is given in Kutser (2009). The Baltic Sea (including the Gulf of Finland) comprises optically complex Case 2 waters that are dominated by colored dissolved organic matter (CDOM), and therefore the production of accurate estimates of water quality parameters from remote sensing imagery is complicated (Darecki and Stramski 2004; Schroeder et al. 2007; Sorensen et al. 2007; Kratzer et al. 2008; HELCOM 2009; Kutser 2009). Despite these problems, previous studies have demonstrated that remote-sensing data can be successfully used for systematic monitoring of the Chl *a* distribution and temporal variability (Krężel et al. 2005b; Koponen et al. 2007; Kratzer et al. 2008). Also, the chlorophyll distribution related to coastal upwelling was explained by combined use of SST and Chl *a* retrievals from remote sensing data (Krężel et al. 2005a; Lass et al. 2010).

Kutser (2004) used remote sensing data for quantitative detection of chlorophyll in cyanobacterial blooms in the Gulf of Finland and also pointed to problems connected with the comparability of remote sensing and in situ data. Using bio-optical modeling, Metsamaa et al. (2006) and Kutser et al. (2006) showed that MERIS bands 6 and 7 can be used to separate cyanobacteria from green algae if the concentration of cyanobacteria is high (Chl *a* concentration > 8–10 mg m⁻³).

Due to the high cloudiness level in the Baltic Sea region, a relatively small fraction (10–50%) of optical/infrared images is suitable for processing (Kreżel et al. 2005a). Since Synthetic Aperture Radar (SAR) data are not influenced by solar illumination or the atmosphere, they provide additional information as they allow the sea surface to be monitored in cloudy conditions and during the nighttime. Previous studies have shown that SAR data could contribute to the study of upwelling-related fronts, eddies, and filaments (Clemente-Colon and Yan 1999; Clemente-Colon and Yan 2000; Svejkovsky and Shandley 2001; Askari 2009; Li et al. 2009; Ryan et al. 2010; Kozlov et al. 2012; Kudryavtsev et al. 2012).

1.2 Motivation and objectives

Coastal upwelling is a process that strongly influences the surface layer temperature and Chl *a* distribution in the warm period of the year. Therefore, it usually has thermal and biogenic signatures on the sea surface which can be observed from space-borne satellite sensors. Remote-sensing data provide valuable information about the characteristics of upwelling events, related filaments and eddies, and their effect on the surface distribution of temperature and phytoplankton blooms at basin scale, thus complementing the field data.

As the remote-sensing data provide indirect measurements, the quality of the data needs to be evaluated against in situ measurements. In this study, existing algorithms and products were used and evaluated to estimate the suitability of SST and Chl *a* retrievals from remote-sensing data for describing their variability in the cases of highly variable conditions (i.e. during upwelling).

Many global-scale validations carried out using satellite SST and in situ buoy temperature to evaluate the remote sensing sensor performance in the world ocean have shown that large regional differences can occur in biases of SST estimates (e.g. Corlett et al. 2006; Noyes et al. 2006; Reynolds et al. 2010). However, relatively few studies of the accuracy of SST retrievals have been carried out for the Baltic Sea and Gulf of Finland area with high-resolution remote sensing SST data (Karagali et al. 2012). Therefore the performance of space-borne SST sensors (MODIS) in variable conditions (i.e. upwelling) in the Gulf of Finland needs to be estimated.

The estimation of water quality parameters from remote sensing data in the optically complex Case 2 waters dominated by CDOM like the Baltic Sea (including the Gulf of Finland) is complicated. Therefore, the results of standard algorithms should be corrected using in situ data when estimating Chl *a*, suspended particulate matter, and CDOM from remote sensing data in the Gulf of Finland.

Interdisciplinary case studies have shown the important role of summer coastal upwelling events in nutrient and phytoplankton dynamics in the Gulf of Finland (e.g. Vahtera et al. 2005; Lips et al. 2009). Therefore the combined use of SST and Chl *a* imagery, complemented by field measurements and wind information, provides a basis for investigating the role of upwelling events in the surface layer spatio-temporal variability of temperature and chlorophyll (phytoplankton) fields at basin scale.

The main aim of the thesis is to improve the knowledge on the characteristics of upwelling and related features (filaments, eddies, fronts) and the influence of upwelling on the Chl *a* distribution using data from different types of remote sensing sensors (visible and infra-red range spectrometers, Synthetic Aperture Radar (SAR), and in situ data.

The main objectives of the study are:

- to compare MODIS SST data and in situ temperature data in the Gulf of Finland and to quantify the differences between in situ temperature and SST;
- to define the wind speed threshold value when the FT temperature measurements at ~ 4 m depth can be used for validation of satellite SST retrievals in dynamic conditions;
- to evaluate the suitability of the MERIS Chl *a* retrievals for the Gulf of Finland using in situ Chl *a* data;
- to determine the characteristics of summer upwelling events and their dependence on wind forcing and bottom topography in the Gulf of Finland;
- to assess and explain the spatial and temporal variability of the Chl *a* field caused by consecutive upwelling events in the Gulf of Finland using MERIS data;
- to examine how temperature differences and the structure of biogenic slicks affect the manifestation of cold-upwelling-related mesoscale eddies in SAR images by using complementary multi-sensor data (SAR, optical remote sensing, and in situ measurements).

2 MATERIAL AND METHODS

2.1 Field data

Flow-through (FT) temperature measurements were conducted at ~4 m depth from ships of opportunity between Helsinki and Travemünde and between Tallinn and Helsinki with a spatial resolution of about 150 m. The FT measurements between Tallinn and Helsinki were carried out by two different measuring systems belonging to (1) the framework of the project Alg@line (Leppänen et al. 1994; with six transects from the years 2003–2005, and (2) a Ferrybox system operated by the Marine Systems Institute (MSI) at Tallinn University of Technology with five transects from the years 2007–2009 (Lips et al. 2008; Kikas et al. 2010) (Fig. 1). Alg@line data collected on 24 September 2008 along the transect between Helsinki and Travemünde were also used (Kaitala et al. 2008). In addition, near surface (about 20 cm depth) FT temperature data with a spatial resolution of 5–7 m were collected along the transect from Tallinn to Lehtma (Hiiumaa Island) on 29 July 2002 (Fig. 1).

Additionally, CTD temperature profile data collected by the MSI research vessel along five of the seven transects from Tallinn to Helsinki in July–August 2006 were used (Fig. 1).

The upper mixed layer Chl *a* data were obtained from (1) pooled samples collected along the five transects from Tallinn to Helsinki by MSI in July–August 2006 and analyzed in the laboratory (HELCOM 1988; Kuvaldina et al. 2010) and (2) from ship of opportunity FT measurements by deriving Chl *a* from fluorescence data on 24 September 2008 between Helsinki and Travemünde (Kaitala et al. 2008) (Fig. 1). An overview of the in situ data is given in Table 1.

2.2 Wind data

Wind data from the Kalbådagrund weather station for the period May–September in 2000–2006 (Finnish Meteorological Institute) were used for the calculation of the approximate along-gulf component of the cumulative wind stress (the product of the wind stress and its duration) to estimate the wind forcing during the observed upwelling events and to count the summer wind events that were favorable for upwelling. The gaps in the Kalbådagrund wind-data record (September 2000 and July 2003) were filled out with the wind data from the Utö weather station (Finnish Meteorological Institute). Kalbådagrund wind data were also used for estimating the effect of wind speed on SST retrievals from MODIS data and for defining suitable and valid wind conditions when FT temperature data at 4 m depth can be used for validation of satellite SST.

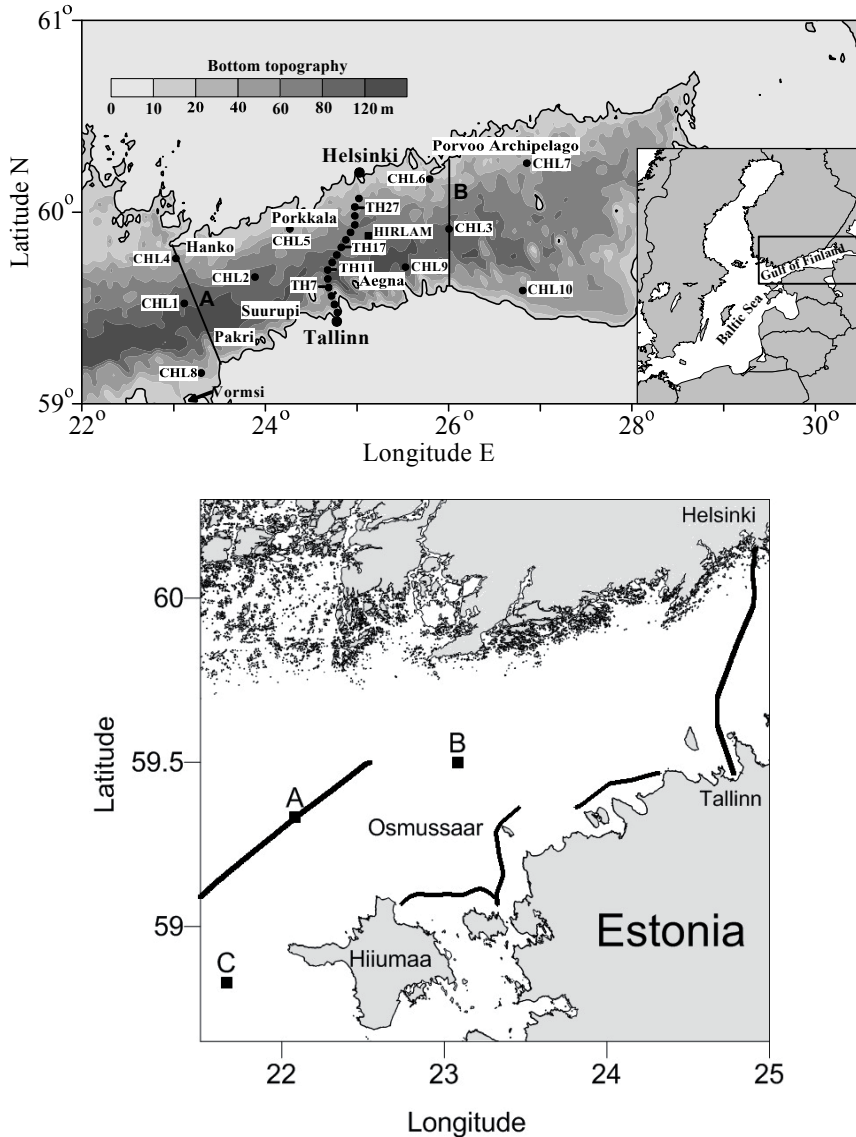


Figure 1. Upper panel: Map of the Gulf of Finland with the depth contours drawn from the gridded topography (Seifert et al. 2001). The solid circles (•) represent the locations of the in situ sampling stations (TH1–TH27) and the locations of the MERIS chlorophyll time series (CHL1–CHL10, TH7, and TH27). The solid square (■) represents the location of the HIRLAM grid point from which wind data were extracted. The Gulf area is divided into two parts: the western Gulf between lines A and B and the eastern Gulf eastward of line B.

Lower panel: ship tracks where FT data were collected between Tallinn and Hiiumaa in July 2002, between Helsinki and Travemünde in September 2008, and between Tallinn and Helsinki during 2003–2009. Letters A, B, and C mark the locations of eddies detected on SST and SAR imagery on 23–25 September 2008.

To evaluate the comparability of satellite and in situ Chl *a*, wind data from the version of HIRLAM (HIGH Resolution Limited Area Model) of the Estonian Meteorological and Hydrological Institute (Männik and Merilain 2007) were interpolated to the location (25°7.5' E, 59°51.9' N) close to the measurement transect between Tallinn and Helsinki in July–August 2006. The spatial resolution of HIRLAM is 11 km, and the forecast interval of 54 h is recalculated after every 6 h with temporal resolution of 1h.

To characterize wind-induced mixing the depth of the turbulent Ekman boundary layer (h) was estimated by the formula $h = 0.1u_*/f$ (Csanady 1982), where $u_* = (\tau/\rho_w)^{1/2}$ is the friction velocity (m s^{-1}), $\tau = \rho_a C_a u^2$ is the wind stress (N m^{-2}), $\rho_a = 1.3 \text{ kg m}^{-3}$ is the air density, $C_a = 1.2 \times 10^{-3}$ is the dimensionless wind drag coefficient, u is the wind speed (m s^{-1}), $\rho_w = 1005 \text{ kg m}^{-3}$ is the water density, and $f = 1.25 \times 10^{-4} \text{ s}^{-1}$ is the Coriolis parameter. This equation does not take into account the setup time.

2.3 Remote sensing SST data and processing

2.3.1 SST imagery

Data from MODIS sensors onboard the Terra and Aqua satellites were used for estimation of SST in the Gulf of Finland. Only sufficiently cloud-free SST images during the warm period of year (May–September) depicting well-expressed coastal upwelling events in the Gulf of Finland were used in the study. The number of SST images, other associated images used (Chl *a*, SAR), and in situ measurements is given in Table 1.

In total, 19 MODIS images (2003–2009) were used for comparison with FT measurements. MODIS images covered three upwelling events along the Finnish coast and three events along the Estonian coast. As the resolution of in situ measurements was higher than the pixel size ($1 \times 1 \text{ km}$) of the SST images, the mean in situ temperature value corresponding to each pixel was calculated. The correlation, mean bias, and root mean square difference (RMSD) were calculated for each dataset.

From the seven-year (2000–2006) MODIS SST data archive, 20 images with well-expressed upwelling were selected to calculate the upwelling areas, filament areas and locations, and temperature differences between upwelled and surrounding waters.

For calculation of the mean upwelling areas, 61 MODIS images from four upwelling events along the southern coast and 86 images from eight upwelling events along the northern coast during the years 2000–2009 were selected from the archive.

A series of upwelling events in the Gulf in July–August 2006 was investigated to determine the spatio-temporal variability of SST. Altogether 200 MODIS images were examined in order to extract the SST data from 60 images that were sufficiently cloud-free during July–August 2006.

Additionally, three MODIS images were used to complement the SAR data in September 2008 in the western Gulf.

2.3.2 SST data processing

MODIS Level 2 products, MOD28L2 and MYD28L2, provide SST at 1×1 km resolution (<http://oceancolor.gsfc.nasa.gov/>; <http://disc.gsfc.nasa.gov/>). The retrieval algorithms of SST products were developed by NASA Ocean Biology Processing Group (http://oceancolor.gsfc.nasa.gov/DOCS/modis_sst/). The nighttime SST products calculated from the short wavelength bands (brightness temperatures at 3.959 and 4.050 μm) and long-wavelength bands (brightness temperatures at 11 μm and 12 μm) were used in the study. The Level 2 flags provided with the product were used to mask the invalid pixels when visualizing and analyzing the images. Only the data with the highest quality flag were used.

2.3.3 Parameters calculated from SST

For detection of the border of the upwelling water (including filaments) the SST images were overlaid by isotherms with a fixed contour interval of 0.5 $^{\circ}\text{C}$ starting from the upwelling center or centers. All sea-surface isotherms either form closed contours or intersect the basin boundary. The contour of the warmest isotherm intersecting the basin boundaries is considered the upwelling water open sea border. The total area of upwelling water was calculated from the known pixel area for each particular SST image. Using 147 images (2000–2009), composite maps showing the average upwelling areas for the northern and southern coasts of the Gulf were calculated. The average temperature was calculated for each pixel location of the Gulf of Finland.

The filament location was defined coinciding with the filament width center along the edge of the upwelling front. The filament length was defined as the distance from the filament location to the farthest filament pixel. Filaments with lengths larger than their respective widths and areas larger than 50 km^2 were taken into account.

2.4 Remote sensing Chl *a* data and processing

MERIS reduced-resolution (about 1×1 km) images from 10 July to 18 August 2006 (31 sufficiently cloud free images altogether) were used for the estimation of Chl *a* concentration (Table 1). The MERIS images were processed using the Free University of Berlin (FUB) algorithm for Case 2 waters (Schroeder et al. 2007a; Schroeder et al. 2007b) to apply an atmospheric correction and obtain the reflectance values in order to calculate the Chl *a* concentration. For the purpose of comparison, Chl *a* and reflectance values were calculated using the Case 2 regional water (C2RW) processor (Doerffer and Schiller 2007). In addition to the time series analysis, MERIS data were also used for phytoplankton bloom area estimation, defined as Chl *a* >7 mg m^{-3} , which determines the border from

where the Chl *a* concentration starts to increase significantly along the northern coast.

Relative Chl *a* changes were estimated from the MODIS standard OC3 product (O'Reilly et al. 1998; Darecki and Stramski 2004) during a case study in the western Gulf of Finland in September 2008. However, the location of band centers of the MODIS instrument is not suitable for correct estimation of Chl *a* and other parameters in optically complex Case 2 waters like the Baltic Sea (e.g. Reinart and Kutser 2006). The standard MODIS Chl *a* product tends to overestimate the Chl *a* values in the Baltic Sea (Darecki and Stramski 2004), and therefore we preferred MERIS data for the calculation of Chl *a* concentrations during upwelling events in July–August 2006.

2.5 SAR data

The manifestation of biogenic slicks and temperature differences on SAR imagery was investigated during a case study in September 2008 at the entrance to the Gulf of Finland using two vertically polarized (VV) C-band (5.6 cm) ENVISAT/ASAR (Advanced Synthetic Aperture Radar) Wide Swath Mode (WSM) images with a pixel spacing of 75 m (Closa et al. 2003; Rosich et al. 2003). The ASAR images (Table 1) were calibrated, and normalized radar cross-section (NRCS in dB) values were calculated (Closa et al. 2003). In order to remove the range trend of ASAR imagery, an NRCS contrast ($K_{\sigma^{\circ}}$) was calculated using the following formula: $K_{\sigma^{\circ}} = (\sigma^{\circ} - \sigma^{\circ}_{\text{mean}})/\sigma^{\circ}_{\text{mean}}$, where the mean σ° ($\sigma^{\circ}_{\text{mean}}$) is defined as NRCS averaged in the azimuth direction and σ° is NRCS at the transect point.

Table 1. Overview of the summer remote-sensing images (SST, Chl *a*, and SAR), in situ FT and CTD temperature (T), Chl *a* data (laboratory analysis and calculated from FT fluorescence) measured along transects Tallinn–Helsinki (11) and Helsinki-Travemünde (1), and sources of wind data used in the present study.

Period	SST images	In situ transects	Chl <i>a</i> images	SAR images	Wind data
2003–2009	19 (MODIS)	11 (FT: T)	–	–	r/v weather station
2000–2009	147 (MODIS)	–	–	–	Kalbådgrund, Utö
2006	60 (MODIS)	5 (CTD: T and sampled Chl <i>a</i>)	31 (MERIS)	–	HIRLAM
2008	3 (MODIS)	1 (FT: T and Chl <i>a</i>)	1 (MODIS)	2 (ASAR)	–

3 COMPARISON OF REMOTE SENSING AND IN SITU DATA

3.1 Comparison of MODIS and in situ temperature data

The differences between in situ temperature and remote sensing SST retrievals can vary significantly in different conditions, regions, and periods. Studies by Brown and Minnett (1999) and Reinart and Reinhold (2008) showed that the accuracy of SST estimates from MODIS sensors is ± 0.5 °C. MODIS/Aqua has been found to have a bias (between SST and in situ temperature) of 0.01 °C with a standard deviation of 0.5 °C for daytime SST retrievals while MODIS/Terra has a mean bias of -0.20 °C with a standard deviation of 0.5 °C (Haines et al. 2007). Mathur et al. (2005) found an RMSD of 0.79 °C, a bias of 0.44 °C, and a correlation of 0.80 between infra-red radiation pyrometer and MODIS daytime SST retrievals in the study conducted in the Arabian Sea. Reynolds et al. (2010) showed that large biases occur between data from different space-borne sensors in the coastal sea areas. Noyes et al. (2006) showed that different space-borne sensors can have biases of up to 0.6 °C. Donlon et al. (2002) showed that in situ temperature measurements at 5 m depth can be used in moderate wind conditions for validation of satellite SST data. They showed that in cases of wind speeds below 6 m s^{-1} the difference between SST_{skin} (surface skin layer $\sim 500 \mu\text{m}$) measured by SISTeR radiometers and $\text{SST}_{5\text{m}}$ (at 5 m depth) measured by CTD increases, especially for the daytime SST retrievals. At wind speeds greater than 6 m s^{-1} the variability of $\Delta T_{5\text{m}}$ ($\Delta T_{5\text{m}} = \text{SST}_{\text{skin}} - \text{SST}_{5\text{m}}$) diminishes and the mean value of $\Delta T_{5\text{m}}$ approximates a constant cool bias of -0.14 ± 0.1 °C RMSD. They concluded that in situ temperature measurements at a specified depth can be used for validation of satellite SST products when the wind speed is greater than 6 m s^{-1} .

Considering the variable accuracy of SST retrievals, the biases between in situ FT temperature and remote sensing SST products as well as the biases between SST products obtained from different remote-sensing sensors need to be quantified for the Gulf of Finland. Comparing in situ and remote-sensing temperatures in the Gulf of Finland, the influence of possible surface accumulations of cyanobacteria should be taken into account. According to Kahru et al. (1993) the massive surface accumulations of cyanobacteria can cause a local increase of surface temperature up to 1.5 °C in the Baltic Sea. We assume that this effect was observed near Osmussaar Island in late July 2002 (Paper III), when the FT temperature was ~ 2 °C lower compared to MODIS SST in the region where surface accumulations were present. Several studies have shown the existence of massive cyanobacterial blooms at the entrance of the Gulf of Finland in July 2002 (Kutser 2004; Reinart and Kutser 2006). A filament of cyanobacterial bloom reached from the open sea bloom to the coastal zone of Osmussaar Island, where it probably influenced the SST data along the transect

of FT measurements (Paper III, Sipelgas et al. 2004). The pixels influenced by cyanobacteria surface accumulations were excluded from further analysis.

Comparison between different MODIS SSTs and near-surface in situ temperatures at ~20 cm depth showed that RMSD was lower in the case of MODIS/Aqua SST (0.57 °C) compared to the MODIS/Terra SST (0.75 °C) (Table 1 in Paper III). We also calculated the RMSD for the data obtained during a time interval of ± 0.5 h around the over-flight of the Aqua satellite. As expected the RMSD was smaller (0.31 °C) for the shorter time intervals.

The comparability of FT temperature and remote sensing SST products depending on wind speed (upper mixed layer depth) was evaluated using 11 FT transects and 17 MODIS images (Table 1). One or two SST images (MODIS/Aqua, MODIS/Terra) were acquired during each FT transect. The biases (SST minus FT temperature) were calculated (a) for 11 transects using SST from all images and (b) using only SST and FT data pairs within an interval of 1 h from the satellite overpass. The calculated biases against wind speed at the time of image acquisition are presented in Fig. 2. In the cases of wind speeds below 5 m s^{-1} , the bias between FT temperature and SST retrievals starts to increase, even in the case of the 1 h time window. Thus, the wind-speed value of 5 m s^{-1} was treated as a threshold for comparison between satellite SST retrievals and FT temperature at a depth of 4 m.

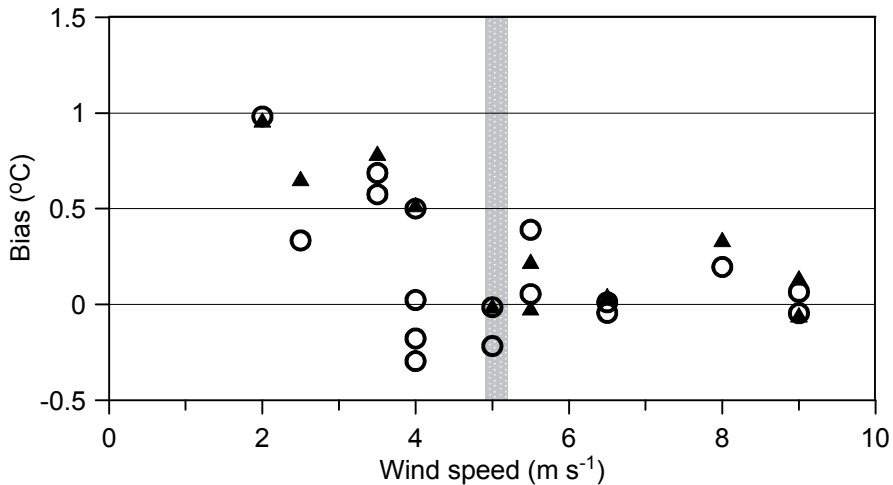


Figure 2. Bias between SST retrievals and FT temperature as a function of wind speed. Circles represent the bias using all SST images (17 images) and triangles represent the bias using FT data within an interval of 1 h from the satellite overpass (12 images). The gray line represents the wind speed threshold.

We calculated the statistics for all data and for the subset where the data pairs corresponding to a wind speed below 5 m s^{-1} were excluded (Table 2). There was no significant change in correlation values while the bias of MODIS

retrievals was reduced by 0.13 °C to 0.11 °C and RMSD was reduced by 0.18 °C to 0.28 °C. In the case of MODIS/Aqua the bias and RMSD were reduced to 0.08 °C and 0.23 °C respectively. The corresponding values for MODIS/Terra were 0.16 °C and 0.36 °C. The improved wind-selective statistics show that the FT data measured at 4 m depth can be used for validation of MODIS SST retrievals in the cases when the wind speed is $\geq 5 \text{ m s}^{-1}$.

Table 2. Correlation coefficient (r), mean bias (SST minus FT temperature), and RMSD between remote sensing SST and FT temperature.

Data	r	Mean bias (°C)	RMSD (°C)	Number of data pairs
All data used				
MODIS/all	0.96	0.24	0.46	730
MODIS/Aqua	0.97	0.26	0.46	435
MODIS/Terra	0.96	0.21	0.46	295
Data corresponding to wind speed $\geq 5 \text{ m s}^{-1}$				
MODIS/all	0.97	0.11	0.28	278
MODIS/Aqua	0.97	0.08	0.23	164
MODIS/Terra	0.97	0.16	0.36	115

3.2 Evaluation of remote sensing Chl *a* retrievals

The Gulf of Finland comprises optically complex Case 2 waters and therefore it is necessary to evaluate the quality of remote sensing Chl *a* data using in situ measurements. Retrievals of Chl *a* concentration from MERIS (FUB algorithm) imagery were validated against in situ Chl *a* data collected during the period when chlorophyll distribution was influenced by a sequence of upwelling events in July–August 2006 (Paper I). In situ Chl *a* concentrations along the cross-gulf transect varied within a wide range from 1.6 to 15.5 mg m^{-3} during the period of field measurements. Low Chl *a* concentrations were observed during the first half of July in the upwelling region along the northern coast. From 25 July, when upwelling along the northern coast was in the relaxation phase, the Chl *a* concentrations increased off the northern coast and decreased off the southern coast. The highest (15.5 mg m^{-3}) and lowest (1.6 mg m^{-3}) Chl *a* concentrations were observed on 8 August off the northern and southern coasts respectively.

The remote sensing imagery represents the situation at the sea surface. Variable wind conditions prevailed during July–August, whilst wind speeds were mainly moderate with gusts over 10 m s^{-1} (Fig. 2b in Paper I). The Chl *a* concentration was measured from the pooled sample representing the UML, and therefore we may suggest that these two datasets are comparable if the depth of the turbulent Ekman boundary layer roughly persists during the time interval between the acquisition of the MERIS image and the collection of water

samples. Kutser et al. (2008) also pointed out that a Chl *a* sample taken from one depth represents the biomass in the whole mixed layer in the case of strong wind mixing. The estimated depth of the turbulent Ekman boundary layer from wind data showed that the differences were small (Fig. 2c in Paper I).

The comparability of in situ and MERIS Chl *a* data is also supported by the Maximum Chlorophyll Index (MCI) calculated from all MERIS data using the algorithm provided by Gower et al. (2008). The MCI showed that no surface algal accumulations were observed during the study period as the index value was negative or close to zero most of the time. The highest MCI values (up to 0.9 mW/(m² sr nm)) were observed on 6 August 2006 at the location of a filament at the entrance to the Gulf of Finland, which is larger than the detection criterion of about 0.2 mW/(m² sr nm) used in Gower (2005).

The Chl *a* concentrations calculated with the FUB processor from the MERIS data were correlated with in situ Chl *a* for two time windows: intervals of 24 h and 2 h (before or after) from the satellite overpass (Fig. 3). According to Kratzer et al. (2008) a 2 h window is sufficient for validating satellite Chl *a* measurements with in situ data. A total of seven data pairs fulfilled the 2 h criterion. The FUB processor underestimated Chl *a* compared with in situ Chl *a*; the average underestimation was 25% (1.3 mg m⁻³), which is of the same magnitude or better compared to previous studies in the Baltic Sea (Kratzer et al. 2008, ~56%). The correlation (r^2) for data points within the 2 h window was 0.67 and that for the 24 h window (66 data pairs) was also relatively high, 0.56. The linear regression for the 2 h window with 95% confidence limits was Chl *a* = 0.48 (\pm 0.39) * X + 3.6 (\pm 1.8), where X is the FUB processor output. The standard deviation of the residuals (i.e. the standard error of the estimation) was 0.51 mg m⁻³. For the 24 h window the slope and y-intercept of the linear regression were 0.44 (\pm 0.097) and 2.9 (\pm 0.60) mg m⁻³ respectively. The standard deviation of the residuals for the 24 h window was 1.43 mg m⁻³.

In addition to the FUB processor we also evaluated the Case 2 regional water processor (C2RW) for Chl *a* (data not shown). The correlation for the FUB processor (r^2 = 0.67) was significantly higher compared to the C2RW processor (r^2 = 0.17). Also, the Chl *a* overestimation of C2RW by 52% is poorer compared with the underestimation (25%) by the FUB processor (Table 3).

On the basis of the above analysis, the FUB algorithm was used to calculate Chl *a* from MERIS data in the Gulf of Finland. The equation obtained with linear regression for the 2 h window was applied to calibrate MERIS Chl *a* data. The average statistics are of the same magnitude or better than in the previous studies (e.g. Kratzer et al. 2008).

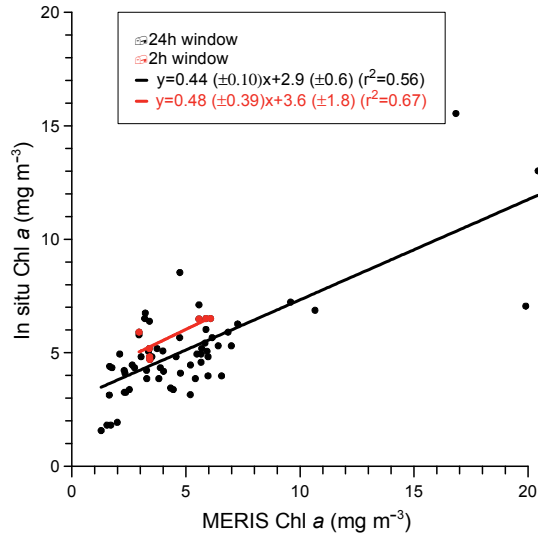


Figure 3. Scatter plot of in situ Chl *a* and MERIS Chl *a* derived by the FUB processor. Black dots represent all data pairs from 11, 18, and 25 July and 7 and 16 August 2006 (24 h window), and red dots represent data pairs from 11 and 25 July 2006 (2 h window). The data points corresponding to the 2 h window were used for bias estimation of the FUB processor Chl *a* (1.3 mg m^{-3} , 25 %). The correlation (r^2) for the 24 h window data points was 0.56, and that for the 2 h window was 0.67.

Table 3. Correlation (r^2) and relative bias (%) of the two Chl *a* remote sensing algorithms for the two time windows (remote-sensing in situ) in the Gulf of Finland in July–August 2006. The results of Kratzer et al. (2008) from the coastal area of the western Baltic Proper are also presented for comparison.

Algorithm	Time window	r^2	Relative bias (%)
FUB	2h	0.67	–25
FUB	24h	0.56	–18
FUB (Kratzer et al. 2008)	2h	–	–56
C2RW	2h	0.17	52
C2RW	24h	0.18	78

4 CHARACTERISTICS OF UPWELLING AND RELATED PHENOMENA

4.1 Upwelling area

Wind conditions are the most important factor behind the formation of coastal upwelling in the Gulf of Finland (Myrberg and Andrejev 2003). The wind data records from June to the end of September (2000–2005) showed five to eight (about six on average) upwelling-favorable wind events per year, which occurred in the summer and had absolute along-gulf components of cumulative wind stress larger than $0.1 \text{ N m}^{-2} \text{ d}$ (Paper II). The frequency of wind events able to generate upwelling differed between the Estonian and Finnish coasts and varied considerably from year to year. Although the southwesterly winds dominating in the Baltic Sea region more often generate upwelling along the northern coast of the Gulf of Finland, there are periods with quite persistent winds from easterly and northeasterly directions (Keevallik and Soomere, 2009) causing upwelling events along the southern coast (Paper I). We found one to four (on average about two) wind events yearly (June–September) that might generate upwelling along the Estonian coast and three to five (on average about four) wind events that might generate upwelling along the Finnish coast during the study period. Considering that SST imagery is influenced by clouds we did not observe all upwelling events. Analysis of the wind data showed that we observed 20% of the potential upwelling events along the northern coast and about 40% along the southern coast.

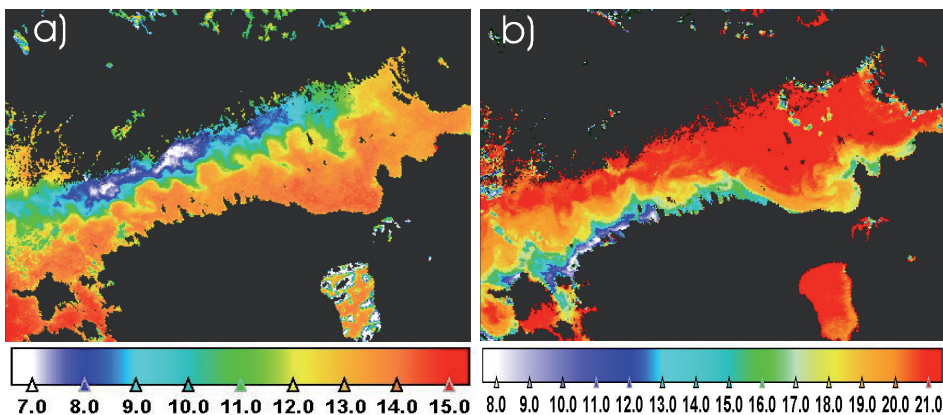


Figure 4. Extreme upwelling events: along the northern coast on 24 September 2003 when 38% of the Gulf area was covered by upwelling water (a), and along the southern coast on 9 August 2006 when 20% of the Gulf area was covered by upwelling water (b).

Satellite SST data analysis from the years 2000–2006 (Paper II) showed that during the strongest upwelling events along the northern and southern coasts of the Gulf of Finland the upwelled water can cover remarkably large areas, corresponding to about 38% (12 140 km²) and 20% (6480 km²), respectively, of the total surface area of the Gulf (about 29 500 km²) (Fig. 4).

Calculations of the areas covered by upwelling water and the percentages they represented were performed separately for the eastern and western parts of the Gulf of Finland considering the shape of the Estonian coastline (separation line along 26.0 °E). On several occasions when clouds were partly covering either the Finnish or the Estonian coastal sea the percentages were calculated for the cloud-free cross-Gulf stripe.

The average area covered by the upwelling water was 4820 km², which is about 15% of the total Gulf area. The average upwelling areas were larger along the Finnish coast (6120 km² and 19%) than along the Estonian coast (4070 km² and 13%). Upwelling events were more extensive in the western part of the Gulf, where the average area covered by the upwelling water was 3100 km² (22%) compared with 2420 km² (13%) in the eastern part. The average upwelling water areas along the Finnish and Estonian coasts were 3680 km² (26%) and 2630 km² (19%), respectively, in the western part of the Gulf. The corresponding estimates for the eastern part of the Gulf were 3440 km² (19%) and 1890 km² (10%). The discrepancies between eastern and western Gulf are probably caused by the different orientations of the coastline, especially in the southeastern part of the Gulf.

The composite upwelling maps calculated from 147 images (61 images along the southern coast and 86 images along the northern coast) depicting upwelling in the Gulf of Finland during the period 2000–2009 also showed that the upwelling area is larger along the northern coast (Fig. 5). The upwelling area during that period along the northern coast was 5642 km², which is 8% less than that for the period 2000–2006. Along the southern coast the upwelling area was 4% smaller, being 3917 km², compared to the years 2000–2006. Also the upwelling area was larger in the western Gulf compared to the eastern region.

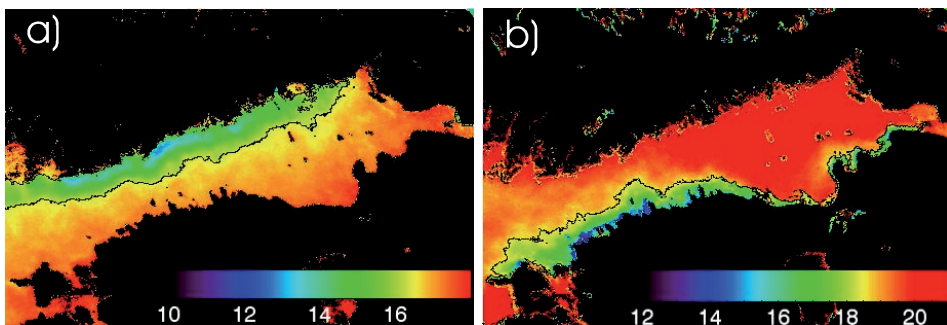


Figure 5 Average upwelling regions for the northern and southern coasts. Isotherms of 16.5 °C along the northern coast and 18.5 °C along the southern coast represent the upwelling border lines.

Considerably larger upwelling areas along the Finnish coastline could be explained by a larger westerly along-gulf component of cumulative wind stress that generated the observed upwelling events (Table 1 in Paper II). The cumulative wind stress was calculated from the beginning of the upwelling-favorable wind until the time of the satellite overpass. The approximate offshore displacement (ΔX) of the upwelling front is $\Delta X = W/\rho_0 f h_E$, where W is the along-gulf component of cumulative wind stress, ρ_0 is the reference density, h_E is the surface Ekman layer depth, and $f = 1.25 \times 10^{-4} \text{ s}^{-1}$ is the Coriolis parameter (Austin and Lentz 2002). This equation does not take into account the upwelling setup time, and there are also no data available from which to estimate the Ekman layer depth. Nevertheless, the observed larger upwelling water areas along the Finnish coast were in accordance with larger cumulative wind stresses (Table 1 in Paper II).

Observed temperature differences between the upwelling and the surrounding water varied in a wide range, from 3.5 to 15.2 °C (Table 1 in Paper II). For the upwelling events along the Estonian coast the temperature differences were between 7.9 and 15.2 °C. During upwelling events along the Finnish coast the temperature differences were smaller, from 3.5 to 7.9 °C. The upwelling events detected off the Estonian coast occurred mainly in July–August when the surface heating was strong and therefore the temperature difference between the upwelling and the surrounding waters was large while upwelling events along the Finnish coast occurred mostly in June and September and therefore the temperature difference was lower (Table 1 in Paper II).

To conclude, the analysis of satellite SST data showed that the upwelling water covered a considerable area of the Gulf. Most likely due to the different atmospheric forcings, the upwelling events off the northern coast were more extensive and the upwelling water covered larger areas of the coastal sea.

4.2 Upwelling filaments

Upwelling-related filaments are an important mechanism for transporting cold nutrient-rich upwelled water offshore. Knowledge about upwelling filaments would give valuable information about areas where the nutrient rich waters are transported offshore. Therefore, the location and area of upwelling filaments in the Gulf of Finland were analyzed (Paper II).

In total, 32 filaments, excluding the filaments of coinciding location observed on the successive SST images of the same upwelling event, were identified (Fig. 6). The filaments predominantly stretched out from the upwelling front along the Finnish coast and in the western part of the Gulf. Only eight filaments were related to the upwelling events along the Estonian coast and six of those were observed during the strongest upwelling event along the Estonian coast in August 2006. The length of filaments was up to 35 km and in several cases the filaments observed along the northern coast were cyclonically turned. For example, on the SST images from 24 to 26 September 2005 the cyclonically

turned filaments can be detected along the Finnish coast (Fig. 4a in Paper II), which further on formed a rotating vortex pair and an eddy (Fig. 4b, c in Paper II). The area of single filaments varied in a wide range from 80 to 680 km². The area covered by filaments was significantly larger for the upwelling events along the northern coast as the filaments were rarely formed in the case of upwelling events along the southern coast (Table 1 in Paper II). In the case of the largest upwelling event along the Finnish coast observed on 24 September 2003 (Fig. 4) the area of filaments was 1420 km² (Table 1 in Paper II), which made up 12% of the total area of the upwelled water in the Gulf. The share of upwelling filaments was higher in the western part of the Gulf. For example, during the upwelling along the Finnish coast on 24 September 2005 (Fig. 4a in Paper II) the area of filaments was 1330 km² (30%) and during a large upwelling along the Estonian coast on 25 August 2006 (Fig. 2b in Paper II) the area of filaments was 1100 km² (27%).

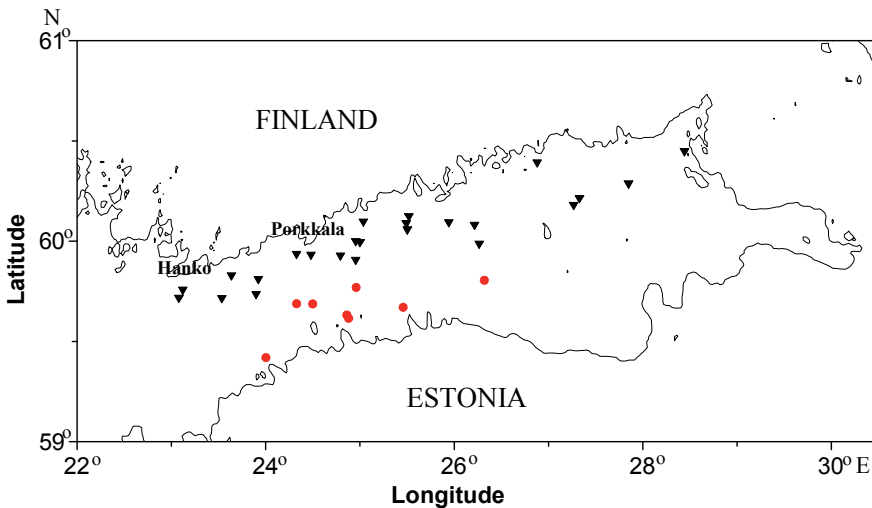


Figure 6. Locations of upwelling filaments related to upwelling events along the Finnish (▲) and Estonian (●) coasts.

Many observed filaments were cyclonically turned. The model simulations by Zhurbas et al. (2006) demonstrated the growth of wave-like perturbations forming mostly cyclonic meanders (filaments) of the upwelling jet which further on detached from the jet and formed mesoscale cyclonic eddies. Such a development was also observed on a series of SST images (Fig. 4 in paper II) at a time scale of a few days.

The generation of filaments is related to the instability of longshore baroclinic jets associated with the upwelling. Blumsack and Gierasch (1972) and de Szoeke (1975) showed that in the case of sloping bottoms the baroclinic instability of a longshore upwelling jet strongly depends on the ratio of the bottom slope to the isopycnal slope, α . When the isopycnal slope is smaller than

the bottom slope ($\alpha > 1$) then the baroclinic instability of the upwelling jet is not expected to occur. A numerical study by Zhurbas et al. (2006) using the characteristic summer stratification in the Baltic Sea also showed that no baroclinic instability of an upwelling jet was observed when the bottom slope exceeded the isopycnal slope. The cross-shore scale for the region of sloping isopycnals for the upwelling event is the baroclinic Rossby radius of deformation (Allen 1980). According to Alenius et al. (2003) the baroclinic Rossby radius of deformation is about 3 km in the Gulf of Finland in summer and the depth of the upper mixed layer is approximately 10 m, which gives a rough estimate of 0.003 for the isopycnal slope. Although the bottom topography of the Gulf of Finland is complicated (Fig. 1) the approximate estimates of the bottom slope off the Estonian coast, 0.006, and off the Finnish coast, 0.002, could be used. Thus, in the Finnish coastal sea $\alpha \approx 0.7$ while in the Estonian coastal sea $\alpha > 1$; that is, baroclinic instability of the upwelling jet along the Finnish coast is more probable. Another reason for the observed difference between the occurrence of upwelling filaments along the Finnish and Estonian coasts is likely due to the different atmospheric forcings. Zhurbas et al. (2006) showed that the rate of growth of instability depends on the cumulative wind stress and increases considerably for sufficiently large cumulative wind stresses. Our data also revealed that the along-gulf component of cumulative wind stress was smaller during the upwelling events along the Estonian coast, except for the upwelling on 25 August 2006 (Table 1 in Paper II).

4.3 Manifestation of SST signatures and biogenic slicks on SAR

Different upwelling-related surface layer phenomena like biogenic slicks and low sea surface temperature areas (upwelling zone, eddies, filaments) influence the backscatter values on SAR imagery. The low-backscatter areas are induced by two mechanisms: (i) the cooler surface water in the upwelling region changes the marine boundary layer and decreases the wind stress, which contributes to producing the lower sea surface roughness, and (ii) upwelling water also brings the biogenic slicks that dampen the Bragg waves in the sea surface (Friehe et al. 1991; Clemente-Colon and Yan 2000; Li et al. 2009). The manifestation of these upwelling-related phenomena on SAR images is restricted by low and moderate wind conditions (Kozlov et al. 2012). In the case of wind speeds over 10 m s^{-1} the effects of the upwelling temperature front and related biogenic slicks are not detectable (Ryan et al. 2010; Kozlov et al. 2012).

The dependence of NRCS on temperature and biogenic slicks is shown as follows (Paper IV). The upwelling-related eddies found on both images (SAR and SST) match with respect to their location, scale, and boundaries (Fig. 7a, b). The minima of in situ temperature and remote sensing SST on the transect were well detected and coincided with eddy centers on SAR images (Fig. 8). Thus,

SAR images allow eddy locations to be monitored when optical (SST) imagery is not available due to cloud cover. Also the cyclonic rotation of the eddies can be observed well on SAR imagery due to the cyclonically turned dark stripe-like slicks surrounding the eddy core and originating from the upwelling zone, while it cannot be observed from SST or Chl *a* imagery. Biogenic films allow the direction of rotation of the eddies to be detected. Figure 7c shows an enlarged fragment of the eddy on the SAR image depicting the dark small-scale elongated features in the periphery of the eddy due to the accumulation of surfactants in the zone of surface current convergence associated with mesoscale dynamics.

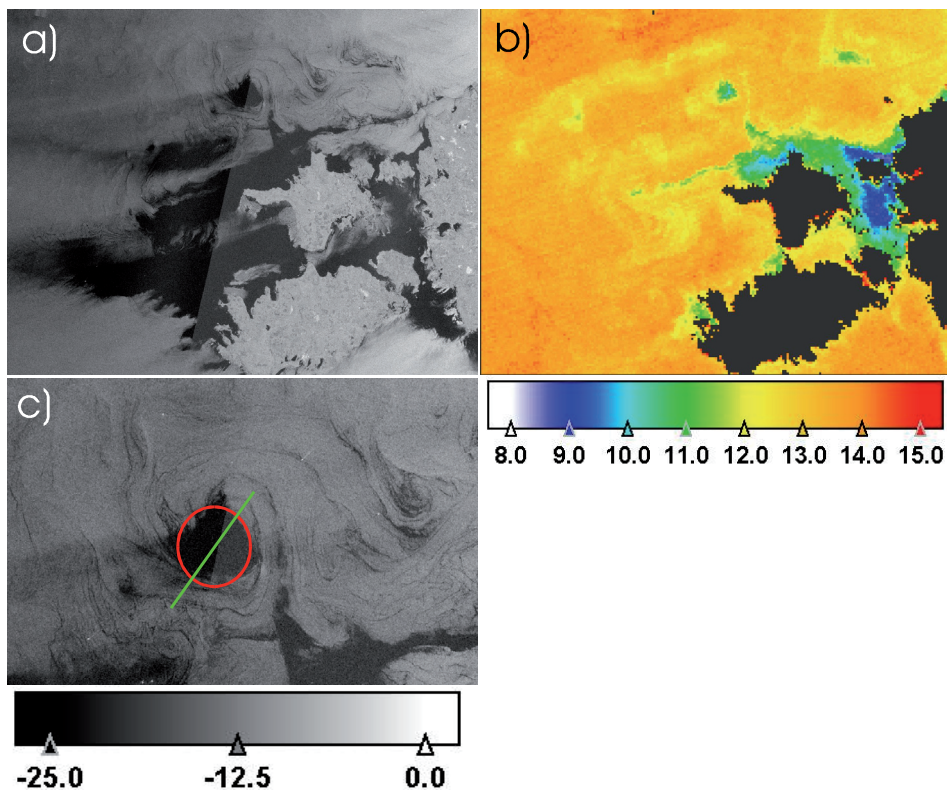


Figure 7. Upwelling and eddy manifestation on 24 September 2008 on (a) Envisat ASAR NRCS at 09.04 UTC, (b) MODIS SST at 11.00 UTC, and (c) zoomed area of SAR image (rectangle on panel (a)) demonstrating eddy rotation. The red circle indicates the eddy core (diameter 12 km) and the green line roughly indicates the diameter (22 km) of the eddy velocity field (c).

The correlation coefficient between NRCS and SST in the region of the upwelling-related eddy was $r = 0.19$ and $r = 0.52$ for two consecutive days. SAR data along the transect correlated better with in situ Chl *a* and turbidity data, with the correlations being up to 0.70 and 0.73, respectively. However, the good correlation with biological parameters might be due to the coincidence of the

range trend on the ASAR image explained by Kozlov et al. (2012) and the increase of Chl *a* concentration from the northern Baltic Proper toward the Gulf of Finland. The effect of surface temperature on SAR backscatter is lower compared to the effect of biogenic slicks (Paper IV; Li et al. 2009).

Differences caused by SST on C-band NRCS were estimated to be 1–2 dB per 1 °C by Li et al. (2009) as well as by Kozlov et al. (2012), while Clemente-Colon and Yan (1999) estimated the backscatter’s sensitivity to temperature to be of the order of 0.5–1.0 dB per 1 °C. Lin et al. (2002) estimated that the increase of Chl *a* concentration by 1 mg m⁻³ caused attenuation of the NRCS by 5 dB.

Our data (Paper IV) showed that the difference in NRCS between the eddy center and the surrounding area was about 11 dB (Fig. 7c). Kozlov et al. (2012) found that the differences in NRCS in the frontal zone should be over 3 dB for reliable detection of the upwelling front, and thus the NRCS difference in our study was well beyond the sufficient level for detection of fronts and eddies. The corresponding temperature difference observed from MODIS imagery was 2–3.5 °C and the difference observed from in situ measurements was 2.5 °C. Considering the abovementioned estimates of NRCS attenuation (from the literature), the SST contribution to the NRCS attenuation in the eddy center is up to 7 dB.

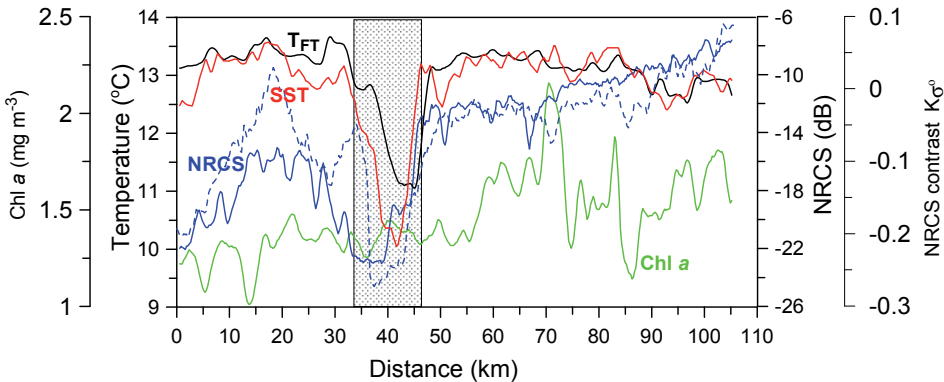


Figure 8. Transect data from 59.10 N, 21.50 E to 59.60 N, 23.10 E showing the manifestation of the upwelling-related eddy on different datasets: T_{FT} denotes FT temperature measurements (black), Chl *a* denotes chlorophyll *a* data obtained from in situ fluorescence measurements (green), SST denotes MODIS SST data (red), and NRCS denotes the normalized radar cross-section (σ^0) on SAR images (solid blue) as well as contrast NRCS (K_{σ^0}) values along the transect with the range trend removed ($K_{\sigma^0} = (\sigma^0 - \sigma_{\text{mean}}^0) / \sigma_{\text{mean}}^0$) (dashed blue). The shaded box indicates the region of the eddy. FT data were collected on 24 September 2008 between 18.42 and 21.08 UTC. SAR and SST images were acquired on 24 September 2008 at 09.04 and 11.00 UTC respectively.

Previous studies (Asakari 2001; Clement-Colon 2001; Lin et al. 2002) showed that the upwelling water is associated with high Chl *a* concentrations. These studies carried out at lower latitudes compared to the Baltic Sea showed

good spatial correlation between the locations of Chl *a* filaments (high Chl *a* content) and cold SST filaments related to the upwelling front. They demonstrated that both phenomena (low SST and high Chl *a*) contribute simultaneously to the dampening of Bragg waves. However, in the case of our study in the Baltic Sea, the time lag between the upwelling event (surfacing water) and increase of Chl *a* concentration has to be considered (e.g. Vahtera et al. 2005). The low temperature values in the upwelling-related eddy core were associated with Chl *a* concentrations that were not significantly lower compared to the background concentrations (Fig. 8). In the autumn the bloom may not occur at all due to the generally low water temperature and “poor” light conditions. Thus the Bragg wave dampening in the eddy core is only due to the low SST. Meanwhile, outside the eddy core where Chl *a* concentrations were often higher and the influence of the SST variability was almost missing, only phytoplankton contributes to Bragg wave dampening. Therefore the rotation of the eddy is observed on the SAR imagery as cyclonically turned dark stripes (Fig. 7a, c). Due to the manifestation of the two phenomena (1) the core of the eddy becomes visible on the SAR image in the region where low temperature contributes to the attenuation of NRCS and (2) the area influenced by the eddy rotation becomes visible due to Chl *a* variability in the vicinity of the eddy core. The eddy core dimensions observed from three different data sets (SAR, FT, and SST) coincide (Fig. 8). The eddy core diameter observed from the SAR image on 24 September 2008 was ~12 km while the diameter of the total area influenced by the eddy velocity field was ~22 km (Fig. 7c). It was also shown by Laanemets et al. (2005, Fig. 6) that the eddy core diameter is smaller compared to the eddy rotation field.

5 EFFECT OF UPWELLING EVENTS ON CHL *a* DISTRIBUTION

5.1 Upwelling-related temperature variability

The spatio-temporal variability of SST and the Chl *a* field caused by a series of coupled upwelling and downwelling events along the northern and southern coasts of the Gulf of Finland in July–August 2006 was investigated using remote sensing (MODIS and MERIS) and in situ data (Paper I).

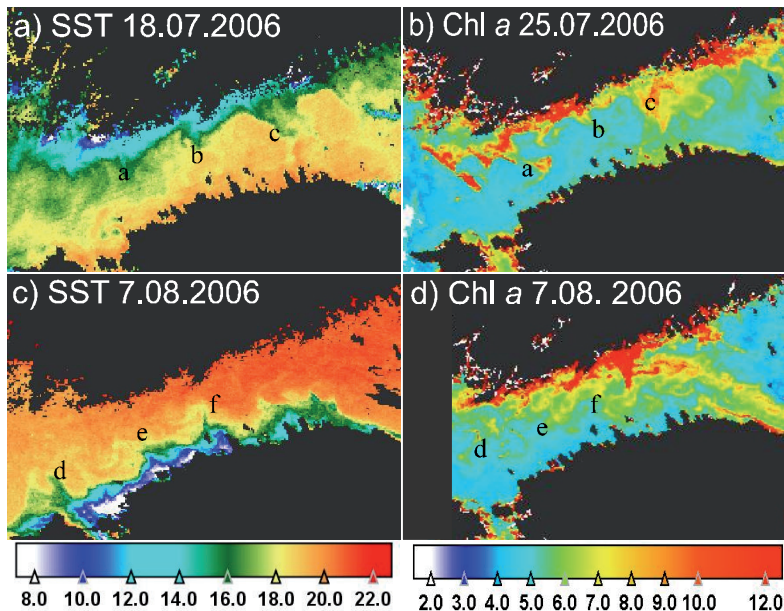


Figure 9. MODIS SST and MERIS Chl *a* images showing (a) peak of upwelling along the northern coast of the Gulf on 18 July 2006; (b) chlorophyll-rich filaments (letters a, b, and c) on 25 July 2006 at the same locations as low temperature filaments on (a); (c) upwelling front and the related cold filaments (d, e, and f) along the southern coast of the Gulf on 7 August 2006; and (d) upwelling induced bloom (by earlier event on 18 July 2006) along the northern coast and filaments with low chlorophyll content (d, e, and f) at the same locations as the low-temperature filaments on 7 August 2006.

Westerly winds dominated in the Gulf area from 10 to 29 July (Fig. 2a in Paper I). The development of upwelling along the northern coast of the Gulf was observed from 10 July (Fig. 3 in Paper I), and the temperature difference between the upwelling and the surrounding water was around 5 °C for most of the time (the maximum difference was up to 12 °C), according to the MODIS SST data (Figs. 9a and 10a). After 29 July, easterly winds were dominant in the Gulf of Finland area until 16 August (Fig. 2a in Paper I), and as a result, a zone

of upwelling formed along the southern coast (Fig. 4 in Paper I). The zone was well-expressed along the northwest coast of Estonia, from Vormsi Island to Aegna Island, with several upwelling centers near the Pakri Islands, Vormsi Island, and off the coast of the Suurupi Peninsula. An extremely low temperature of upwelled water of about 2 °C was observed near Vormsi island (e.g. Figs. 9c and 10b). The temperature difference between the upwelled and surrounding waters was up to 18 °C (Figs. 9c and 10b), and the upwelled water covered 31% of the western Gulf area (22–26° E) on 9 August (Table 1 in Paper II).

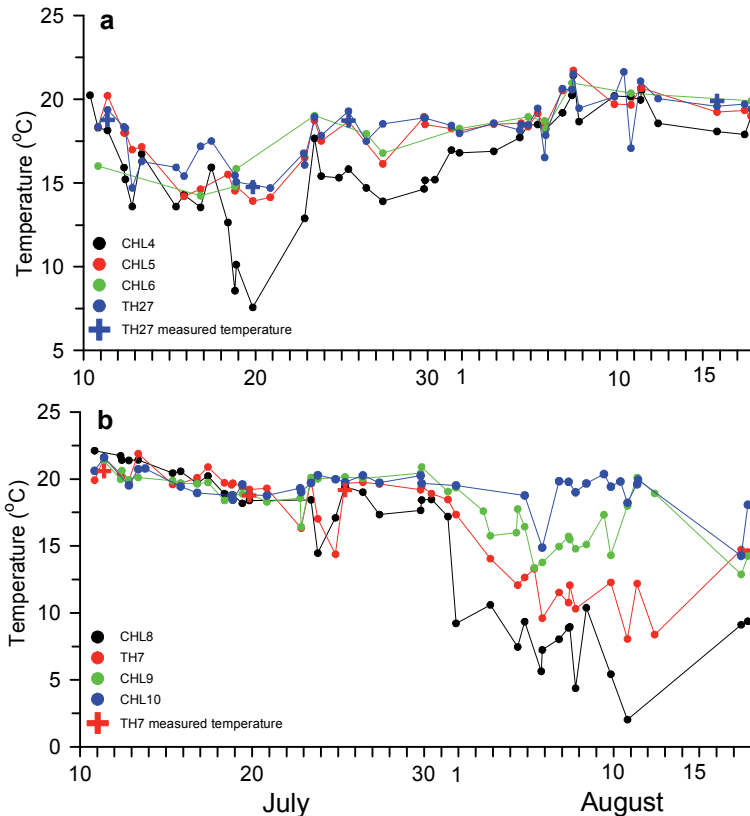


Figure 10. Temporal courses of surface layer temperature (MODIS SST) from 10 July to 16 August 2006 at stations CHL4, CHL5, CHL6, and TH27 (northern part of the Gulf) (a) and at stations CHL8, CHL9, CHL10, and TH7 (southern part of the Gulf) (b). The in situ surface temperature (bold cross) is given for stations TH7 and TH27. The locations of stations are shown in Fig. 1.

5.2 Chl *a* variability caused by upwelling events

The upwelling caused high variability in the surface Chl *a* distribution. In July–August 2006 the Chl *a* concentrations were generally higher along the northern coast compared with those in the open sea area and along the southern coast (Fig. 11). In July the Chl *a* concentrations along the northern coast varied in the

range of 4–9 mg m⁻³. After the relaxation of upwelling along the northern coast, Chl *a* concentrations reached high values of up to 13–14 mg m⁻³.

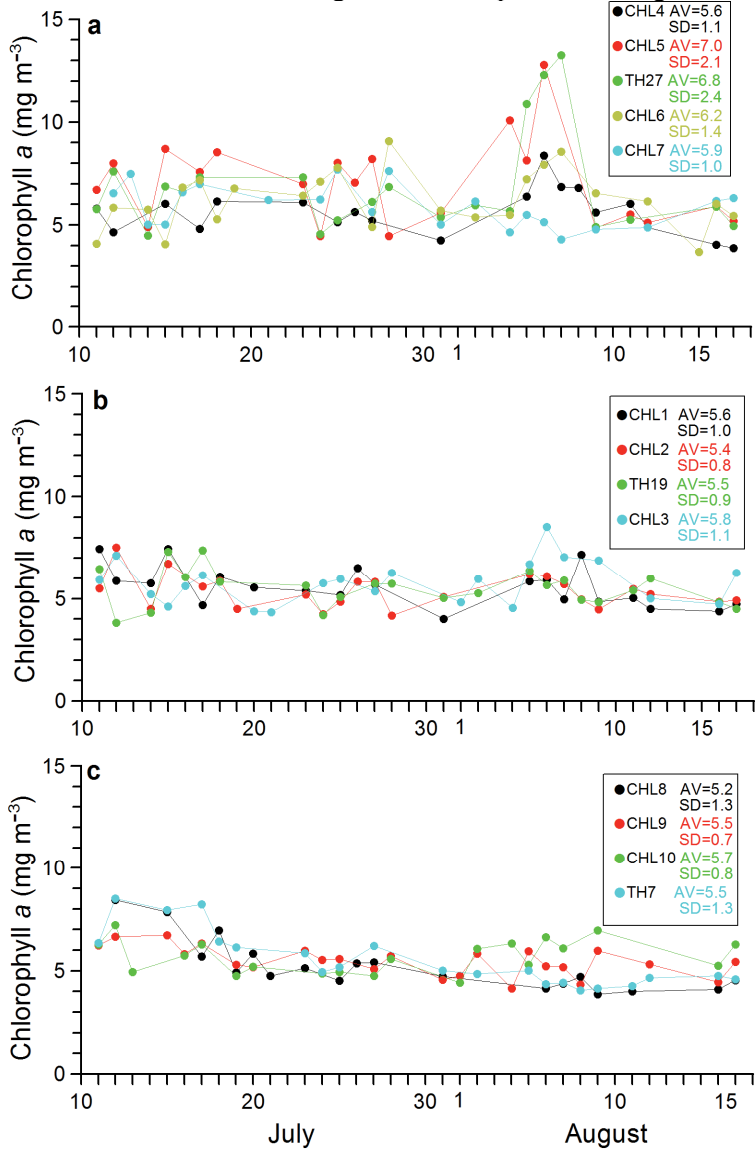


Figure 11. Distribution of MERIS Chl *a* at selected locations (Fig. 1) (a) along the northern coast, (b) along the Gulf axis, and (c) along the southern coast in July–August 2006. The locations’ of time series data are shown on Fig. 1.

Along the southern coast, Chl *a* concentrations varied between 4 and 8.5 mg m⁻³ in July–August (Fig. 11). Higher Chl *a* concentrations (up to 8.5 mg m⁻³)

were observed in the western part of the Gulf during the upwelling along the northern coast between 11 and 18 July. In early August, when upwelling developed along the southern coast, the temperature dropped below 12 °C (Fig. 10c), and Chl *a* concentrations were below 5 mg m⁻³ (Fig. 11b) in a narrow area along the southern coast (Fig 11c). The temporal course of Chl *a* along the southern coast was less variable compared with the northern coast during the whole study period.

The largest increase of Chl *a* was observed from 4 to 8 August along the narrow northern coastal zone (Fig. 9e, f in Paper I; Fig. 11a) after the decrease of the surface Chl *a* concentration from 31 July to 4 August (Fig. 11a), which was most likely caused by a strong wind event increasing the UML depth (Fig. 2b, c in Paper I) and mixing the phytoplankton deeper.

At locations along the Gulf axis in the western and central Gulf of Finland, the variability of the surface Chl *a* field (Fig. 11b) was related to mesoscale activity (filaments). In July, when upwelling occurred along the northern coast, filaments carried cold nutrient-rich water with low chlorophyll content offshore. Observational evidence that filaments carry nutrients from upwelling zones offshore is shown by Vahtera et al. (2005). In August, filaments carried chlorophyll-poor water from the southern upwelling zone into the central part of the Gulf.

Chlorophyll-rich filaments were observed off the Hanko and Porkkala peninsulas and the Porvoo Archipelago after 23 July, when upwelling along the northern coast was in the relaxation phase. The location of chlorophyll-rich filaments coincided well with locations of cold filaments observed on the SST map (Fig. 9a, b). The high variability of Chl *a* along the Gulf axis observed in August (Fig. 11b, locations CHL1, CHL2, and TH19) was a result of chlorophyll-rich and -poor filaments from the northern and southern coastal sea areas, respectively (Fig. 9b)

In the shallower eastern part of the Gulf, the mesoscale activity estimated from SST imagery (e.g. Kahru et al. 1995) and numerical simulations (Laanemets et al. 2011) was lower. This was also confirmed by the MERIS Chl *a* data, as the mean concentrations of the whole period were relatively persistent (5.7–5.9 mg m⁻³) with small standard deviations (0.8–1.1 mg m⁻³) at the easternmost locations.

The temporal course of spatially averaged SST and Chl *a* along the northern coast showed that the increase of Chl *a* started after the peak of upwelling on 20 July (Fig. 12). There are probably two reasons for the increase of Chl *a* concentration in the narrow northern coastal zone. One reason could be the phytoplankton growth promoted by nutrient input during the upwelling in July along the northern coast. The numerical simulation of nutrient transport during upwelling events in summer 2006 showed that the main area along the northern coast of the Gulf, where nutrients (nitrogen and phosphorus) were brought to the surface layer, was from the Hanko Peninsula to the Porvoo Archipelago region (Laanemets et al. 2011). By 20 July most of the nitrogen and phosphorus (about

325 and 400 tonnes respectively) had been brought into the upper layer. This area coincided with the area of intensive upwelling along the northern coast depicted on the SST maps (Fig. 3b, c in Paper I). After the upwelling began to relax, the temperature in the northern coastal zone rose above 15 °C by 23 July (Figs. 10a and 12). Previous studies have shown that phytoplankton growth is promoted in areas covered by upwelled nutrient-rich water (Vahtera et al. 2005). To confirm this assumption, we also compared the upwelled water area and the extended Chl *a* area along the northern coast. The area where the temperature was < 14 °C, that is, the narrow area along the northern coast where nutrients were probably brought to the surface layer, was 1317 km² (about 7% of the study area) on 18 July. Moreover, the area along the coast of water with a temperature < 17 °C due to offshore transport and covering the filaments was 4879 km² (about 25%). The upwelling-induced area with a slightly increased Chl *a* concentration (over 7 mg m⁻³) on 25 July was 5507 km². This area remained approximately the same until 6 August (the bloom peak), when it was 5526 km². This suggests that the observed phytoplankton increase occurred mainly in the region of possible nutrient input by upwelling with a two-week lag. Of course, some differences in the spatial distribution were due to the development of upwelling (and filaments) along the southern coast (Fig. 4a, b in Paper I).

The second possible reason for the higher Chl *a* concentrations and variability along the northern coast could be the Ekman transport of phytoplankton biomass in the surface layer from the open sea area towards the northern coast during the upwelling event along the southern coast and the simultaneous convergence due to downwelling along the northern coast in early August. Surface transport and a higher Chl *a* concentration in the downwelling zone were also observed in previous studies (Pavelson et al. 1999; Kanoshina et al. 2003; Lips and Lips 2010).

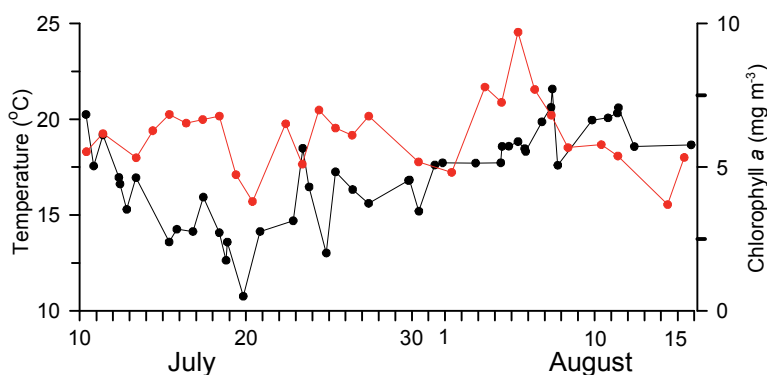


Figure 12. Temporal course of spatially averaged (locations CHL4, CHL5, and CHL6) Chl *a* concentration (red line) and SST (black line) on the northern coast in July–August 2006. Peak of upwelling observed on 20 July and peak of bloom observed on 6 August.

CONCLUSIONS

The aim of the thesis was to improve the knowledge about spatio-temporal variability of near-surface layer temperature and chlorophyll distribution caused by upwelling events at basin scale. Estimations of upwelling characteristics showed that summer coastal upwelling is an important process that transports cold water from deeper layers to the surface layer and the area influenced by upwelled water might cover up to 40% of the total Gulf area. Due to the bottom topography and wind forcing the upwelling filaments were mainly observed in the northern coastal sea area. The combined use of remote sensing SST and Chl *a* data allows spatio-temporal changes in the Chl *a* field to be linked with upwelling and related filaments. It was demonstrated that SAR imagery can provide information about the scale and dynamics of upwelling-related eddies.

SST and Chl *a* concentration from MODIS and MERIS data were evaluated against in situ measurements. The results of MERIS chlorophyll-retrieval algorithms in optically complex Case 2 waters like the Baltic Sea were adjusted according to the in situ data.

The main results of the present thesis are as follows:

- The upwelling water covered a considerable part of the total Gulf area: 15% on average and 38% in the case of the largest upwelling event. The upwelling events off the northern coast were more extensive (19%) compared to the southern coast (13%), probably due to the larger eastward along-gulf cumulative wind stress. Upwelling events were more extensive in the western part of the gulf than in the eastern part. Temperature differences between upwelling and surrounding waters were up to 15.2 °C.
- The upwelling filaments were predominantly observed off the northern coast due to the bottom topography (smaller bottom slope) and larger eastward along-gulf cumulative wind stress. The area of filaments varied from 80 to 680 km²; during the strongest upwelling the total area of filaments was 1420 km². The share of upwelling filaments was higher in the western part of the Gulf.
- The spatio-temporal variability of Chl *a* in July–August 2006 showed the evident influence of upwelling events and related filaments. The variability of Chl *a* was largest in the western and central parts of the Gulf, where mesoscale activity was the highest. Upwelling events had only a minor influence in the eastern part of the study area, where Chl *a* concentrations were relatively high and persistent throughout the study period.
- The highest Chl *a* concentrations along the northern coast in July–August 2006 were observed about two weeks after the upwelling peak. The high Chl *a* concentrations were induced by (1) growth of phytoplankton promoted by nutrient input, and (2) the northward Ekman transport of surface waters caused by easterly wind forcing at the beginning of August.

- Comparison of the upwelling areas on the SST images and post-upwelling high Chl *a* areas on MERIS images in July–August 2006 showed structural similarities. The upwelling area along the northern coast and the high Chl *a* area about two weeks later roughly coincided. Also, the filaments with high Chl *a* content coincided with the locations of cold filaments from the preceding upwelling front along the northern coast. In the case of intensive upwelling along the southern coast, the low Chl *a* regions coincided with the cold upwelled water area and filaments.
- SAR data allowed the diameter of the eddy core and the diameter of the eddy rotation field to be estimated. The SST differences of 2–3.5 °C resulted in attenuation of NRCS in a range of 10–12 dB in the region of the upwelling-related eddy.

The results from the comparison of remote-sensing and in situ data are as follows.

- The mean RMSD between MODIS SST and ship-of-opportunity FT temperature (~4 m) was 0.46 °C. MODIS SST had a warm bias of 0.24 °C compared to FT temperature. The RMSD between MODIS SST and near-surface FT temperature from the research vessel (20 cm) was between 0.57 °C and 0.77 °C (low wind speed).
- The in situ temperature data measured at 4 m depth can be used for validation of MODIS SST retrievals if the wind speed is over 5 m s⁻¹.
- The Chl *a* concentration obtained from MERIS data using the FUB Case 2 waters processor was well correlated with in situ measurements ($r^2 = 0.67$), but was underestimated on average by 25%.

REFERENCES

- Alenius, P., Myrberg, K., and Nekrasov, A. 1998. The physical oceanography of the Gulf of Finland: a review. *Boreal Environment Research* 3, 97–125.
- Alenius, P., Nekrasov, A., and Myrberg, K. 2003. Variability of the baroclinic Rossby radius in the Gulf of Finland. *Continental Shelf Research* 23(6), 563–573 DOI: 10.1016/S0278-4343(03)00004-9.
- Allen, J.S. 1980. Models of wind driven currents on the continental shelf. *Annual Review of Fluid Mechanics* 12, 389–433.
- Askari, F. 2001. Multi-sensor remote sensing of eddy-induced upwelling in the southern coastal region of Sicily. *International Journal of Remote Sensing*, 22(15), 2899–2910. DOI: 10.1080/01431160119443.
- Austin, J.A. and Lentz, S.J. 2002. The inner shelf response to wind-driven upwelling and downwelling. *Journal of Physical Oceanography* 32, 2171–2193.
- Bergström, S., Alexandersson, H., Carlsson B., Josefsson. W., Karlsson, K.G., and Westring. G. 2001. Climate and hydrology of the Baltic basin. In: *A Systems Analysis of the Baltic Sea*, F. Wulff, L. Rahm, and P. Larsson (eds.), Ecological Study 148, Springer, Berlin, Heidelberg, 75–112.
- Blumsack, S.L. and Gierasch, P.J. 1972. Mars: the effects of topography on baroclinic instability. *Journal of the Atmospheric Sciences* 29, 1081–1089.
- Bradtke, K., Herman, A., and Urbanski, J.A. 2010. Spatial and interannual variations of seasonal sea surface temperature patterns in the Baltic Sea. *Oceanologia* 52(3), 345–362. <http://dx.doi.org/10.5697/oc.52-3.345>.
- Brown, O.B. and Minnett, P.J. 1999. MODIS infrared sea surface temperature algorithm theoretical basis document, ver. 2.0. Available at http://modis.gsfc.nasa.gov/data/atbd/atbd_mod25.pdf. 02.01.2013
- Clemente-Colon, P. and Yan, X.H. 1999. Observations of East Coast upwelling conditions in Synthetic Aperture Radar imagery. *IEEE Transactions on Geoscience and Remote Sensing* 37(5), 2239–2248. DOI: 10.1109/36.789620.
- Clemente-Colon, P. and Yan, X.H. 2000. Low-backscatter ocean features in synthetic aperture radar imagery. *Johns Hopkins APL Technical Digest* 21(1), 116–121.
- Clemente-Colon, P. 2001. Evolution of upwelling-associated biological features in the Middle Atlantic sight as captured by SAR, SST, and ocean color sensors. *IEEE International Symposium on Geoscience and Remote Sensing (IGARSS)*, Proceedings 1–7, 2616–2618.
- Closa, J., Rosich, B. and Monti-Guarnieri, A. 2003. The ASAR wide swath mode products. *IEEE International Symposium on Geoscience and Remote Sensing (IGARSS)*, Proceedings, 1118–1120.

- Corlett, G.K., Barton, I.J., Donlon, C.J., Edwards, M.C., Good, S.A., Horrocks, L.A., Llewellyn-Jones, D.T., Merchant, C.J., Minnett, P.J., Nightingale, T.J., Noyes, E.J., O'Carroll, A.G., Remedios, J.J., Robinson, I.S., Saunders, R.W., Watts, J.G. 2006. The accuracy of SST retrievals from AATSR: An initial assessment through geophysical validation against in situ radiometers, buoys and other SST data sets. *Natural Hazards and Oceanographic Processes from Satellite Data*, Book Series: Advances in Space Research 37(4), 764–769 DOI:10.1016/j.asr.2005.09.037.
- Csanady, G.T., 1982. *Circulation in the Coastal Ocean*, D. Reidel Publ. Co., Dordrecht, 279.
- Darecki, M. and Stramski, D. 2004. An evaluation of MODIS and SeaWiFS bio-optical algorithms in the Baltic Sea. *Remote Sensing of Environment* 89(3), 326–350. DOI: 10.1016/j.rse.2003.10.012.
- de Szoeke R.A. 1975. Some effects of bottom topography on baroclinic instability. *Journal of Marine Research* 33, 93–122.
- Doerffer, R., Sorensen K. and Aiken, J. 1999. MERIS potential for coastal zone applications, *International Journal of Remote Sensing* 20 (9), 1809–1818. <http://dx.doi.org/10.1080/014311699212498>.
- Doerffer, R. and Schiller, H. 2007. The MERIS case 2 water algorithm. *International Journal of Remote Sensing* 28(3–4), 517–535, <http://dx.doi.org/10.1080/01431160600821127>.
- Doerffer, R. and Schiller H. 2008. MERIS regional Coastal and Lake Case-2 Water Project – Atmospheric Correction ATBD, GKSS Research Centre 21502, Geerthacht Version 1.018. May 2008.
- Donlon, C.J., Minnett, P.J., Gentemann, C., Nightingale, T.J., Barton, I.J., Ward, B. and Murray, M.J. 2002. Toward improved validation of satellite sea surface skin temperature measurements for climate research. *Journal of Climate* 15(4), 353–369. DOI: 10.1175/1520-442(2002)015<0353:TIVOSS>2.0.CO;2.
- Eilola, K. and Stigebrandt, A. 1998. Spreading of juvenile freshwater in the Baltic proper. *Journal of Geophysical Research – Oceans*, 103(C12), 27795–27807 DOI:10.1029/98JC02369.
- Elken, J., Raudsepp, U. and Lips, U. 2003. On the estuarine transport reversal in deep layers of the Gulf of Finland. *Journal of Sea Research* 49, 267–274.
- Friehe, C.A., Shaw, W.J., Rogers, D.P., Davidson, K.L., Large, W.G., Stage, S.A., Crescenti, G.H., Khalsa, S.J.S., Greenhut, G.K., and Li, F. 1991. Air-sea fluxes and surface-layer turbulence around a sea surface temperature front. *Journal of Geophysical Research – Oceans* 96(C5), 8593–8609. DOI:10.1029/90JC02062.
- Gade, M., Seppke, B., and Dreschler-Fischer, L. 2012. Mesoscale surface current fields in the Baltic Sea derived from multi-sensor satellite data. *International Journal of Remote Sensing* 33(10), 3122–3146. DOI: 10.1080/01431161.2011.628711.

- Gidhagen, L. 1987. Coastal upwelling in the Baltic – satellite and in situ measurements of sea surface temperatures indicating coastal upwelling, *Estuarine, Coastal and Shelf Science* 24(4), 449–462. [http://dx.doi.org/10.1016/0272-7714\(87\)90127-2](http://dx.doi.org/10.1016/0272-7714(87)90127-2).
- Gitelson, A.A., Gurlin, D., Moses, W.J., and Barrow, T. 2009. A bio-optical algorithm for the remote estimation of the chlorophyll-a concentration in case 2 waters. *Environmental Research Letters* 4(4), article no. 045003. DOI:10.1088/1748-9326/4/4/045003.
- Gower, J., King, S., Borstad, G., and Brown, L. 2005. Detection of intense plankton blooms using the 709 nm band of the MERIS imaging spectrometer. *International Journal of Remote Sensing* 26(9), 2005–2012. DOI:10.1080/01431160500075857.
- Gower, J., King, S., Borstad, G., and Brown, L. 2008. The importance of a band at 709 nm for interpreting water-leaving spectral radiance. *Canadian Journal of Remote Sensing* 34(3), 287–295.
- Haapala, J. 1994. Upwelling and its influence on nutrient concentration in the coastal area of the Hanko Peninsula, entrance of the Gulf of Finland. *Estuarine, Coastal and Shelf Science* 38, 507–521.
- Haines, S.L., Jedlovec, G.J., and Lazarus, S.M. 2007. MODIS sea surface temperature composites for regional applications. *IEEE Transactions on Geoscience and Remote Sensing* 45(9), 2919–2927. DOI:10.1109/FGRS.2007.898274.
- HELCOM. 1988. Guidelines for the Baltic Monitoring Programme for the third stage. *Baltic Sea Environment Proceedings* no. 27D.
- HELCOM. 2009. Eutrophication in the Baltic Sea – An integrated thematic assessment of the effects of nutrient enrichment and eutrophication in the Baltic Sea region. *Baltic Sea Environment Proceedings* no. 115B.
- Horstmann, U. 1983. Distribution patterns of temperature and water colour in the Baltic Sea as recorded in satellite images: Indicators for phytoplankton growth, *Ber. Inst. Meeresk., Kiel*, 106, 147.
- Kahru, M., Leppänen, J. M., and Rud, O. 1993. Cyanobacterial blooms cause heating of sea surface. *Marine Ecology Progress Series* 101, 1–7.
- Kahru, M., Håkansson, B., and Rud, O. 1995. Distributions of the sea-surface temperature fronts in the Baltic Sea as derived from satellite imagery. *Continental Shelf Research* 15, 663–679.
- Kaitala, S., Seppala, J., Raateoja, M., Hallfors, S., Flerning-Lehtinen, V., Maunula, P., Helminen, J., Ylostalo, P. 2008. Recent advances in ferrybox monitoring on board FINNMAID ferry. *IEEE/OES US/EU-Baltic International Symposium*, 116–120.
- Kanoshina, I., Lips, U., and Leppänen, J.M. 2003. The influence of weather conditions (temperature and wind) on cyanobacterial bloom development in the Gulf of Finland (Baltic Sea). *Harmful Algae* 2(1), 29–41. [http://dx.doi.org/10.1016/S1568-9883\(02\)00085-9](http://dx.doi.org/10.1016/S1568-9883(02)00085-9).

- Karagali, I., Hoyer, J., and Hasager, C. 2012. SST diurnal variability in the North Sea and the Baltic Sea. *Remote Sensing of Environment* 121, 159–170. DOI:10.1016/j.rse.2012.01.016.
- Kawai, Y. and Wada, A. 2007. Diurnal sea surface temperature variation and its impact on the atmosphere and ocean: A review. *Journal of Oceanography* 63(5), 721–744. DOI: 10.1007/s10872-007-0063-0.
- Keevallik, S. 2003. Possibilities of reconstruction of the wind regime over Tallinn Bay. *Proceedings of the Estonian Academy of Sciences. Engineering* 9(3), 209–219.
- Keevallik S. and Soomere T. 2009. Seasonal and diurnal variations of wind parameters at Pakri. *Estonian Journal of Engineering* 15(3), 227–239.
- Keevallik, S. and Soomere, T. 2010. Towards quantifying variations in wind parameters across the Gulf of Finland. *Estonian Journal of Earth Sciences* 59(4), 288–297.
- Kikas, V., Norit, N., Meerits, A., Kuvaldina, N., Lips, I., and Lips, U. 2010. High-resolution monitoring of environmental state variables in the surface layer of the Gulf of Finland (during a dynamic spring bloom in March–May 2010). *Baltic International Symposium (BALTIC), 2010 IEEE/OES US/EU*. DOI: 10.1109/BALTIC.2010.5621627.
- Koponen, S., Attila, J., Pulliainen, J., Kallio, K., Pyhälähti, T., Lindfors, A., Rasmus, K., and Hallikainen, M. 2007. A case study of airborne and satellite remote sensing of a spring bloom event in the Gulf of Finland. *Continental Shelf Research* 27(2), 228–244. <http://dx.doi.org/10.1016/j.csr.2006.10.006>.
- Kozlov, I.E., Kudryavtsev, V.N., Johannessen, J.A., Chapron, B., Dailidienė, I., and Myasoedov, A.G. 2012. ASAR imaging for coastal upwelling in the Baltic Sea. *Advances in Space Research* 50(8), 1125–1137. DOI: 10.1016/j.asr.2011.08.017.
- Kratzer, S., Brockmann, C. and Moore, G. 2008. Using MERIS full resolution data to monitor coastal waters – A case study from Himmerfjärden, a fjord-like bay in the northwestern Baltic Sea. *Remote Sensing of Environment* 112(5), 2284–2300. <http://dx.doi.org/10.1016/j.rse.2007.10.006>.
- Kreżel, A., Ostrowski, M., and Szymelfenig, M. 2005a. Sea surface temperature distribution during upwelling along the Polish Baltic coast. *Oceanologia* 47(4), 415–432.
- Kreżel, A., Szymanek, L., Kozłowski, L., and Szymelfenig, M. 2005b. Influence of coastal upwelling on chlorophyll a concentration in the surface water along the Polish coast of the Baltic Sea. *Oceanologia* 47(4), 433–452.
- Kudryavtsev, V., Myasoedov, A., Chapron, B., Johannessen, J.A., Collard, F. 2012. Imaging mesoscale upper ocean dynamics using synthetic aperture radar and optical data. *Journal of Geophysical Research – Oceans* 117, C04029. DOI:10.1029/2011JC007492.
- Kutser, T. 2004. Quantitative detection of chlorophyll in cyanobacterial blooms by satellite remote sensing. *Limnology and Oceanography* 49(6), 2179–2189.

- Kutser, T., Metsamaa, L., Strombeck, N., and Vahtmae, E. 2006. Monitoring cyanobacterial blooms by satellite remote sensing. *Estuarine Coastal and Shelf Science* 67(1/2), 303–312. DOI: 10.1016/j.ecss.2005.11.024.
- Kutser, T., Metsamaa, L., and Dekker, A.G. 2008. Influence of the vertical distribution of cyanobacteria in the water column on the remote sensing signal. *Estuarine Coastal and Shelf Science* 78(4), 649–654. DOI:10.1016/j.ecss.2008.02.024.
- Kutser, T. 2009. Passive optical remote sensing of cyanobacteria and other intense phytoplankton blooms in coastal and inland waters. *International Journal of Remote Sensing* 30(17), 4401–4425. DOI:10.1080/01431160802562305.
- Kuvaldina, N., Lips I., Lips U., and Liblik T. 2010. The influence of a coastal upwelling event on chlorophyll a and nutrient dynamics in the surface layer of the Gulf of Finland, Baltic Sea. *Hydrobiologia* 639(1), 221–230, <http://dx.doi.org/10.1007/s10750-009-0022-4>.
- Laanemets, J., Pavelson, J., Lips, U. and Kononen, K. 2005. Downwelling related mesoscale motions at the entrance to the Gulf of Finland: observations and diagnosis. *Oceanological and Hydrobiological Studies* 34(2), 15–36.
- Laanemets, J., Zhurbas, V., Elken, J., and Vahtera E. 2009. Dependence of upwelling-mediated nutrient transport on wind forcing, bottom topography and stratification in the Gulf of Finland: model experiments. *Boreal Environmental Research* 14(1), 213–225.
- Laanemets, J., Väli, G., Zhurbas, V., Elken, J., Lips, I., and Lips, U. 2011. Simulation of mesoscale structures and nutrient transport during summer upwelling events in the Gulf of Finland in 2006. *Boreal Environmental Research* 16(suppl. A), 15–26.
- Lass, H.U., Mohrholz, V., Nausch, G., and Siegel, H. 2010. On phosphate pumping into the surface layer of the eastern Gotland Basin by upwelling. *Journal of Marine Systems* 80(1/2), 71–89. <http://dx.doi.org/10.1016/j.jmarsys.2009.10.002>.
- Lehmann, A., Krauss, W., and Hinrichsen, H.H. 2002. Effects of remote and local atmospheric forcing on circulation and upwelling in the Baltic Sea. *Tellus Series A – Dynamic Meteorology and Oceanography* 54(3), 299–316. DOI:10.1034/j.1600-0870.2002.00289.x.
- Lehmann, A. and Myrberg, K. 2008. Upwelling in the Baltic Sea – A review, *Journal of Marine Systems* 74 (Suppl.), S3–S12, <http://dx.doi.org/10.1016/j.jmarsys.2008.02.010>.
- Lehmann, A., Getzlaff, K., and Harlaß, J. 2011. Detailed assessment of climate variability in the Baltic Sea area for the period 1958 to 2009. *Climate Research* 46, 185–196. DOI:10.3354/cr00876.
- Lehmann, A., Myrberg, K., and Höfllich, K. 2012. A statistical approach to coastal upwelling in the Baltic Sea based on the analysis of satellite data for 1990–2009. *Oceanologia* 54(3), 369–393. DOI:10.5697/oc.54-3.369.

- Leppänen, J.M., Rantajarvi, E., Maunumaa, M., Larinmaa, M., and Pajala, J. 1994. Unattended algal monitoring system – a high resolution method for detection of phytoplankton blooms in the Baltic Sea. OCEANS '94. Oceans Engineering for Today's Technology and Tomorrow's Preservation. Proceedings 1, 461–463. DOI:10.1109/OCEANS.1994.363971.
- Li, X.M., Li, X.F., and He, M.X. 2009. Coastal upwelling observed by multi-satellite sensors. Science in China Series D-Earth Sciences 52(7), 1030–1038. DOI:10.1007/s11430-009-0088-x.
- Liblik, T. and Lips, U. 2011. Characteristics and variability of the vertical thermohaline structure in the Gulf of Finland in summer. Boreal Environmental Research 16(suppl. A), 73–83.
- Lin, I., Wen, L.S., Liu, K.K., Tsai, W.T., and Liu, A.K. 2002. Evidence and quantification of the correlation between radar backscatter and ocean colour supported by simultaneously acquired in situ sea truth. Geophysical Research Letters 29(10), article no. 1464. DOI:10.1029/2001GL014039.
- Lips, U., Lips, I., Kikas, V. and Kuvaldina, N. 2008. Ferrybox measurements: a tool to study meso-scale processes in the Gulf of Finland (Baltic Sea). US/EU-Baltic International Symposium, IEEE/OES, DOI: 10.1109/BALTIC.2008.4625536.
- Lips, U., Lips, I., Kikas, V., and Kuvaldina, N. 2008. Ferrybox measurements: a tool to study meso-scale processes in the Gulf of Finland (Baltic Sea). US/EU-Baltic International Symposium, IEEE/OES. DOI: 10.1109/BALTIC.2008.4625536.
- Lips I. and Lips, U. 2008. Abiotic factors influencing cyanobacterial bloom development in the Gulf of Finland (Baltic Sea). Hydrobiologia 614(1), 133–140. <http://dx.doi.org/10.1007/s10750-008-9449-2>.
- Lips, I., Lips, U., and Liblik, T. 2009. Consequences of coastal upwelling events on physical and chemical patterns in the central Gulf of Finland (Baltic Sea), Continental Shelf Research 29(15), 1836–1847. <http://dx.doi.org/10.1016/j.csr.2009.06.010>.
- Lips, I. and Lips, U. 2010. Phytoplankton dynamics affected by the coastal upwelling events in the Gulf of Finland in July–August 2006, Journal of Plankton Research 32(9), 1269–1282. <http://dx.doi.org/10.1093/plankt/fbq049>.
- Llewellyn-Jones, D., Edwards, M.C., Mutlow, C.T., Birks, A.R., Barton, I.J., and Tait, H. 2001. AATSR: Global-change and surface-temperature measurements from Envisat. ESA Bulletin – European Space Agency 105, 11–21.
- Mathur, A., Subrahmanyam, M.V., Gohil, B.S., Reddy, K.G., and Agarwal, V.K. 2005. In situ validation of sea surface temperature derived from satellite microwave and infrared sensors: a case study of TRMM/TMI and TERRA/MODIS. Proceedings of the XXVIII URSI General Assembly in New Delhi 1–4.

- Metsamaa, L., Kutser, T., and Strombeck, N. 2006. Recognising cyanobacterial blooms based on their optical signature: a modelling study. *Boreal Environmental Research* 11(6), 493–506.
- Mietus, M. 1998. The climate of the Baltic Sea basin. Marine meteorology and related oceanographic activities. Report 41, WMO/TD 933, Geneva.
- Männik A. and Merilain M., 2007, Verification of different precipitation forecasts during extended winter-season in Estonia, *HIRLAM Newsletter*, 52, 65–70.
- Myrberg, K. and Andrejev, O. 2003. Main upwelling regions in the Baltic Sea – a statistical analysis based on three dimensional modelling. *Boreal Environmental Research* 8, 97–112.
- Myrberg, K., Lehmann, A., Raudsepp, U., Szymelfenig, M., Lips, I., Lips, U., Matciak, M., Kowalewski, M., Krężel, A., Burska, D., Szymanek, L., Ameryk, A., Bielecka, L., Bradtke, K., Gałkowska, A., Gromisz, S., Jędrasik, J., Kaluźny, M., Kozłowski, L., Krajewska-Sołtys, A., Ołdakowski, B., Ostrowski, M., Zalewski, M., Andrejev, O., Suomi, I., Zhurbas, V., Kauppinen, O.-K., Soosaar, E., Laanemets, J., Uiboupin, R., Talpsepp, L., Golenko, M., Golenko, N. and Vahtera, E. 2008. Upwelling events, coastal offshore exchange, links to biogeochemical processes. Highlights from the Baltic Sea Science Congress at Rostock University, *Oceanologia* 50(1), 95–113.
- Noyes, E.J., Minnett, P.J., Remedios, J.J., Corlett, G.K., Good, S.A. and Llewellyn-Jones, D.T. 2006. The accuracy of the AATSR sea surface temperatures in the Caribbean. *Remote Sensing of Environment* 101(1), 38–51. DOI:10.1016/j.rse.2005.11.011.
- O'Reilly, J.E., Maritorena, S., Mitchell, B.G., Siegel, D.A., Carder, K.L., Garver, S.A., Kahru, M., and McClain, C. 1998. *Journal of Geophysical Research* 103(C11), 24937–24953. DOI:10.1029/98JC02160.
- Palmén, E. 1930. Untersuchungen über die Strömungen in den Finland umgebenden Meeren. *Soc. Sci. Fenn., Comm. Phys. – Math.* 5, 1–94.
- Pavelson, J., Kononen, K., and Laanemets, J. 1999. Chlorophyll distribution patchiness caused by hydrodynamical processes: a case study in the Baltic Sea. *ICES Journal of Marine Science* 56(suppl.), 87–99. <http://dx.doi.org/10.1006/jmsc.1999.0610>.
- Petersen, W., Wehde, H., Krasernann, H., Colijn, F., and Schroeder F. 2008. FerryBox and MERIS – Assessment of coastal and shelf sea ecosystems by combining in situ and remotely sensed data. *Estuarine Coastal and Shelf Science* 77(2), 296–307. <http://dx.doi.org/10.1016/j.ecss.2007.09.023>.
- Rantajärvi, E., Olsonen, R., Hallfors, S., Leppanen, J.M., and Raateoja, M. 1998. Effect of sampling frequency on detection of natural variability in phytoplankton: unattended high-frequency measurements on board ferries in the Baltic Sea. *ICES Journal of Marine Science* 55(4), 697–704. <http://dx.doi.org/10.1006/jmsc.1998.0384>.

- Reinart, A. and Kutser, T. 2006. Comparison of different satellite sensors in detecting cyanobacterial bloom events in the Baltic Sea. *Remote Sensing of Environment* 102(1/2), 74–85. DOI:10.1016/j.rse.2006.02.013.
- Reinart, A., and Reinhold, M. 2008. Mapping surface temperature in large lakes with MODIS data. *Remote Sensing of Environment* 112(2), 603–611 DOI: 10.1016/j.rse.2007.05.015.
- Reynolds, R.W., Gentemann, C.L., and Corlett, G.K. 2010. Evaluation of AATSR and TMI Satellite SST Data. *Journal of Climate* 23(1), 152–165. DOI:10.1175/2009JCLI3252.1.
- Rosich, B., Zink, M., Torres, R., Closa, J., and Buck, C. 2003. ASAR instrument performance and product quality status. *IGARSS 2003: IEEE International Geoscience and remote Sensing Symposium, Proceedings* 1109–1111.
- Ryan, J.P., Fischer, A.M., Kudela, R.M., McManus, M.A., Myers, J.S., Paduan, J.D., Ruhsam, C.M., Woodson, C.B., and Zhang, Y. 2010. Recurrent frontal slicks of a coastal ocean upwelling shadow. *Journal of Geophysical Research – Oceans* 115, C12070. DOI:10.1029/2010JC006398.
- Schroeder, T., Behnert, I., Schaale, M., Fischer, J., and Doerffer, R. 2007a. Atmospheric correction algorithm for MERIS above Case-2 waters. *International Journal of Remote Sensing* 28(7), 1469–1486. <http://dx.doi.org/10.1080/01431160600962574>.
- Schroeder, T., Schaale, M., and Fischer, J. 2007b. Retrieval of atmospheric and oceanic properties from MERIS measurements: A new Case-2 water processor for BEAM. *International Journal of Remote Sensing* 28(24), 5627–5632. <http://dx.doi.org/10.1080/01431160701601774>.
- Seifert, T., Tauber, F., and Kayser, B. 2001. A high resolution spherical grid topography of the Baltic Sea, revised edition. In: *Baltic Sea Science Congress 2001: Past, Present and Future – A Joint Venture, Abstract Volume*, Stockholm University, 298.
- Siegel, H., Gerth, M., Rudolff, R., and Tschersich, G. 1994. Dynamic features in the western Baltic Sea investigated using NOAA-AVHRR data, *Dt. Hydrogr. Zet.*, 46, 191–209. <http://dx.doi.org/10.1007/BF02226949>.
- Siegel, H., Gerth, M., and Tschersich, G. 2006. Sea surface temperature development of the Baltic Sea in the period 1990–2004. *Oceanologia* 48(S), 119–131.
- Sipelgas, L., Arst, H., Raudsepp, U., Kõuts, T. and Lindfors, A. 2004. Optical properties of coastal waters of northwestern Estonia: in situ measurements. *Boreal Environmental Research* 9(5), 447–456.
- Soomere, T. and Keevallik, S. 2003. Directional and extreme wind properties in the Gulf of Finland, *Proceedings of the Estonian Academy of Science. Engineering* 9, 73–90.
- Sorensen, K., Aas, E., and Hokedal, J. 2007. Validation of MERIS water products and bio-optical relationships in the Skagerrak. *International Journal of Remote Sensing* 28(3/4), 555–568. <http://dx.doi.org/10.1080/01431160600815566>.

- Svejkovsky, J. and Shandley, J. 2001. Detection of offshore plankton blooms with AVHRR and SAR imagery. *International Journal of Remote Sensing* 22(2/3), 471–485. DOI:10.1080/014311601450040.
- Vahtera, E., Laanemets, J., Pavelson, J., Huttunen, M. and Kononen K. 2005. Effect of upwelling on the pelagic environment and bloom-forming cyanobacteria in the western Gulf of Finland, Baltic Sea. *Journal of Marine Systems* 58(1/2), 67–82. <http://dx.doi.org/10.1016/j.jmarsys.2005.07.001>.
- Zhurbas, V.M., Stipa, T., Mälkki, P., Paka, V.T., Kuzmina, N.P., and Sklyarov, V.E. 2004. Mesoscale variability of upwelling in the southeast Baltic: infrared images and numerical modeling. *Oceanology* 44, 495–504.
- Zhurbas, V.M., Oh, I.S., and Park T. 2006. Formation and decay of a longshore baroclinic jet associated with transient coastal upwelling and downwelling: a numerical study with application to the Baltic Sea. *Journal of Geophysical Research* 111(C4), C04014. DOI:0.1029/2005JC003079.
- Zhurbas, V.M., Laanemets, J., and Vahtera, E. 2008. Modeling of the mesoscale structure of coupled upwelling/downwelling events and the related input of nutrients to the upper mixed layer in the Gulf of Finland, Baltic Sea. *Journal of Geophysical Research* 113(C5), C05004. <http://dx.doi.org/10.1029/2007JC004280>.

PUBLICATIONS

Paper I

Uiboupin, R., Laanemets, J., Sipelgas, L., Raag, L., Lips, I., Buhhalko, N. 2012. Monitoring the effect of upwelling on the chlorophyll a distribution in the Gulf of Finland (Baltic Sea) using remote sensing and in situ data. *Oceanologia*, 54(3), 395 - 419.

**Monitoring the effect
of upwelling on the
chlorophyll *a* distribution
in the Gulf of Finland
(Baltic Sea) using remote
sensing and in situ data***

doi:10.5697/oc.54-3.395
OCEANOLOGIA, 54 (3), 2012.
pp. 395–419.

© Copyright by
Polish Academy of Sciences,
Institute of Oceanology,
2012.

KEYWORDS
MERIS
MODIS
Upwelling
Chlorophyll *a*
SST
Baltic Sea
Gulf of Finland

RIVO UIBOUPIN*
JAAN LAANEMETS
LIIS SIPELGAS
LAURA RAAG
INGA LIPS
NATALIA BUHHALKO

Marine Systems Institute,
Tallinn University of Technology,
Akadeemia 15a, Tallinn 12618, Estonia;

e-mail: rivo.uiboupin@msi.ttu.ee

*corresponding author

Received 12 March 2012, revised 17 April 2012, accepted 8 May 2012.

Abstract

The spatio-temporal variability of chlorophyll *a* (Chl *a*) caused by a sequence of upwelling events in the Gulf of Finland in July–August 2006 was studied using remote sensing data and field measurements. Spatial distributions of sea surface temperature (SST) and Chl *a* concentration were examined using MODIS and MERIS data respectively. The MERIS data were processed with an algorithm

* The study was supported by the Estonian Science Foundation (grants No. 7467, No. 6752, No. 7633, No. 7581 & No. 8968). The remote sensing data were provided by ESA via Cat-1 project No. 6855.

The complete text of the paper is available at <http://www.ioopan.gda.pl/oceanologia/>

developed by the Free University of Berlin (FUB) for case 2 waters. Evaluation of MERIS Chl *a* versus in situ Chl *a* showed good correlation ($r^2 = 0.67$), but the concentration was underestimated. The linear regression for a 2 h window was applied to calibrate MERIS Chl *a*. The spatio-temporal variability exhibited the clear influence of upwelling events and related filaments on Chl *a* distribution in the western and central Gulf. The lowest Chl *a* concentrations were recorded in the upwelled water, especially at the upwelling centres, and the highest concentrations (13 mg m^{-3}) were observed about two weeks after the upwelling peak along the northern coast. The areas along the northern coast of upwelled water (4879 km^2) on the SST map, and increased Chl *a* (5526 km^2) two weeks later, were roughly coincident. The effect of upwelling events was weak in the eastern part of the Gulf, where Chl *a* concentration was relatively consistent throughout this period.

1. Introduction

Remote sensing data have been widely used for monitoring the ecological and physical state of the Baltic Sea. Satellite imagery has been used for detecting interannual, seasonal and mesoscale variability of the sea surface temperature (SST) (Horstmann 1983, Gidhagen et al. 1987, Siegel et al. 1994, Krężel et al. 2005a, Siegel et al. 2006, Bradtke et al. 2010). Previous studies have demonstrated that remote sensing imagery can be used for the systematic monitoring of the chlorophyll *a* (Chl *a*) distribution and variability (Krężel et al. 2005b, Koponen et al. 2007, Kratzer et al. 2008). Coastal upwelling is an important process that brings cold, nutrient-rich deep water to the surface layer, and can be monitored using different remote sensing data (Krężel et al. 2005a, Lass et al. 2010). The combined use of SST and Chl *a* imagery, complemented by in situ measurements and wind information, provides a basis for describing and analysing the spatial variability of phytoplankton blooms promoted by upwelling.

The Gulf of Finland is an area of the Baltic Sea well known for frequent upwelling events (Kahru et al. 1995, Myrberg & Andrejev 2003, Lehmann & Myrberg 2008, Myrberg et al. 2008). Satellite SST data have shown that during the strongest upwelling events along the northern and southern coasts of the Gulf of Finland, the upwelled water can cover remarkably large areas, corresponding to about 40% and 20%, respectively, of the total surface area of the Gulf (which is about $29\,500 \text{ km}^2$) (Uiboupin & Laanemets 2009). During upwelling events the surface phytoplankton community is transported offshore and replaced by species normally resident in the upper part of the thermocline (Kanoshina et al. 2003, Vahtera et al. 2005, Lips & Lips 2010). Numerical simulations by Zhurbas et al. (2008) and field measurements by Lips et al. (2009) have shown that in the narrow, elongated Gulf of Finland, upwelling along one coast is accompanied by downwelling along the opposite coast, i.e. two longshore baroclinic jets and

their related thermohaline fronts develop simultaneously. The instability of a longshore baroclinic jet leads to the increasing development of filaments and eddies, and thus coastal offshore mixing, resulting in a substantial horizontal variability of the surface layer temperature, upwelled nutrients and phytoplankton/chlorophyll.

The spatio-temporal variability of hydrographic and biological-chemical parameters can be regularly monitored from autonomous ship-of-opportunity measurements that collect temperature, salinity and chlorophyll *a* fluorescence data, as well as water samples for nutrient and phytoplankton analysis, along fixed transects in the Baltic Sea (Rantajärvi et al. 1998, Lips & Lips 2008, Petersen et al. 2008). However, for obtaining information about the phytoplankton abundance/biomass, and surface distribution over large sea areas, remote sensing imagery is invaluable. The Baltic Sea (including the Gulf of Finland) comprises optically complex case 2 waters that are dominated by coloured dissolved organic matter, and it is therefore a considerable challenge to produce accurate estimates of water quality parameters from remote sensing imagery (Schroeder et al. 2007a, Sorensen et al. 2007, Kratzer et al. 2008). This optical complexity affects satellite Chl *a* retrievals, so it is important to validate the algorithm using in situ measurements. Satellite imagery with sufficient temporal resolution is regularly available from MERIS (Medium Resolution Imaging Spectrometer) and MODIS (Moderate Resolution Imaging Spectroradiometer) for the Baltic Sea region. MERIS was designed to monitor coastal waters (Doerffer et al. 1999), and it therefore has sufficient spectral resolution in the visible range to monitor turbid waters like the Baltic Sea. In principle, MERIS operates in a range enabling the detection of pigments like phycocyanin (cyanobacteria), which have specific absorption minima near wavelength 630 nm and local maxima at wavelength 650 nm (Kutser et al. 2006).

A series of upwelling events along the northern and southern coasts of the Gulf of Finland occurred in July–August 2006. Westerly winds were dominant in July, generating moderate upwelling along the northern coast of the Gulf. Easterly winds then prevailed during the whole of August, and as a result, very intense upwelling was observed along the southern coast. The upwelling events were well documented by several studies based on in situ measurements of physical, biological and chemical parameters (Suursaar & Aps 2007, Lips et al. 2009, Lips & Lips 2010). In addition, remote sensing data (MERIS and MODIS) are available from that period to monitor the variability of SST and phytoplankton chlorophyll *a* fields.

The objectives of this study were: (1) to validate the MERIS chlorophyll product retrieved with the Free University of Berlin (FUB) case 2 waters processor using in situ measurements of Chl *a*, and (2) to assess the spatial

and temporal variability of the Chl *a* field caused by consecutive upwelling events using MERIS data.

This paper is structured as follows: section 2 describes the in situ, remote sensing and wind data, as well as the methodology; in section 3, the comparability of in situ and satellite chlorophyll *a* data is evaluated, the sequence of upwelling events is described on the basis of MODIS SST, MERIS chlorophyll is compared with in situ chlorophyll *a*, and the upwelling-related variability of the chlorophyll *a* field from MERIS data is described; section 4 discusses the results of the SST and chlorophyll *a* surface distributions; the final conclusions are drawn in section 5.

2. Data and methodology

2.1. In situ data

The in situ data were obtained during five surveys (Table 1) conducted along the same transect between Tallinn and Helsinki (Kuvaldina et al. 2010). Water samples for phytoplankton and Chl *a* analysis were collected from 14 stations, each about 5.2 km apart (Figure 1). Three (but two in the case of the shallow upper mixed layer) water samples were taken from the upper mixed layer (UML, from a depth of 1 m down to the seasonal thermocline) to form a pooled sample for each station. The depth of the UML was determined from the CTD profile, which preceded water sampling. Chl *a* content was measured spectrophotometrically (Thermo Helios γ ; photometric accuracy: ± 0.005 A at 1 A) from the pooled samples in the laboratory (HELCOM 1988). On 19–20 July, two (TH19, TH21) out of five pooled samples were cloud-free on the satellite imagery. Because of inclement weather conditions, only surface samples ($n = 8$) were collected at stations TH1–TH15.

Phytoplankton species composition and biomass were analysed for each survey from pooled samples (Lips & Lips 2010).

Table 1. In situ sampling and MERIS acquisition dates, times (UTC) and number of samples used (*N*) in July–August 2006. The figures in brackets indicate the number of samples collected within the 2 h interval from the satellite overpass. On 19–20 July, 2 pooled samples and 8 surface samples were collected

Sampling date	<i>N</i>	MERIS date	MERIS time
11 Jul.	14 (3)	11 Jul.	9.35
19–20 Jul.	10	18 Jul.	9.15
25 Jul.	14 (4)	25 Jul.	8.55
8 Aug.	12	7 Aug.	8.46
15–16 Aug.	9	16 Aug.	9.03

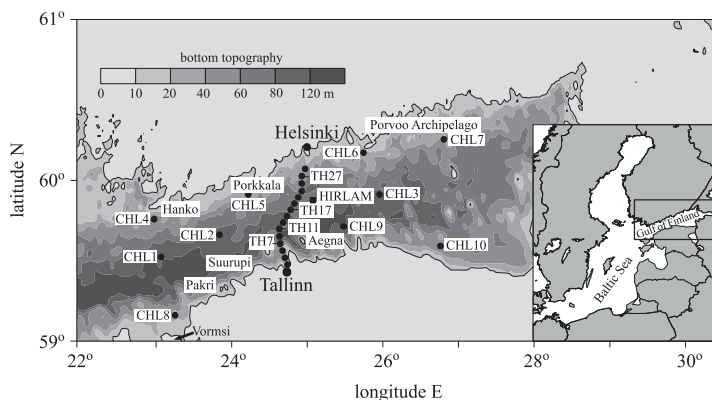


Figure 1. Map of the study area in the Gulf of Finland. The solid circles (●) represent the locations of the in situ sampling stations (TH1–TH27) and the locations of the MERIS chlorophyll time series (CHL1–CHL10, TH7 and TH27). The solid square (■) represents the location of the HIRLAM grid point where wind data were extracted. The bottom topography is drawn from the gridded topography in metres (Seifert et al. 2001)

2.2. MERIS data

MERIS reduced-resolution (about 1×1 km) images from 10 July to 18 August 2006 (altogether 31 sufficiently cloud free images) were used to analyse the spatio-temporal variability of the Chl *a* field. The MERIS images were processed using an algorithm developed by FUB for case 2 waters (Schroeder et al. 2007a, b) to apply an atmospheric correction and to obtain the reflectance values used to calculate the Chl *a* concentration. For the purposes of comparison, we also calculated Chl *a* and reflectance values using the case 2 regional water (C2RW) processor (Doerffer & Schiller 2007).

To compare the MERIS and in situ Chl *a* data, two time frames were selected at 24 h and 2 h intervals (before, or after) from the satellite overpass (Table 1). According to Kratzer et al. (2008) a 2 h window is sufficient for validating satellite Chl *a* measurements with in situ data. The MERIS image pixel covering the location of the sampling station within the given time window was extracted.

To evaluate the suitability of MERIS data for the detection of moderate concentrations of cyanobacteria, the normalized reflectance spectra were calculated according to Wu (2004).

For the detection of surface phytoplankton accumulations a Maximum Chlorophyll Index (MCI) was calculated for each MERIS image using the algorithm provided in Gower et al. (2008).

2.3. MODIS data

To determine the extent of the upwelling zone and to describe the temporal course of SST at selected locations, MODIS data (standard level 2 MODIS SST products) from 10 July to 18 August 2006 were used (<http://oceancolor.gsfc.nasa.gov>). Altogether 200 MODIS/Terra and MODIS/Aqua images (1×1 km pixel spacing) were examined in order to extract the SST data from 60 images that were sufficiently cloud-free.

2.4. Wind data

Wind-induced mixing largely determines the distribution of phytoplankton in the upper layer. To evaluate the comparability of satellite and in situ Chl *a* measurements, wind data from the version of HIRLAM (High Resolution Limited Area Model) of the Estonian Meteorological and Hydrological Institute (Männik & Merilain 2007) were interpolated to the location ($25^{\circ}7.5'E$, $59^{\circ}51.9'N$) close to the measurement transect in July–August 2006 (Figure 1). The spatial resolution of HIRLAM is 11 km, and the forecast interval of 1 h ahead of 54 h is recalculated after every 6 h. To characterize wind-induced mixing we used the depth of the turbulent Ekman boundary layer estimated by the formula $h = 0.1u_*/f$ (Csanady 1982), where $u_* = (\tau/\rho_w)^{1/2}$ is the friction velocity, $\tau = \rho_a C_a u^2$ is the wind stress, $\rho_a = 1.3 \text{ kg m}^{-3}$ is the air density, $C_a = 1.2 \times 10^{-3}$ is the dimensionless wind drag coefficient, u is the wind speed, $\rho_w = 1005 \text{ kg m}^{-3}$ is the water density, and $f = 1.25 \times 10^{-4} \text{ s}^{-1}$ is the Coriolis parameter.

3. Results

3.1. Comparability of in situ and satellite Chl *a*

Generally speaking, remote sensing imagery represents the situation at the sea surface. Variable wind conditions prevailed during July and August, whilst wind speeds were mainly moderate but with some gusts over 10 m s^{-1} (Figure 2b). In this study, the pooled sample represents the UML, and therefore we suggest that these two datasets are comparable if the depth of the turbulent Ekman boundary layer largely persists during the time interval between the acquisition of the MERIS image and the collection of the water samples. The average UML depths estimated from the CTD profiles within

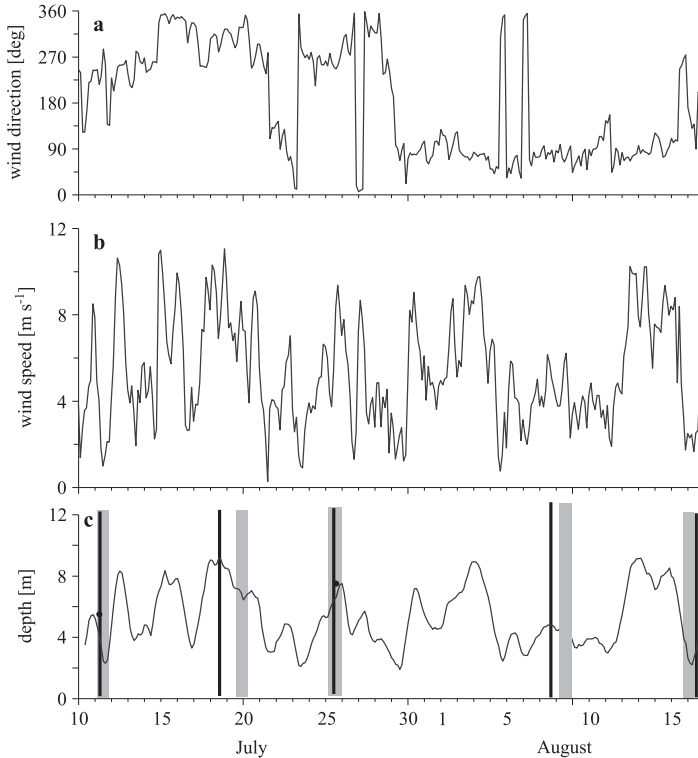


Figure 2. Wind direction (a), wind speed derived from HIRLAM data in July–August 2006 (b), depth of turbulent Ekman boundary layer (c). The grey rectangles mark the time of in situ measurements and the bold lines mark the times of MERIS image acquisition. The black dots represent the UML depths estimated from CTD measurements during the 2 h window on 11 and 25 July

the 2 h windows on 11 July (5.5 m) and 25 July (7.5 m) coincided well with the UML depths estimated from HIRLAM wind data (Figure 2c).

Comparability of in situ and MERIS Chl *a* data is also supported by the MCI calculated from all the MERIS data used. The MCI showed that no surface algal accumulations were observed during the study period. The highest MCI values were observed on 6 August 2006, when a maximum MCI value of $0.9 \text{ mW}/(\text{m}^2 \text{ sr nm})$ was recorded at the location of a filament at the entrance to the Gulf of Finland. The MCI index was close to zero most of the time.

3.2. Upwelling events in July–August

Westerly winds dominated in the Gulf area from 10 to 29 July (Figure 2a). The development of upwelling along the northern coast of the Gulf was observed from 10 July (Figures 3 and 5a), and the temperature difference between the upwelling and the surrounding water was around 5°C for most of the time, according to the MODIS SST data. However, the temperature difference was larger for the upwelling centres because of the

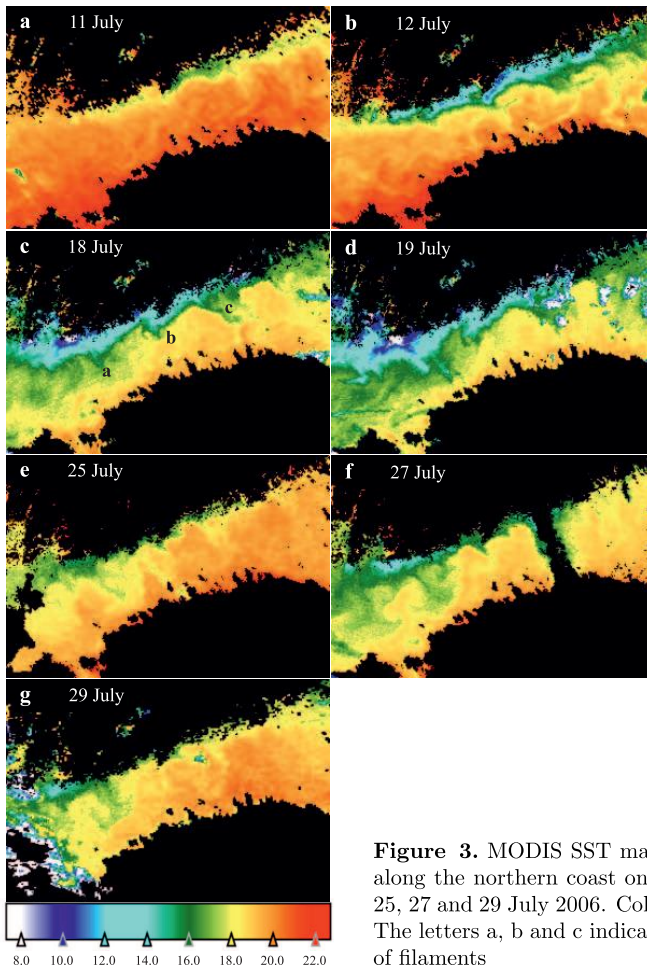


Figure 3. MODIS SST maps of upwelling along the northern coast on 11, 12, 18, 19, 25, 27 and 29 July 2006. Colour scale in °C. The letters a, b and c indicate the locations of filaments

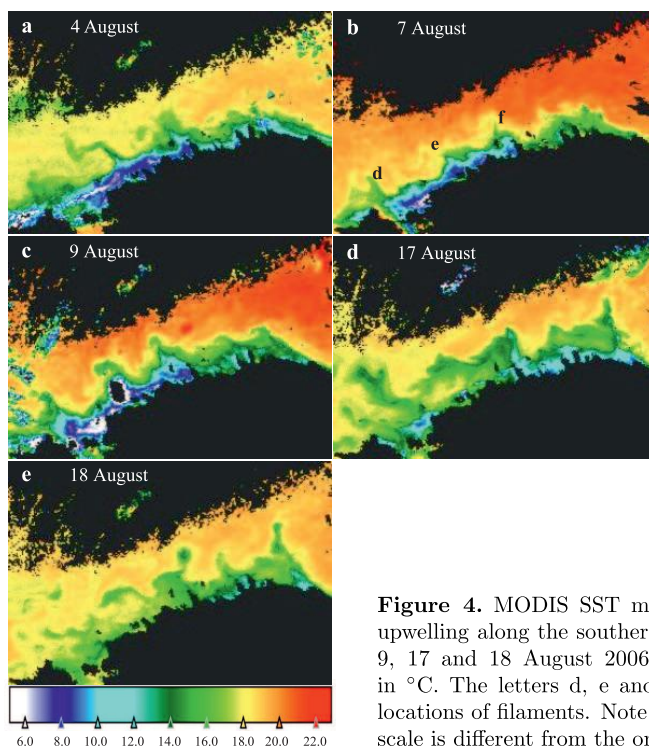


Figure 4. MODIS SST maps of stronger upwelling along the southern coast on 4, 7, 9, 17 and 18 August 2006. Colour scale in °C. The letters d, e and f indicate the locations of filaments. Note that the colour scale is different from the one in Figure 3

significantly lower temperature in the upwelled water. On 12 July the water temperature in the upwelling centre near the Porkkala Peninsula dropped to 8°C (Figure 3b). At the peak of upwelling on 19 July, the upwelling centre was near the Hanko Peninsula (due to the NW wind), and the temperature dropped to 6°C (Figures 3d and 5a), whilst in the middle of the Gulf the temperature was around 16°C, and near the southern coast it was over 18°C (Figure 3d). In the Porkkala region, where the upwelling centre was located on 12 July, the temperature rose to 13°C by 19 July. Relaxation of upwelling along the northern coast started after 20 August as a result of a change in wind forcing (Figure 2). The temperature in the upwelling zone on 25 and 27 July was then in the 14–16°C range, and the surrounding area had temperatures of around 19°C (Figures 3e and f). Because of the start of the upwelling relaxation after 20 July, cold filaments developed off the Hanko and Porkkala Peninsulas, and off the Porvoo Archipelago during the upwelling along the northern coast (Figure 3c).

After 29 July, easterly winds were dominant in the Gulf of Finland area until 16 August (Figure 2a), and as a result, a zone of upwelling formed along the southern coast (Figure 4). The strongest such zone developed along the NW coast of Estonia, from Vormsi Island to Aegna Island, with several upwelling centres near the Pakri Islands, Vormsi Island and off the coast of the Suurupi Peninsula, where the minimum temperature of the upwelled water was about 2°C (Figure 4 and 5b). The temperature difference between the upwelled and the surrounding water was as much as 18°C (Figures 4 and 5b), and the upwelled water covered 31% of the western Gulf area

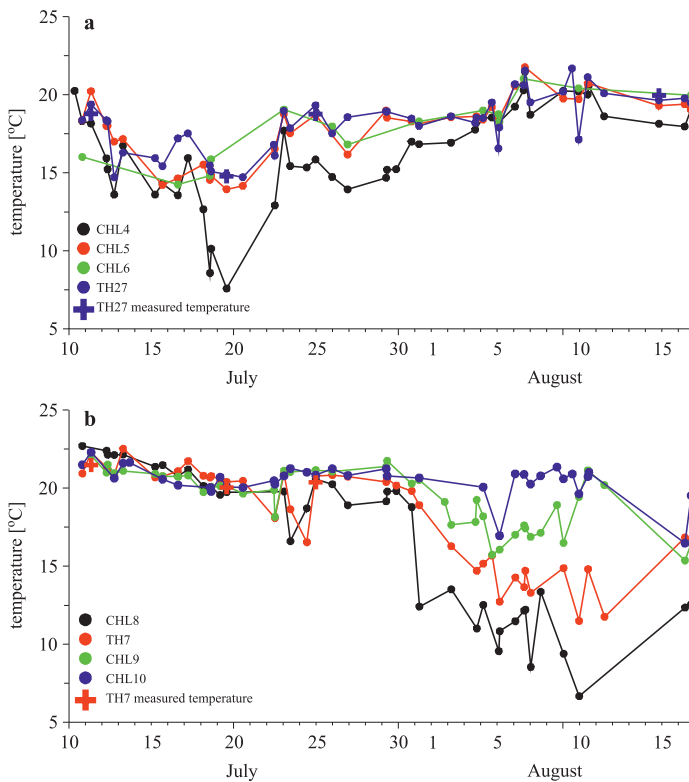


Figure 5. Temporal courses of surface layer temperature (MODIS SST) from 10 July to 16 August 2006 at stations CHL4, CHL5, CHL6 and TH27 (northern part of the Gulf) (a) and at stations CHL8, CHL9, CHL10 and TH7 (southern part of the Gulf) (b). The in situ surface temperature (bold cross) is given for stations TH7 and TH27

(22–26°E) on 9 August. After 16 August, the wind turned to the S and SW (data not shown), thus causing the upwelling to relax. Several cold upwelling filaments developed along the southern coast between longitudes 23 and 27°E, and a few of them transformed into eddies (Figure 4). The filaments were persistent at three locations: north of Hiiumaa, and off Pakri and Tallinn (Figure 4b).

3.3. Evaluation of the FUB Chl *a* processor using in situ Chl *a*

In situ Chl *a* concentrations along the transect varied in a wide range from 1.57 to 15.54 mg m⁻³ during the period of field measurements (Figure 6). Low Chl *a* values were observed during the first half of July in the upwelling region along the northern coast. From 25 July, when upwelling along the northern coast was in the relaxation phase, the Chl *a* concentrations increased off the northern coast, and decreased off the southern coast. The highest (15.5 mg m⁻³) and lowest (1.6 mg m⁻³) Chl *a* concentrations were observed on 8 August off the northern and southern coasts respectively.

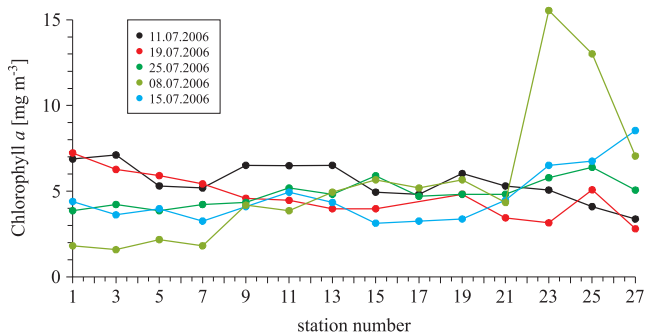


Figure 6. In situ Chl *a* distribution along the sampling transect on 11, 19 and 25 July, and 8 and 15 August 2006

The Chl *a* concentrations calculated with the FUB processor from the MERIS data was correlated with in situ Chl *a* for two time windows: 24 h and 2 h intervals (before or after) from the satellite overpass. A scatterplot of selected data pairs is shown in Figure 7. A total of 7 data pairs fulfilled the 2 h criterion: 3 samples (TH9, TH11 and TH13) from 11 July and 4 samples (TH11, TH13, TH15 and TH17) from 25 July (Table 1). For the 2 h window the FUB processor underestimated Chl *a* compared with in situ Chl *a* (Figure 7); the average underestimation was 25% (1.3 mg m⁻³),

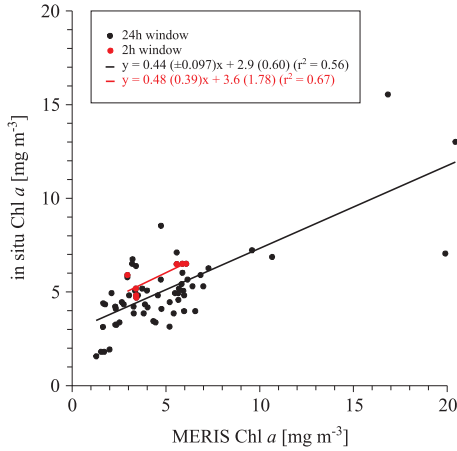


Figure 7. Scatterplot of in situ Chl *a* and MERIS Chl *a* derived by the FUB processor. Black dots represent all data pairs from 11, 18 and 25 July, and 7 and 16 August 2006 (24 h window), and red dots represent data pairs from 11 and 25 July 2006 (2 h window). The data corresponding to the 2 h window were used to estimate bias and to calibrate the FUB Chl *a* processor. The correlation (r^2) for 24 h window data points was 0.56 and for the 2 h window it was 0.67

which is of the same magnitude as in previous studies in the Baltic Sea (Kratzer et al. 2008). The correlation (r^2) for data points within the 2 h window was 0.67 and for the 24 h window was also relatively high at 0.56. The linear regression for the 2 h window with 95% confidence limits was $\text{Chl } a = 0.48(\pm 0.39) \times X + 3.6(\pm 1.8)$, where X is the FUB processor output. The standard deviation of the residuals (i.e. standard error of the estimation – SEE) was 0.51. For the 24 h window the slope and y-intercept of the linear regression were 0.44 (± 0.097) and 2.9 (± 0.60) respectively. The standard deviation of the residuals for the 24 h window was 1.43.

In addition to the FUB processor we also evaluated the case 2 regional water processor (C2RW) for Chl *a* (data not shown). The correlation for the FUB processor (0.67) was much higher compared to the C2RW processor (0.17). Also, the Chl *a* overestimation of C2RW by 52% is poorer compared with the underestimation (25%) by the FUB processor.

On the basis of the above analysis, the FUB algorithm was used to calculate Chl *a* from MERIS data in the Gulf of Finland. The equation obtained with linear regression for the 2 h window was applied to calibrate MERIS Chl *a* data.

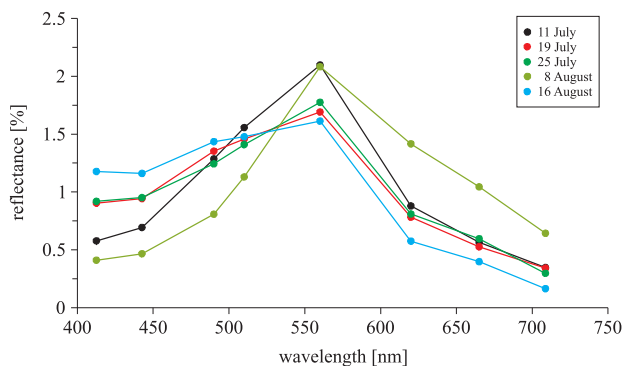


Figure 8. Normalized reflectance spectra calculated according to Wu (2004) on 11, 19 and 26 July; 8 and 16 August 2006 at location TH25

In order to assess the suitability of MERIS data (processed with the FUB algorithm) for detecting cyanobacteria, we analysed the temporal changes of reflectance spectra at the location of the largest increase in Chl *a* off the northern coast (Figure 6). We used MERIS images with the smallest time displacement from the time of the in situ measurements (Table 1). The distinct peak around wavelengths 620–650 nm, which is related to phycocyanin, was not detected on any of the normalized spectra (Figure 8).

3.4. Upwelling-related Chl *a* variability from MERIS imagery

To describe the spatio-temporal variability of the Chl *a* field, we used maps (Figures 9 and 10) and time series (Figure 11) at selected locations (Figure 1) formed from calibrated MERIS Chl *a* data. Different locations were selected to describe the temporal variability of Chl *a* along the northern and southern coasts, and along the axis of the Gulf (open sea area).

In July–August the Chl *a* concentrations were generally higher along the northern coast compared with those in the open sea area, and along the southern coast (Figure 11). In July the Chl *a* concentrations along the northern coast varied in the range of 4–9 mg m⁻³ (Figure 11a). After the relaxation of upwelling along the northern coast, Chl *a* concentrations reached high values of up to 13–14 mg m⁻³ at locations CHL5 and TH27 on 7 August. The increase in Chl *a* was also observed at other locations along the northern coast, reaching values of up to 8.5 mg m⁻³. Elevated Chl *a* along the northern coast and in the filaments was observed starting from 23 July and peaked on 6–7 August (Figures 9e, 10b and c). By 6 August, 26% of the area between longitudes 23–27°E was covered by Chl *a*

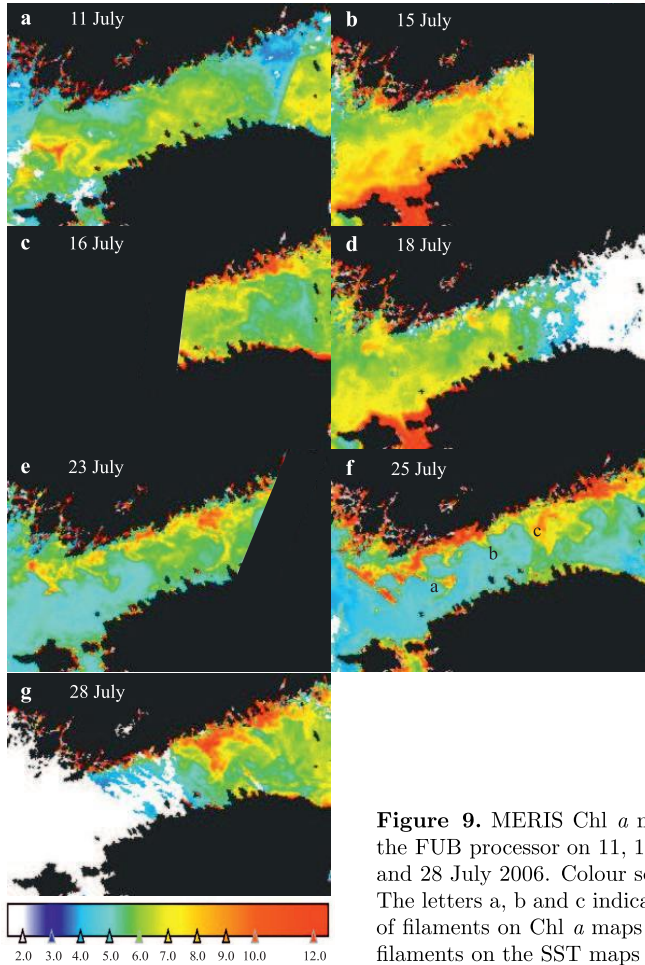


Figure 9. MERIS Chl *a* maps derived by the FUB processor on 11, 15, 16, 18, 23, 25 and 28 July 2006. Colour scale in mg m^{-3} . The letters a, b and c indicate the locations of filaments on Chl *a* maps coincident with filaments on the SST maps (see Figure 3c)

concentrations above 7 mg m^{-3} (Figure 10b and c). The development of the Chl *a* field was characterized by high spatial and temporal variability; standard deviations were 2.1 and 2.4 mg m^{-3} at locations CHL5 and TH27 respectively. Chlorophyll-rich filaments were observed off the Hanko and Porkkala Peninsulas and the Porvoo Archipelago after 23 July, when upwelling along the northern coast was in the relaxation phase. Relatively high and persistent Chl *a* concentrations were observed in the easternmost

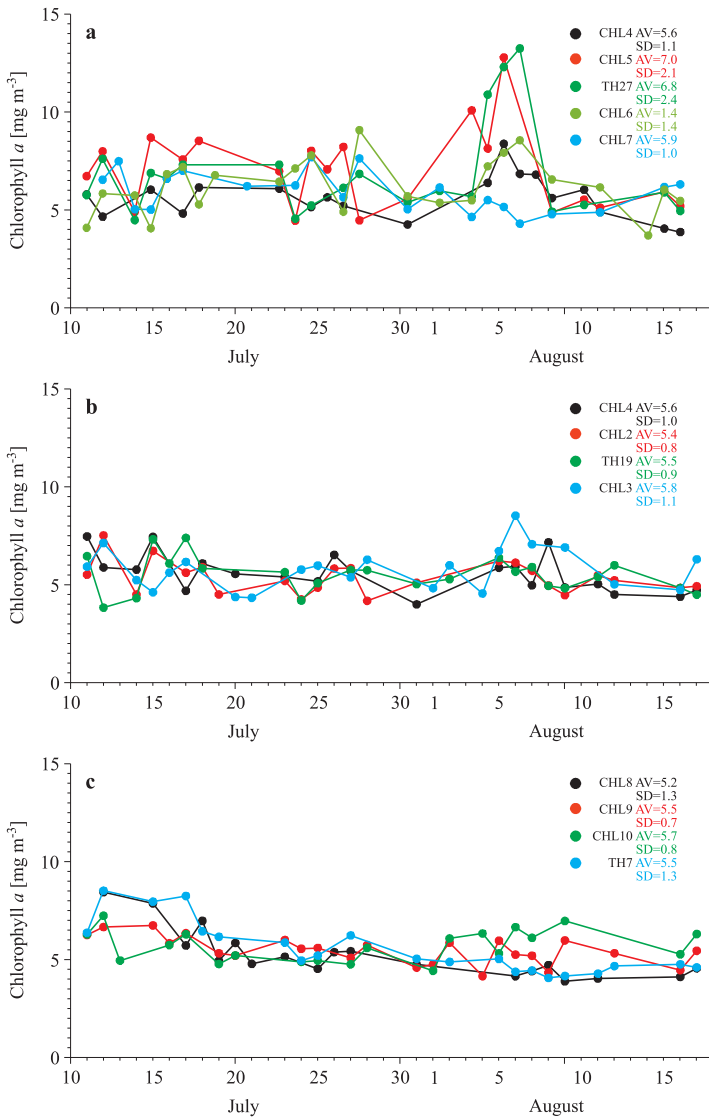


Figure 11. Distribution of MERIS Chl *a* at selected locations (see Figure 1) along the northern coast (a), along the Gulf axis (b), and along the southern coast (c) in July–August 2006

period (Figure 11c). By 16 (and 18) August, when upwelling started to relax (Figure 4e), the Chl *a* concentrations increased slightly in the upwelling region (Figure 9c, CHL8 and TH7). Again, relatively high and persistent Chl *a* concentrations were found in the easternmost part of the study area (CHL10, mean = 5.7 mg m⁻³, SD = 0.8 mg m⁻³).

During the whole study period the temporal course of Chl *a* along the Gulf axis (Figure 11b) displayed less variability, mainly between 4 and 8 mg m⁻³, compared with the northern coast. Chl *a* variations were larger between 11 and 18 July (Figures 9 and 11b), when the upwelling front and related filaments with low chlorophyll contents (Figures 3a–d) reached the open part of the Gulf. The high variability of Chl *a* at locations along the Gulf axis observed in August (Figure 11b, CHL1, CHL2 and TH19) was a result of chlorophyll-rich filaments from the northern, and chlorophyll-poor filaments from the southern, coastal sea areas (Figure 10).

4. Discussion

July–August 2006 was characterized by quite a rare wind regime in the Gulf of Finland: westerly winds prevailed until 29 July, whereas after 30 July easterly winds remained dominant for quite a long time. In the long, narrow Gulf of Finland, westerly winds cause upwelling along the northern coast, and downwelling along the southern coast, and vice versa when winds are blowing from the east. A high-resolution numerical study showed that the instability of the longshore baroclinic jet and related thermohaline fronts, caused by coupled upwelling and downwelling events, leads to the development of cold and warm mesoscale filaments and eddies contributing to coastal offshore exchange (Zhurbas et al. 2008). The maps of mean mesoscale (eddy) kinetic energy in the surface layer (simulation for July–August 2006), showed that the coastal offshore exchange caused by filaments and eddies is larger in the narrow western and the central parts of the Gulf (Laanemets et al. 2011).

Spatio-temporal variability of the Chl *a* field observed from MERIS imagery in July–August 2006 clearly reflected the influence of mesoscale physical processes, coupled upwelling/downwelling events and related filaments. Wind mixing may also decrease the surface Chl *a* concentration by mixing phytoplankton deeper into the water column. Chl *a* concentrations varied in a wide range, from 4 to 14 mg m⁻³, which is also expressed in the variations of mean concentrations (5.2–7.0 mg m⁻³) and standard deviations (SD = 1.4–2.4 mg m⁻³) (Figures 9, 10 and 11). Chl *a* concentrations were the lowest in the upwelling zones along both coasts. The highest mean Chl *a* and standard deviation were recorded along the northern coast: up to 7.0 and 2.4 mg m⁻³ respectively. In this region the upwelling and possible

upwelling-related nutrient input to the surface layer occurred earlier, during the first half of July, and therefore most likely promoted phytoplankton growth after the relaxation of the upwelling and the warming of the surface layer.

At locations along the Gulf axis in the western and central Gulf of Finland, the variability of the surface Chl *a* field (Figure 11b) was related to mesoscale activity. In July, when upwelling was taking place along the northern coast, filaments carried cold water with low chlorophyll concentrations offshore. In August, filaments carried chlorophyll-poor water from the southern upwelling zone and chlorophyll-rich water from the northern downwelling zone, into the central part of the Gulf.

In the shallower eastern part of the Gulf, the mesoscale activity estimated from SST imagery (Kahru et al. 1995, Uiboupin & Laanemets 2009) and numerical simulations (Laanemets et al. 2011) was lower. This was also reflected by the MERIS Chl *a* data, as concentrations were relatively persistent (mean 5.7–5.9 mg m⁻³) with small standard deviations (0.8–1.1 mg m⁻³).

The largest increase in Chl *a* was observed from 4 to 8 August along the northern coast (Figures 11a and 12) after the decrease of the surface Chl *a* concentration from 31 July to 4 August (Figures 11a and b), which was most likely caused by a strong wind event increasing the UML depth (Figures 2b and c) and mixing the phytoplankton deeper. There are probably two reasons for the increase of Chl *a* concentration in the narrow northern coastal zone and the cold filaments (Figure 9e) starting after the peak of upwelling

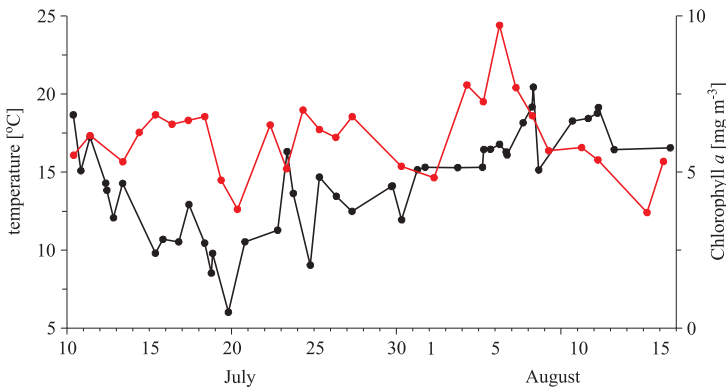


Figure 12. Temporal course of average (CHL4, CHL5 and CHL6) Chl *a* concentration (red line), and SST (black line) on the northern coast in July–August 2006

on 20 July (Figure 12). One reason could be the phytoplankton growth promoted by nutrient input during the upwelling in July along the northern coast. The numerical simulation of nutrient transport during upwelling events in summer 2006 showed that the main area along the northern coast of the Gulf, where nutrients (nitrogen and phosphorus) were brought to the surface layer, was from the Hanko Peninsula to the Porvoo Archipelago region (Laanemets et al. 2011). By 20 July most of the nitrogen and phosphorus (about 325 and 400 tonnes respectively) had been brought into the upper layer (Laanemets et al. 2009). This area coincided with the area of intensive upwelling along the northern coast depicted on the SST maps (Figures 3b and c). After the upwelling began to relax, the temperature in the northern coastal zone rose to above 15°C by 23 July (Figures 5a and 12). Previous studies have shown that phytoplankton growth is promoted in an area covered by upwelled nutrient-rich water (Vahtera et al. 2005). To confirm this assumption, we also compared the upwelled water area and the extended Chl *a* area along the northern coast. The area where the temperature was <14°C, i.e. the narrow area along the northern coast where nutrients were probably brought to the surface layer, was 1317 km² (about 7% of the study area) on 18 July. Moreover, the area along the coast of water with a temperature <17°C due to offshore transport and also covering the filaments was 4879 km² (about 25%). The upwelling-induced area with a slightly increased Chl *a* (concentrations over 7 mg m⁻³) on 25 July was 5507 km². This area remained approximately the same until 6 August (the bloom peak) – 5526 km². This suggests that the observed phytoplankton increase occurred mainly in the region of possible nutrient input by upwelling with a two week lag. Of course, some differences in the spatial distribution were due to the development of upwelling along the southern coast (Figures 4a and b).

The second possible reason responsible for the higher Chl *a* concentrations and variability along the northern coast could be the Ekman transport of phytoplankton biomass in the surface layer from the open sea area towards the northern coast during the upwelling event along the southern coast and the simultaneous downwelling along the northern coast in early August. Surface transport and a higher Chl *a* concentration in the downwelling zone were also observed in previous studies (Pavelson et al. 1999, Kanoshina et al. 2003, Lips & Lips 2010). In addition, Lips & Lips (2010) found a relationship between high phytoplankton biomass and a mesoscale anticyclonic feature in the northern part of the study area on 8 August. This corresponds to Zhurbas et al. (2006), who showed that instability of the longshore baroclinic jet, associated with downwelling, results in the formation of an anticyclonic eddy. The highest biomass values in the same area coincided

with this mesoscale feature, where domed isopycnals caused shallowing of the UML to only 5 m, against the background of a relatively deep UML in the remainder of the downwelling area on the transect. The northward surface transport of cold upwelled water and the spreading of filaments with low chlorophyll content are clearly visible on the SST and Chl *a* maps (Figures 4a, b, c and 10a, b, c, d).

The distinct feature (the peak around 630 nm) in the red part of the reflectance spectrum can be used to detect phycocyanin (cyanobacteria) (Dekker 1993, Dekker & Peters 1993, Reinart & Kutser 2006, Kutser et al. 2006). Bio-optical modelling results by Metsamaa et al. (2006) showed that MERIS bands 6 and 7 can be used to separate cyanobacteria and green algae if the concentration of Chl *a* in the cyanobacteria is 8–10 mg m⁻³. The calculated reflectance spectra showed that despite the dominance of phycocyanin-containing cyanobacteria (Chl *a* about 9 mg m⁻³) off the northern coast on 8 August (Lips & Lips 2010), the peak around 630 nm was not detected (Figure 8). Thus, our estimates based on in situ data confirmed the bio-optical modelling result. Previous field measurements have shown that Chl *a* in cyanobacteria during blooms were usually 10 mg m⁻³ in the Gulf of Finland area (Kononen et al. 1996, Vahtera et al. 2005, Suikkanen et al. 2007), i.e. cyanobacteria blooms are not detectable on MERIS imagery before the appearance of surface accumulations.

5. Conclusions

Upwelling events along the northern (southern) coast of the Gulf of Finland led to a minimum temperature of around 6°C (2°C) with a temperature difference between the upwelled and surrounding water of up to 12°C (18°C).

The Chl *a* concentration obtained from MERIS data using the FUB processor was well correlated with in situ measurements ($r^2 = 0.67$), but was underestimated on average by 25%. The Chl *a* concentration in cyanobacteria was not high enough to detect the characteristic feature of phycocyanin around wavelengths 620–650 nm in the reflectance spectra.

The spatio-temporal variability of Chl *a* estimated from MERIS data showed the evident influence of upwelling events and related filaments. The variability of Chl *a* was largest in the western and central parts of the Gulf, where mesoscale activity was the highest.

The highest Chl *a* concentrations (up to 14 mg m³) along the northern coast were observed about two weeks after the upwelling peak. The high Chl *a* was induced by (1) growth of phytoplankton promoted by nutrient input, and (2) the northward Ekman transport of surface waters caused by easterly wind forcing at the beginning of August.

Comparison of the upwelling areas on the SST images and high Chl *a* areas on MERIS images showed structural similarities. The upwelling area along the northern coast (4879 km²) and the high Chl *a* area (5526 km²) about two weeks later were roughly coincident. Also, the filaments with high Chl *a* coincided with the locations of cold filaments extending from the upwelling front along the northern coast. In the case of intensive upwelling along the southern coast, the low Chl *a* regions coincided with the cold filaments.

Upwelling events had only a minor influence in the eastern part of the study area, where Chl *a* concentrations were relatively high and persistent throughout the study period.

Acknowledgements

Our thanks go to the staff of the Marine Systems Institute who conducted the measurement campaigns.

References

- Bradtke K., Herman A., Urbański J. A., 2010, *Spatial and interannual variations of seasonal sea surface temperature patterns in the Baltic Sea*, *Oceanologia*, 52 (3), 345–362, <http://dx.doi.org/10.5697/oc.52-3.345>.
- Csanady G. T., 1982, *Circulation in the coastal ocean*, D. Reidel Publ. Co., Dordrecht, 279 pp.
- Dekker A. G., 1993, *Detection of optical water quality parameters for eutrophic waters by high resolution remote sensing*, Ph.D. thesis, Free University, Amsterdam.
- Dekker A. G., Peters S. W. M., 1993, *The use of the thematic mapper for the analysis of eutrophic lakes – a case-study in the Netherlands*, *Int. J. Remote Sens.*, 14 (5), 799–821, <http://dx.doi.org/10.1080/01431169308904379>.
- Doerffer R., Sorensen K., Aiken J., 1999, *MERIS potential for coastal zone applications*, *Int. J. Remote Sens.*, 20 (9), 1809–1818, <http://dx.doi.org/10.1080/014311699212498>.
- Doerffer R., Schiller H., 2007, *The MERIS case 2 water algorithm*, *Int. J. Remote Sens.*, 28 (3–4), 517–535, <http://dx.doi.org/10.1080/01431160600821127>.
- Gidhagen L., 1987, *Coastal upwelling in the Baltic – satellite and in situ measurements of sea surface temperatures indicating coastal upwelling*, *Estuar. Coast. Shelf Sci.*, 24 (4), 449–462, [http://dx.doi.org/10.1016/0272-7714\(87\)90127-2](http://dx.doi.org/10.1016/0272-7714(87)90127-2).
- Gower J., King S., Borstad G., Brown L., 2008, *The importance of a band at 709 nm for interpreting water-leaving spectral radiance*, *Can. J Remote Sens.*, 34 (3), 287–295.

- HELCOM, 1988, *Guidelines for the Baltic Monitoring Programme for the third stage*, Baltic Sea Environ. Proc., 27D.
- Horstmann U., 1983, *Distribution patterns of temperature and water colour in the Baltic Sea as recorded in satellite images: Indicators for phytoplankton growth*, Ber. Inst. Meeresk., Kiel, 106, 147 pp.
- Kahru M.H., Håkansson B., Rud O., 1995, *Distributions of the sea-surface temperature fronts in the Baltic Sea as derived from satellite imagery*, Cont. Shelf Res., 15 (6), 663–679, [http://dx.doi.org/10.1016/0278-4343\(94\)E0030-P](http://dx.doi.org/10.1016/0278-4343(94)E0030-P).
- Kanoshina I., Lips U., Leppänen J.-M., 2003, *The influence of weather conditions (temperature and wind) on cyanobacterial bloom development in the Gulf of Finland (Baltic Sea)*, Harmful Algae, 2 (1), 29–41, [http://dx.doi.org/10.1016/S1568-9883\(02\)00085-9](http://dx.doi.org/10.1016/S1568-9883(02)00085-9).
- Kononen K., Kuparinen J., Mäkelä K., Laanemets J., Pavelson J., Nömmann S., 1996, *Initiation of cyanobacterial blooms in a frontal region at the entrance to the Gulf of Finland, Baltic Sea*, Limnol. Oceanogr., 41 (1), 98–112.
- Koponen S., Attila J., Pulliainen J., Kallio K., Pyhälähti T., Lindfors A., Rasmus K., Hallikainen M., 2007, *A case study of airborne and satellite remote sensing of a spring bloom event in the Gulf of Finland*, Cont. Shelf Res., 27 (2), 228–244, <http://dx.doi.org/10.1016/j.csr.2006.10.006>.
- Kratzer S., Brockmann C., Moore G., 2008, *Using MERIS full resolution data to monitor coastal waters – A case study from Himmerfjärden, a fjord-like bay in the northwestern Baltic Sea*, Remote Sens. Environ., 112 (5), 2284–2300, <http://dx.doi.org/10.1016/j.rse.2007.10.006>.
- Kreżel A., Ostrowski M., Szymelfenig M., 2005a, *Sea surface temperature distribution during upwelling along the Polish Baltic coast*, Oceanologia, 47 (4), 415–432.
- Kreżel A., Szymanek L., Kozłowski L., Szymelfenig M., 2005b, *Influence of coastal upwelling on chlorophyll a concentration in the surface water along the Polish coast of the Baltic Sea*, Oceanologia, 47 (4), 433–452.
- Kutser T., Metsamaa L., Strömbeck N., Vahtmäe E., 2006, *Monitoring cyanobacterial blooms by satellite remote sensing*, Estuar. Coast. Shelf Sci., 67 (1–2), 303–312, <http://dx.doi.org/10.1016/j.ecss.2005.11.024>.
- Kuvaldina N., Lips I., Lips U., Liblik T., 2010, *The influence of a coastal upwelling event on chlorophyll a and nutrient dynamics in the surface layer of the Gulf of Finland, Baltic Sea*, Hydrobiologia, 639 (1), 221–230, <http://dx.doi.org/10.1007/s10750-009-0022-4>.
- Laanemets J., Väli G., Zhurbas V., Elken J., Lips I., Lips U., 2011, *Simulation of mesoscale structures and nutrient transport during summer upwelling events in the Gulf of Finland in 2006*, Boreal Environ. Res., 16 (suppl. A), 15–26.
- Laanemets J., Zhurbas V., Elken J., Vahtera E., 2009, *Dependence of upwelling-mediated nutrient transport on wind forcing, bottom topography and stratification in the Gulf of Finland: model experiments*, Boreal Environ. Res., 14 (1), 213–225.

- Lass H. U., Mohrholz V., Nausch G., Siegel H., 2010, *On phosphate pumping into the surface layer of the eastern Gotland Basin by upwelling*, J. Marine Syst., 80 (1–2), 71–89, <http://dx.doi.org/10.1016/j.jmarsys.2009.10.002>.
- Lehmann A., Myrberg K., 2008, *Upwelling in the Baltic Sea – A review*, J. Marine Syst., 74 (Suppl.), S3–S12, <http://dx.doi.org/10.1016/j.jmarsys.2008.02.010>.
- Lips I., Lips U., 2008, *Abiotic factors influencing cyanobacterial bloom development in the Gulf of Finland (Baltic Sea)*, Hydrobiologia, 614 (1), 133–140, <http://dx.doi.org/10.1007/s10750-008-9449-2>.
- Lips I., Lips U., 2010, *Phytoplankton dynamics affected by the coastal upwelling events in the Gulf of Finland in July–August 2006*, J. Plankton Res., 32 (9), 1269–1282, <http://dx.doi.org/10.1093/plankt/fbq049>.
- Lips I., Lips U., Liblik T., 2009, *Consequences of coastal upwelling events on physical and chemical patterns in the central Gulf of Finland (Baltic Sea)*, Cont. Shelf Res., 29 (15), 1836–1847, <http://dx.doi.org/10.1016/j.csr.2009.06.010>.
- Männik A., Merilain M., 2007, *Verification of different precipitation forecasts during extended winter-season in Estonia*, HIRLAM Newsletter, 52, 65–70.
- Metsamaa L., Kutser T., Strombeck N., 2006, *Recognising cyanobacterial blooms based on their optical signature: a modelling study*, Boreal Environ. Res., 11 (6), 493–506.
- Myrberg K., Andrejev O., 2003, *Main upwelling regions in the Baltic Sea – a statistical analysis based on three-dimensional modelling*, Boreal Environ. Res., 8 (2), 97–112.
- Myrberg K., Lehmann A., Raudsepp U., Szymelfenig M., Lips I., Lips U., Matciak M., Kowalewski M., Krężel A., Burska D., Szymanek L., Ameryk A., Bielecka L., Bradtke K., Gałkowska A., Gromisz S., Jędrasik J., Kaluźny M., Kozłowski L., Krajewska-Sołtys A., Ołdakowski B., Ostrowski M., Zalewski M., Andrejev O., Suomi I., Zhurbas V., Kauppinen O.-K., Soosaar E., Laanemets J., Uiboupin R., Talpsepp L., Golenko M., Golenko N., Vahtera E., 2008, *Upwelling events, coastal offshore exchange, links to biogeochemical processes – Highlights from the Baltic Sea Science Congress at Rostock University, Germany, 19–22 March 2007*, Oceanologia, 50 (1), 95–113.
- Pavelson J., Kononen K., Laanemets J., 1999, *Chlorophyll distribution patchiness caused by hydrodynamical processes: a case study in the Baltic Sea*, ICES J. Mar. Sci., 56 (Suppl.), 87–99, <http://dx.doi.org/10.1006/jmsc.1999.0610>.
- Petersen W., Wehde H., Krasemann H., Colijn F., Schroeder F., 2008, *FerryBox and MERIS – Assessment of coastal and shelf sea ecosystems by combining in situ and remotely sensed data*, Estuar. Coast. Shelf Sci., 77 (2), 296–307, <http://dx.doi.org/10.1016/j.ecss.2007.09.023>.
- Rantajärvi E., Olsonen R., Hallfors S., Leppanen J. M., Raateoja M., 1998, *Effect of sampling frequency on detection of natural variability in phytoplankton: unattended high-frequency measurements on board ferries in the Baltic Sea*, ICES J. Mar. Sci., 55 (4), 697–704, <http://dx.doi.org/10.1006/jmsc.1998.0384>.

- Reinart A., Kutser T., 2006, *Comparison of different satellite sensors in detecting cyanobacterial bloom events in the Baltic Sea*, Remote Sens. Environ., 102 (1–2), 74–85.
- Schroeder T., Behnert I., Schaale M., Fischer J., Doerffer R., 2007a, *Atmospheric correction algorithm for MERIS above Case-2 waters*, Int. J. Remote Sens., 28 (7), 1469–1486, <http://dx.doi.org/10.1080/01431160600962574>.
- Schroeder T., Schaale M., Fischer J., 2007b, *Retrieval of atmospheric and oceanic properties from MERIS measurements: A new Case-2 water processor for BEAM*, Int. J. Remote Sens., 28 (24), 5627–5632, <http://dx.doi.org/10.1080/01431160701601774>.
- Seifert T., Tauber F., Kayser B., 2001, *A high resolution spherical grid topography of the Baltic Sea – 2nd edition*, Baltic Sea Science Congress, Stockholm 25–29 November 2001, Poster No. 147, [<http://www.io-warnemuende.de/iowtopo>].
- Siegel H., Gerth M., Rudolf R., Tschersich G., 1994, *Dynamic features in the western Baltic Sea investigated using NOAA-AVHRR data*, Dt. Hydrogr. Zet., 46, 191–209, <http://dx.doi.org/10.1007/BF02226949>.
- Siegel H., Gerth M., Tschersich G., 2006, *Sea surface temperature development of the Baltic Sea in the period 1990–2004*, Oceanologia, 48 (S), 119–131.
- Sorensen K., Aas E., Hokedal J., 2007, *Validation of MERIS water products and bio-optical relationships in the Skagerrak*, Int. J. Remote Sens., 28 (3–4), 555–568, <http://dx.doi.org/10.1080/01431160600815566>.
- Suikkanen S., Laamanen M., Huttunen M., 2007, *Long-term changes in summer phytoplankton communities of the open northern Baltic Sea*, Estuar. Coast. Shelf Sci., 71 (3–4), 580–592, <http://dx.doi.org/10.1016/j.ecss.2006.09.\break004>.
- Suursaar Ü., Aps R., 2007, *Spatio-temporal variations in hydrophysical and chemical parameters during a major upwelling event off the southern coast of the Gulf of Finland in summer 2006*, Oceanologia, 49 (2), 209–229.
- Uiboupin R., Laanemets J., 2009, *Upwelling characteristics derived from satellite sea surface temperature data in the Gulf of Finland, Baltic Sea*, Boreal Environ. Res., 14 (2), 297–304.
- Vahtera E., Laanemets J., Pavelson J., Huttunen M., Kononen K., 2005, *Effect of upwelling on the pelagic environment and bloom-forming cyanobacteria in the western Gulf of Finland. Baltic Sea*, J. Marine Syst., 58 (1–2), 67–82, <http://dx.doi.org/10.1016/j.jmarsys.2005.07.001>.
- Wu C., 2004, *Normalized spectral mixture analysis for monitoring urban composition using ETM plus imagery*, Remote Sens. Environ., 93 (4), 480–492, <http://dx.doi.org/10.1016/j.rse.2004.08.003>.
- Zhurbas V. M., Laanemets J., Vahtera E., 2008, *Modeling of the mesoscale structure of coupled upwelling/downwelling events and the related input of nutrients to the upper mixed layer in the Gulf of Finland, Baltic Sea*, J. Geophys. Res., 113 (C5), C05004, <http://dx.doi.org/10.1029/2007JC004280>.

Zhurbas V., Oh I. S., Park T., 2006, *Formation and decay of a longshore baroclinic jet associated with transient coastal upwelling and downwelling: A numerical study with applications to the Baltic Sea*, J. Geophys. Res., 111 (C4), C04014, <http://dx.doi.org/10.1029/2005JC003079>.

Paper II

Uiboupin, R., Laanemets, J. 2009. Upwelling characteristics derived from satellite sea surface temperature data in the Gulf of Finland, Baltic Sea. *Boreal Environment Research*, 14(2), 297 - 304.

Upwelling characteristics derived from satellite sea surface temperature data in the Gulf of Finland, Baltic Sea

Rivo Uiboupin and Jaan Laanemets

*Marine Systems Institute at Tallinn University of Technology, Akadeemia tee 21, 12618 Tallinn, Estonia
(e-mail: Rivo.Uiboupin@phys.sea.ee)*

Received 9 May 2007, accepted 17 March 2008 (Editor in charge of this article: Timo Huttula)

Uiboupin, R. & Laanemets, J. 2009: Upwelling characteristics derived from satellite sea surface temperature data in the Gulf of Finland, Baltic Sea. *Boreal Env. Res.* 14: 297–304.

The seven-year (2000–2006) satellite sea surface temperature (SST) data were examined to determine characteristics of coastal upwellings during the warm period of the year (June–September) in the Gulf of Finland. A total of 20 sufficiently cloud-free SST images depicting well-expressed coastal upwelling were found. The area covered by upwelling water, the temperature difference between the upwelling and surrounding waters, and the location and area of filaments were estimated. The average area covered by the upwelling water was 4820 km² and for the largest upwelling event 12 140 km², i.e. 38% of the Gulf surface area. The average upwelling area along the Finnish coast (6120 km²) was larger than the upwelling area along the Estonian coast (4070 km²) which likely results from a larger cumulative wind stress (the product of wind stress and its duration) of westerly winds during the observed upwellings. The detected upwelling filaments were predominantly related to an upwelling along the Finnish coast. The area of a single filament usually varied from 80 to 680 km² while the total area of filaments reached the maximal value of 1420 km² during the strongest upwelling event.

Introduction

The coastal upwelling caused by the along-shore wind forcing typically brings cold and nutrient-rich deeper water to the surface layer. In the Gulf of Finland, summer upwellings usually transport cold and phosphate rich water from thermocline to the surface thus promoting the growth of nitrogen-fixing cyanobacteria (e.g. Haapala 1994, Vahtera *et al.* 2005). Besides the field measurements and numerical modeling the satellite sea surface temperature (SST) data carries substantial additional information about the spatial extent and structure of wind-driven coastal upwellings. Concerning the Baltic Sea,

the satellite sea surface temperature images have been analysed by Horstmann (1983), Bychkova and Victorov (1986), Gidhagen (1987), Siegel *et al.* (1994) and Kahru *et al.* (1995) to determine upwelling parameters for the period with thermally stratified sea. They found that the temperature difference between the upwelled and surrounding water varies within 2–10 °C, the alongshore extent is of the order of hundreds kilometres and the off-shore scale is tens of kilometres.

The seasonal thermocline in the Gulf of Finland usually forms at the beginning of May, is at its strongest in July–August and erodes by the end of August (e.g. Alenius *et al.* 1998). Its

depth is of 10–15 m and in July–August the temperature difference between the warm surface layer and the cold intermediate layer below the thermocline may be up to 20 °C. Therefore, due to the strong thermal stratification the large sea surface temperature contrasts could be expected in the upwelling regions. Owing to the prevailing south-westerly winds (e.g. Mietus 1998, Soomere and Keevallik 2003) the northern coastal sea of the Gulf of Finland is an active upwelling area in summer as it was shown also by model simulations (Myrberg and Andrejev 2003). Kahru *et al.* (1995) identified from satellite SST images that the northwestern Gulf of Finland is one of the major upwelling front areas in the Baltic Sea. They found two most significant upwelling centres where filaments emerge from the upwelling front off the Hanko and Porkkala peninsulas and move south towards the Estonian coast. The model simulations showed also that the mesoscale disturbances (meanders and eddies) of an alongshore upwelling jet can be attributed to topographic irregularities (e.g. Zhurbas *et al.* 2004).

The objective of this work was to estimate the surface area covered by the upwelling water, the location of upwelling filaments and the temperature difference between the upwelling and surrounding water during summer upwelling events in the Gulf of Finland. The study is based on examination of satellite SST data from the years 2000–2006.

Data and methods

Remote sensing and wind data

The 7-year (2000–2006) SST data measured by MODerate Resolution Imaging Spectroradiometer (MODIS) onboard of Terra and Aqua satellites were used in this study. Both satellites overpass the Baltic Sea daily. MODIS Level 2 products, MOD28L2 and MYD28L2 provide sea surface temperature calculated from the long wavelength (11–12 μm) and the short wavelength (3–4 μm) bands at about 1×1 km resolution. Previous studies (Brown and Minnett 1999, Reinart and Reinhold 2008) have confirmed that the SST measurements can be considered having

the accuracy of up to ± 0.5 °C. The SST images from the warm period of the year (June–September) were analysed in the present study.

Wind data measured at the Kalbådagrund weather station (Fig. 1) (Finnish Meteorological Institute) were used for the calculation of the approximate along-gulf component of the cumulative wind stress (the product of the wind stress and its duration) to estimate the wind forcing during the observed upwelling events and to count the summer wind events favourable for upwelling. Soomere and Keevallik (2003) analysed wind data series from weather stations around the Gulf and found that the wind data measured at the southern coast do not represent adequately marine wind properties. Therefore we used Kalbådagrund weather station data for the calculation of both, easterly and westerly, wind forcing. The gaps in the Kalbådagrund wind data record (September 2000 and July 2003) were filled out with the wind data measured at the Utö weather station (Finnish Meteorological Institute).

Methods

In order to exclude the areas covered by clouds or influenced by coast, the reflectance data from MODIS bands 1 (620–670 nm) and 2 (841–876 nm) were examined together with MODIS SST data.

The line between the Hanko peninsula and the island of Osmussaar is treated as the western boundary of the Gulf of Finland basin (line A in Fig. 1). For detection of the border of the upwelling water (including filaments) the computer software ENVI 4.2 (ENVI 2001) was used. The SST images were overlaid by isotherms with the fixed contour interval of 0.5 °C starting from the upwelling centre(s). All sea surface isotherms either form closed contours or intersect the basin boundary. The contour of the warmest isotherm intersecting the basin boundaries is considered the upwelling water open sea border (Fig. 2a).

The pixels belonging to the upwelling water region were counted and also marked for visual checking of the upwelling water area. The total area of upwelling water was calculated from the known pixel area for each particular SST image.

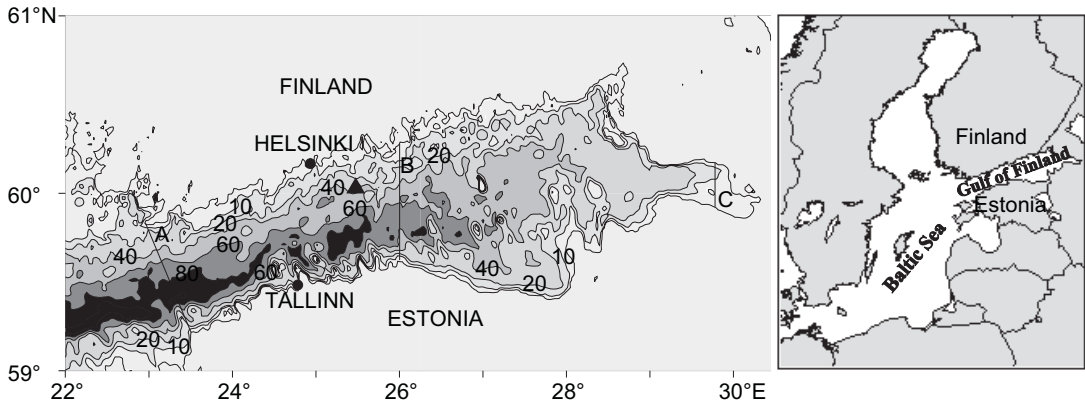


Fig. 1. The Baltic Sea (right panel) and the map of the Gulf of Finland (left panel) with the depth contours drawn from the gridded topography (Seifert *et al.* 2001). Shown is the location of Kalbádagrund (\blacktriangle) weather station. The Gulf area is divided into two parts: western Gulf between lines A and B and eastern Gulf between lines B and C.

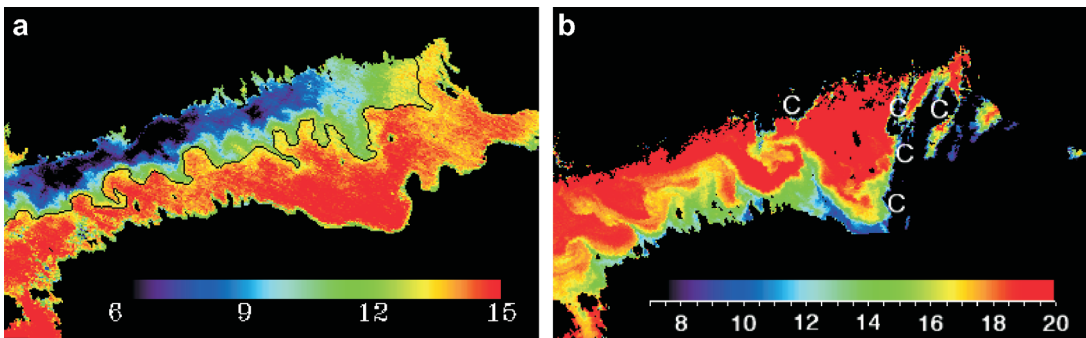


Fig. 2. — **a:** The largest upwelling observed during the study period on 24 September 2003 along the Finnish coast. The determined border of upwelling water is marked by a solid curve. — **b:** A large upwelling observed during the study period on 25 August 2006 along the Estonian coast. C = cloud cover.

The filament location was defined coinciding with the filament width centre along the edge of upwelling front. The filament length was defined as the distance from the filament location to the farthest filament pixel. The filaments with the length larger than the width and with the area larger than 50 km² were taken into account.

Results

Detected and potential upwelling events

We found 20 sufficiently clear sky SST images comprising five upwelling events along the Finnish coast and five events along the Estonian coast during the summers 2000–2006. The wind data records from June to the end of September (2000–2005) showed yearly five to eight (on the

average about six per year) upwelling-favourable wind events per summer which had the absolute along-gulf component of the cumulative wind stress larger than 0.1 N m⁻² d. The frequency of wind events able to generate upwelling were different along the Estonian and Finnish coast and varied considerably from year to year. We found one to four (on the average about two) wind events (June–September) that might generate upwellings along the Estonian coast and three to five (on the average about four) wind events that might generate upwellings along the Finnish coast for the study period. The westerly winds, caused by cyclones passing the Gulf area, are often accompanied by cloudy weather and, therefore, the fraction of SST images reflecting the upwelling events along the Finnish coast from all wind-detected upwelling-favorable events is smaller as compared with those from the similar

upwelling events along the Estonian coast, usually caused by anticyclones. Thus, taking into account the above statistics we observed about 20% from the potential upwelling events along the Finnish coast and about 40% along the Estonian coast during the study period.

Area covered with upwelling water

Calculations of the area covered by the upwelling water and its percentage were performed separately for the eastern and western parts of the Gulf of Finland considering the shape of the Estonian coastline (Fig. 1). On several occasions when clouds were partly covering either the Finnish or the Estonian coastal sea the percentages were calculated for the cloud free cross-Gulf stripe.

The average area covered by the upwelling water was 4820 km² which is about 15% from the total Gulf area. The average upwelling areas were larger along the Finnish coast (6120 km² and 19%) than along the Estonian coast (4070 km² and 13%). The most intensive upwelling along the Finnish coast occurred on 24 September 2003 (Fig. 2) and along the Estonian coast on 9 August 2006 when 38% (12 140 km²) and 20% (6480 km²) of the Gulf area respectively was covered with the upwelling water (Table 1).

Upwellings were more extensive in the western part of the Gulf, where the average area covered by the upwelling water was 3100 km² (22%) compared with 2420 km² (13%) in the eastern part. The average upwelling water areas along the Finnish and the Estonian coast were 3680 km² (26%) and 2630 km² (19%) in the western part of the Gulf. The corresponding esti-

Table 1. Upwelling characteristics in the western (WG) and eastern (EG) parts of the Gulf of Finland. The fraction of the cloudless area is presented in brackets in percents, the area covered with the upwelled water and the corresponding fraction in percents, the area of filaments, the minimum temperature (T_{\min}) in the upwelling region, the maximum temperature (T_{\max}) of the surrounding water across the front, their difference (ΔT) and the absolute along-gulf component of cumulative wind stress W . The areas of eastern and western part of the Gulf were about 18 000 km² and 14 000 km² correspondingly.

Coast	Date	Part of Gulf	Upwelling area (km ²)	Upwelling area (%)	Filament area (km ²)	T_{\min} (°C)	T_{\max} (°C)	ΔT (°C)	W N m ⁻² d
FIN	27 Sep. 2000	WG/EG	3047/2095	22/12	1020	14.4	17.9	3.5	0.52 ^a
FIN	20 Jun. 2002	WG/EG	2917/1227	21/7	160	10.1	16.0	5.9	0.33
FIN	2 Sep. 2002	WG (32)	1808	40*	200	14.3	20.4	6.1	0.47
FIN	4 Sep. 2002	WG(60)/EG	2308/3921	28*/22	600	12.6	19.8	7.2	0.9
EST	17 Jul. 2003	WG/EG	1260/1121	9/6	–	10.7	21.3	10.6	0.21 ^b
EST	19 Jul. 2003	WG/EG	2264/1923	16/11	230	10.1	20.5	10.4	0.23 ^b
EST	21 Jul. 2003	EG(42)	783	10*	–	14.9	24.1	9.2	0.21 ^b
EST	22 Jul. 2003	WG/EG	3598/2696	25/15	510	14.6	23.1	8.5	0.19 ^b
EST	1 Aug. 2003	WG(36)/EG	249/1754	5*/10	–	11.0	25.1	14.2	0.06
EST	2 Aug. 2003	WG/EG	674/2297	5/13	110	10.3	25.5	15.2	0.06
FIN	23 Sep. 2003	WG(44)/EG	796/4951	13*/27	1170	7.7	14.8	7.1	1.52
FIN	24 Sep. 2003	WG/EG	6474/5664	46/31	1420	6.4	14.3	7.9	1.69
EST	9 Jul. 2005	WG(48)	990	14*	–	12.4	20.3	7.9	0.08
FIN	24 Sep. 2005	WG/EG(28)	4383/1108	31/22*	1330	7.9	15.2	7.4	0.98
FIN	25 Sep. 2005	WG	4336	31	1100	8.1	15.2	7.1	1.02
FIN	26 Sep. 2005	WG	3598	26	320	7.5	14.9	7.4	1.06
EST	6 Aug. 2006	WG/EG	2721/1406	19/8	–	7.2	20.1	12.9	0.51
EST	7 Aug. 2006	WG/EG	3666/2385	26/13	180	8.3	19.5	11.2	0.55
EST	9 Aug. 2006	WG/EG	4449/2031	31/11	160	7.2	18.0	10.8	0.59
EST	25 Aug. 2006	WG/EG(41)	4003/1734	29/24*	1400	8.7	19.2	10.5	0.47

* The area was partly covered by clouds; the percentage of area covered by upwelled water was calculated for cloudless area.

^a Utö wind data.

^b Combined wind data from Kalbådagrund and Utö.

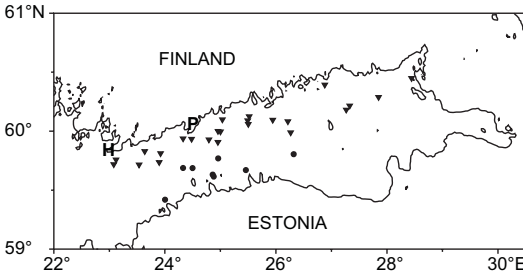


Fig. 3. Locations of upwelling filaments related to upwellings along the Finnish (▼) and Estonian (●) coast. Hanko and Porkkala peninsulas are marked with (H) and (P) correspondingly.

mates for the eastern part of the Gulf were 3440 km² (19%) and 1890 km² (10%).

Observed temperature differences between the upwelling and the surrounding water varied in a wide range, from 3.5 to 15.2 °C (Table 1). For the upwelling events along the Estonian coast the temperature differences were between 7.9 and 15.2 °C. During upwelling events along the Finnish coast the temperature differences were smaller, from 3.5 to 7.9 °C.

Upwelling filaments

Overall 32 filaments, excluding the filaments of coinciding location observed on the successive SST images of the same upwelling event, were identified. The filaments predominantly stretched out from the upwelling front along the Finnish coast and in the western part of the Gulf (Fig. 3). Only eight filaments were related to the upwellings along the Estonian coast thereby 6 of those were observed during the strongest upwelling event along the Estonian coast in August 2006.

The length of filaments was up to 35 km and in several cases the filaments observed along the northern coast were cyclonically turned. For example, on the SST images from 24 to 26 September 2005 the cyclonically turned filaments can be detected along the Finnish coast (Fig. 4a) which further on formed a rotating vortex pair and an eddy (Fig. 4b and c). The area of single filaments varied in a wide range from 80 to 680 km².

The area covered by filaments was significantly larger for the upwellings along the northern coast as the filaments were rarely formed

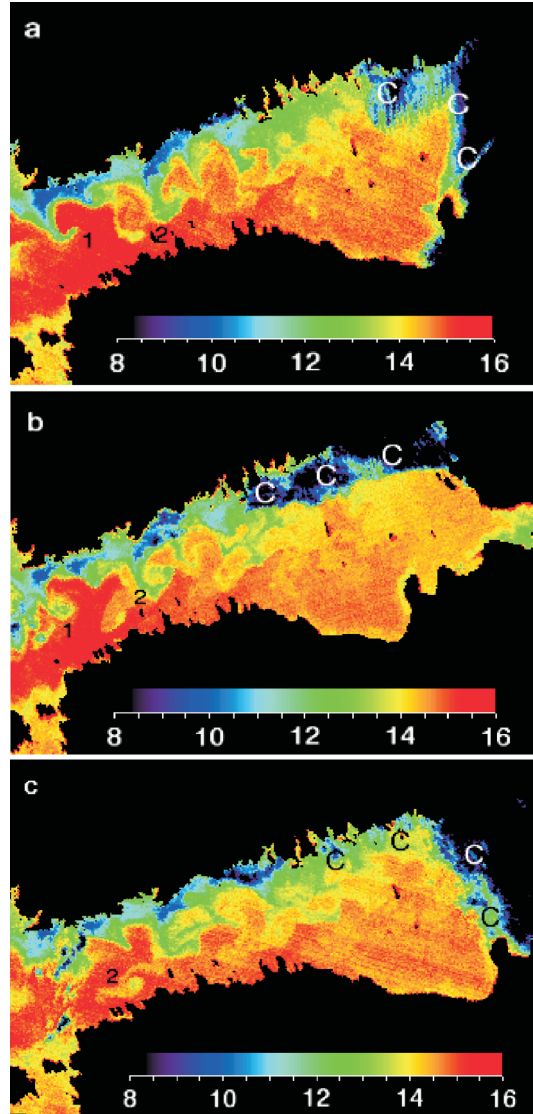


Fig. 4. Series of SST images showing the development of filaments emerging from the upwelling front along the Finnish coast during 24–26 September 2005. Filament marked as 1 in panel a turned into eddy (see b). Filament marked as 2 in panel a formed a rotating vortex pair (see b), one of which turned into eddy (see c). C = cloud cover.

in case of upwellings along the southern coast (Table 1). In case of the largest upwelling event along the Finnish coast observed on 24 September 2003 (Fig. 2a) the area of filaments was 1420 km² (Table 1) which made up 12% from the total area of the upwelled water in the Gulf. The share of upwelling filaments was higher in the western part of Gulf. For example, during the upwelling

along the Finnish coast on 24 September 2005 (Fig. 4a) the area of filaments was 1330 km² (30%) and during a large upwelling along the Estonian coast on 25 August 2006 (Fig. 2b) the area of filaments was 1100 km² (27%).

Discussion and conclusions

Satellite SST images allow upwelling characteristics study all over the entire area of the Gulf. The summer upwellings in the Gulf of Finland are characterized by pronounced temperature contrasts which provide a good premise for identification of upwelling events and their parameters from SST images. Due to the high cloudiness level the weakness of the Baltic Sea satellite SST data are a relatively small fraction (10%–50%) of useful images suitable for processing (e.g. Krężel *et al.* 2005).

Upwelling areas off the Finnish coast, on the average 6120 km², were larger as compared with those off the Estonian coast, 4070 km². During the strongest upwelling events observed on 24 September 2003 along the Finnish and on 9 August 2006 along the Estonian coast the upwelling water (including filaments) may cover remarkable areas, up to ~40 % and ~20% correspondingly from the total Gulf area (Table 1).

Considerably larger upwelling areas along the Finnish coastline could be explained by a larger westerly along-gulf component of cumulative wind stress that generated the observed upwelling events (Table 1). The cumulative wind stress was calculated from the beginning of the action of upwelling-favourable wind until the time of the satellite overpass. The approximate offshore displacement (ΔX) of the upwelling front is $\Delta X = W / \rho_0 f h_E$, where W is the along-gulf component of cumulative wind stress, ρ_0 is the reference density and h_E is the surface Ekman layer depth (Austin and Lentz 2002). This equation does not take into account the upwelling set-up time and there is also no data to estimate the Ekman layer depth. Nevertheless, the observed larger upwelling water areas along the Finnish coast were in accordance with larger cumulative wind stresses (Table 1).

The SST images from the study period showed that the pronounced cold filaments were

related mainly to the upwelling events along the Finnish coast as it was also shown in an earlier study by Kahru *et al.* (1995). Although they found that filaments occurred mainly off Hanko and Porkkala peninsulas there were no easily seen preferred filament generation regions along the northern coast of the Gulf in our study (Fig. 3). The filaments originating from the coast of Estonia were weaker and were observed more rarely. The relatively high portion of upwelling water in the filaments, up to 30% in the western part of Gulf, points to their important role in the offshore transport of the cold and nutrient-rich water.

The generation of filaments is related to the instability of longshore baroclinic jet associated with the upwelling. Blumsack and Gierasch (1972) and de Szoeke (1975) showed that in case of sloping bottom the baroclinic instability of a longshore upwelling jet strongly depends on the ratio of the bottom slope to the isopycnal slope, α . When the isopycnal slope is smaller than the bottom slope ($\alpha > 1$) then the baroclinic instability of the upwelling jet is not expected to occur. A numerical study by Zhurbas *et al.* (2006) using the characteristic summer stratification in the Baltic Sea, also showed that no baroclinic instability of an upwelling jet was observed when the bottom slope exceeded the isopycnal slope. The cross-shore scale for the region of sloping isopycnals for the upwelling event is the baroclinic Rossby radius of deformation (Allen 1980). According to Fennel *et al.* (1991) the baroclinic Rossby radius of deformation is about 3 km in the Gulf of Finland in summer and the upper mixed layer depth is approximately 10 m, which gives a rough estimate for the isopycnal slope of 0.003. Although the bottom topography of the Gulf of Finland is complicated (Fig. 1) the approximate estimates of the bottom slope off the Estonian coast 0.006 and off the Finnish coast 0.002 could be used. Thus, in the Finnish coastal sea $\alpha \approx 0.5$ while in the Estonian coastal sea $\alpha > 1$, i.e. the baroclinic instability of the upwelling jet along the Finnish coast is more probable. Another reason of the observed difference between the occurrence of upwelling filaments along the Finnish and Estonian coasts is likely due to the different atmospheric forcing. The along-gulf component of cumulative wind stress was smaller during

the upwellings along the Estonian coast, except the upwelling on 25 August 2006 (Table 1). Zhurbas *et al.* (2006) showed that the instability growth rate depends on the cumulative wind stress and increases considerably for sufficiently large cumulative wind stresses.

Many filaments were cyclonically turned. The model simulations by Zhurbas *et al.* (2006) demonstrated the growth of wave-like perturbations forming mostly cyclonic meanders (filaments) of the upwelling jet which further on detached from the jet and formed mesoscale cyclonic eddies. Such development was also observed on a series of SST images (Fig. 4) with the time scale of a few days.

The detected upwellings off the Estonian coast occurred in July–August when the surface heating was strong and therefore the temperature difference between the upwelling and the surrounding waters was large while upwellings along the Finnish coast occurred in June and September and therefore the temperature difference was lower (Table 1).

To conclude, the analysis of satellite SST data showed that the upwelling water covered considerable area of the Gulf. Most likely due to the different atmospheric forcing and different topography of the northern and southern coasts of the Gulf the upwelling characteristics differed in the following way: (1) the upwellings off the northern coast were more extensive and the upwelling water covered larger areas of the coastal sea, and (2) the upwelling filaments were predominantly observed off the northern coast.

Acknowledgements: The Kalbådgrund and Utö weather station wind data were kindly provided by the Finnish Meteorological Institute. The temperature data on the transect Helsinki–Tallinn were kindly provided by Alg@line project (Estonian Marine Institute). Likewise, our thanks to Juss Pavelson, Aleksander Toompuu and Liis Sipilgas for valuable comments on the manuscript. This work was supported by Estonian Science Foundation through grant No. 7467.

References

- Allen J.S. 1980. Models of wind driven currents on the continental shelf. *Annu. Rev. Fluid Mech.* 12: 389–433.
- Alenius P., Myrberg K. & Nekrasov A. 1998. The physical oceanography of the Gulf of Finland: a review. *Boreal Env. Res.* 3: 97–125
- Austin J.A. & Lentz S.J. 2002. The inner shelf response to wind-driven upwelling and downwelling. *J. Phys. Oceanogr.* 32: 2171–2193
- Blumsack S.L. & Gierasch P.J. 1972. Mars: the effects of topography on baroclinic instability. *J. Atmos. Sci.* 29: 1081–1089.
- Brown O.B. & Minnett P.J. 1999. *MODIS infrared sea surface temperature algorithm theoretical basis document*, ver. 2.0. Available at http://modis.gsfc.nasa.gov/data/atbd/atbd_mod25.pdf.
- Bychkova I. & Viktorov S. 1986. Use of satellite data for identification and classification of upwelling in the Baltic Sea. *Oceanology* 27: 158–162.
- de Szoeke R.A. 1975. Some effects of bottom topography on baroclinic instability. *J. Mar. Res.* 33: 93–122
- Fennel W., Seifert T. & Kayser B. 1991. Rossby radii and phase speed in the Baltic Sea. *Cont. Shelf Res.* 11: 23–36.
- ENVI 2001. *ENVI user's guide*. Research Systems Inc. Boulder CO.
- Gidhagen L. 1987. Coastal upwelling in the Baltic — satellite and in situ measurements of sea surface temperatures indicating coastal upwelling. *Est. Coast. Shelf Sci.* 24: 449–462.
- Haapala J. 1994. Upwelling and its influence on nutrient concentration in the coastal area of the Hanko Peninsula, entrance of the Gulf of Finland. *Est. Coast. Shelf Sci.* 38: 507–521.
- Horstmann U. 1983. Distribution patterns of temperature and water colour in the Baltic Sea as recorded in satellite images: indicators for phytoplankton growth. *Berichte aus dem Institute für Meereskunde an der Universität Kiel* 106: 1–147.
- Kahru M., Håkansson B. & Rud O. 1995. Distributions of the sea-surface temperature fronts in the Baltic Sea as derived from satellite imagery. *Cont. Shelf Res.* 15: 663–679.
- Krężel A., Ostrowski M. & Szymelfenig M. 2005. Sea surface temperature distribution during upwelling along the Polish Baltic coast. *Oceanologia* 47: 415–432.
- Mietus M. 1998. *The climate of the Baltic Sea basin. Marine meteorology and related oceanographic activities*. Report 41, WMO/TD 933, Geneva.
- Myrberg K. & Andrejev O. 2003. Main upwelling regions in the Baltic Sea — a statistical analysis based on three-dimensional modelling. *Boreal Env. Res.* 8: 97–112.
- Reinart A. & Reinhold M. 2008. Mapping surface temperature in large lakes with MODIS data. *Rem. Sen. Env.* 112: 603–611.
- Seifert T., Tauber F. & Kayser B. 2001. A high resolution spherical grid topography of the Baltic Sea, revised edition. In: *Baltic Sea Science Congress 2001: Past, Present and Future — A Joint Venture*, Abstract Volume, Stockholm University, pp. 298.
- Siegel H., Gerth M., Rudloff R. & Tschersich G. 1994. Dynamic features in the western Baltic Sea investigated using NOAA-AVHRR data. *Dt. hydrogr. Z.* 46: 191–209.
- Soomere T. & Keevallik S. 2003. Directional and extreme wind properties in the Gulf of Finland. *Proc. Estonian*

Acad. Sci. Eng. 9: 73–90.

- Vahtera E., Laanemets J., Pavelson, J., Huttunen M. & Kononen K. 2005. Effect of upwelling on the pelagic environment and bloom-forming cyanobacteria in the western Gulf of Finland. *Baltic Sea. J. Mar. Syst.* 58: 67–82.
- Zhurbas V.M., Stipa T., Mälkki P., Paka V.T., Kuzmina N.P. & Sklyarov V.E. 2004. Mesoscale variability of

upwelling in the southeast Baltic: infrared images and numerical modeling. *Oceanology* 44: 495–504.

- Zhurbas V.M., Oh I.S. & Park T. 2006. Formation and decay of a longshore baroclinic jet associated with transient coastal upwelling and downwelling: a numerical study with application to the Baltic Sea. *J. Geophys. Res.* 111(C4), C04014, doi: 10.1029/2005JC003079.

Paper III

Uiboupin, R., Sipelgas, L.2007. Comparison of satellite sea surface temperature with in situ surface layer temperature. Proceedings of the Estonian Academy of Sciences: Biology, Ecology, 56(1), 47 - 56.

Comparison of satellite sea surface temperature with in situ surface layer temperature

Rivo Uiboupin* and Liis Sipelgas

Marine Systems Institute, Tallinn University of Technology, Akadeemia tee 21, 12618 Tallinn, Estonia; liis@sea.ee

Received 27 January 2006, in revised form 22 August 2006

Abstract. Shipborne measurements of sea surface layer temperature in the western Gulf of Finland in July 2002 were compared with four different MODIS sea surface temperature (SST) products. The root mean square difference of the satellite and shipborne temperature series was calculated. According to the calculations the MODIS Aqua SST products were closer to the shipborne temperature measurements than the MODIS Terra SST products. A criterion of 0.4°C temperature differences was found to detect upwelling regions from MODIS SST products. Comparison of images showed that surface accumulation of cyanobacteria causes a local increase of the sea surface temperature on the SST images.

Key words: sea surface temperature, MODIS Aqua, MODIS Terra, upwelling, Gulf of Finland.

INTRODUCTION

One of the most frequent variables retrieved from satellite sensors used for oceanographic studies is the sea surface temperature. The distribution of the sea surface temperature provides significant information for monitoring the relevant key ocean structures, e.g. fronts, eddies, and upwellings (Gidhagen, 1987; Sur & Ilyin, 1997; Borzella et al., 1999; Kartushinskaya, 2000; Bricaud et al., 2002; Tang et al., 2002). The sea surface temperature is observed from the space by the thermal infrared imagery during cloud-free conditions using the thermal and infrared satellite channels. A wide range of different satellite systems and sensors providing the sea surface temperature (SST) data is and will become available during the next decade (Johannessen et al., 2000). In the Gulf of Finland (Baltic Sea) the summer coastal upwellings caused by the time-variable wind forcing bring up cold and phosphate rich waters from the deeper layers to the surface thus

* Corresponding author, Rivo.Uiboupin@phys.sea.ee

increasing the biomass of cyanobacterial blooms (Laanemets et al., 2004; Vahtera et al., 2005). Therefore, statistical analyses of upwelling parameters (horizontal scales of the upwelled water and the upwelling-related filaments, temperature differences between the upwelled and the surrounding water) as well as the frequency of upwelling events during summer by using SST from satellite remote sensing images is an important task.

The aim of this study is to compare (1) different images obtained within a short time window (Aqua and Terra products) and (2) MODIS products in terms of algorithms (SST and SST4) used for the calculation of the sea surface temperature for the same images.

This comparison shows which MODIS product gives the best results in the Baltic Sea region. The sea surface temperatures calculated by using different MODIS products are compared with the respective shipborne measurements to establish quantitative measures for defining uncertainties of the SST from remote sensing. The results can be used for developing quantitative criteria for the detection of upwelling parameters.

DATA AND METHODS

Shipborne measurements

A field study trip for measurements of the surface layer temperature was made on 29 July 2002 using a flow through (FT) system while the ship was moving. The length of the ship track from Tallinn to Hiiumaa Island (Fig. 1) was about

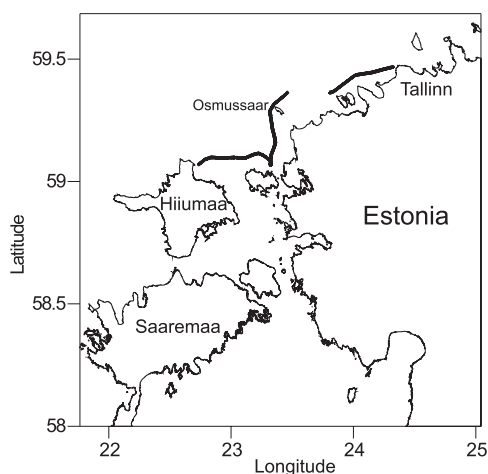


Fig. 1. Study site. Ship track from Tallinn to Hiiumaa.

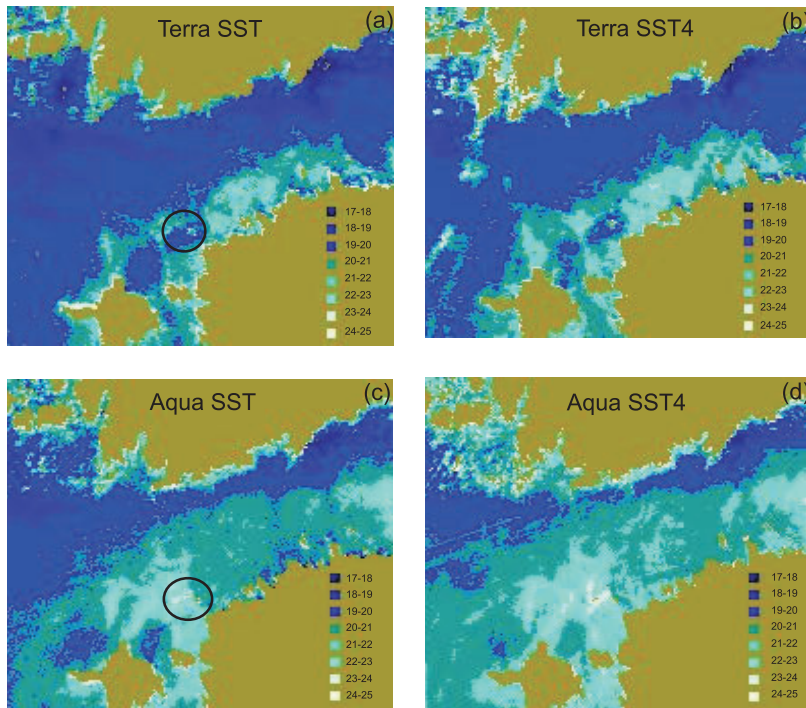


Fig. 2. Sea surface temperature products from satellite images Terra SST (a), Terra SST4 (b), Aqua SST (c), and Aqua SST4 (d). The region of surface accumulation of cyanobacteria is encircled (c).

130 km and it was passed in 7 h. Measurements started at 10.30 UTC. The FT system comprised a Seabird CTD recording temperature and conductivity at 1 s intervals. The ship location was determined by GPS. Seawater was pumped into the FT system from a depth of 20 cm. During the cruise the wind speed and direction were measured once per hour.

Remote sensing images

MODIS (**MOD**erate Resolution Imaging Spectroradiometer) is a key instrument aboard the Terra (EOS AM) and Aqua (EOS PM) satellites. Terra MODIS and Aqua MODIS view the entire Baltic Sea area daily, acquiring data in 36 spectral bands. MODIS Level 2 Sea Surface Temperature Product, MOD28L2, provides a long wavelength (11–12 μm , SST) and a short wavelength (3–4 μm , SST4) sea surface temperature at 1×1 km resolution over the global oceans (Satellite-based Information System on Coastal Areas and Lakes, http://www.siscal.net/documents/EOP_SST_MOD_V03.pdf and GES Distributed Active Archive Centre, <http://disc.gsfc.nasa.gov/data/dataset/>).

Both MODIS Terra (overflight at 9.15 UTC) and MODIS Aqua (overflight at 11.05 UTC) SST products of 29 July 2002 were downloaded from GES Distributed Active Archive Centre (<http://disc.gsfc.nasa.gov/data/dataset/>). Geocorrection was applied to each obtained image. The digital number (DN) values were converted to SST by using the following values of calibration coefficients:
MODIS SST = $0.01 \times \text{DN} - 300$ (GES Distributed Active Archive Centre).

RESULTS AND DISCUSSION

Comparison of images

The SST images of MODIS standard products are shown in Fig. 2. Differences between the products are evident. The major difference in the temperature fields is between the MODIS Aqua and MODIS Terra products (cf. Fig. 2a, b and Fig. 2c, d). The MODIS Aqua SST and SST4 products give generally higher values and the area with a temperature of 20–21 °C is much wider than the temperature fields on MODIS Terra products. This disparity can be partly explained by the surface layer solar heating because the overflight of Aqua took place 1 h and 45 min later. The Aqua SST value averaged along the ship track was 0.183 °C higher than the Terra SST value while the difference between the averaged SST4 values was 0.149 °C. The difference was smaller within the Aqua and Terra products (Fig. 2).

Small-scale areas with significantly higher temperature anomalies can be seen on the north-west Estonian coast in all four MODIS SST images (Fig. 2a, c). The maxima can be explained by the visible massive surface cyanobacteria patches

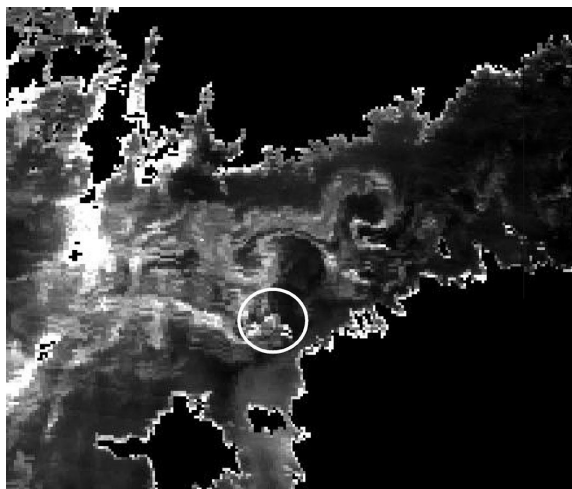


Fig. 3. Radiance data at a waveband of 662–672 nm. The area of measurements that was affected by a cyanobacterial bloom is encircled.

near Osmussaar Island. Kahru et al. (1993) assumed that the massive surface accumulation of cyanobacteria can cause a local increase of the sea surface temperature up to 1.5°C on the SST images for low wind speed (about 2 m s^{-1}). We suggest that this effect was also intermittently present in the area covered by our data (temperature difference between two neighbouring pixels was up to 2°C), in the region encircled in Fig. 2a, c. In the same region maximum values were also observed in the radiance data at the waveband 662–672 nm, which is the range that describes surface accumulation of cyanobacteria (Fig. 3). Therefore in the following data analysis the pixels for which the cyanobacteria surface accumulation was visible were discarded.

Estimation of the Ekman layer depth

To evaluate the correspondence of the shipborne temperature measurements with the satellite SST data the depth of the turbulent Ekman boundary layer h_m was estimated by the formula $h_m = 0.1u_* / f$ for a homogeneous water column (Csanady, 1982). Here $u_* = (\tau / \rho_w)^{1/2}$ is friction velocity, $\tau = \rho_a C_a u^2$ is wind stress, ρ_a is air density, ρ_w is water density, $C_a = 1.2 \times 10^{-3}$ is dimensionless wind drag coefficient, u is wind speed, and $f = 1.3 \times 10^{-4} \text{ s}^{-1}$ is Coriolis parameter. The mean wind speed during the measurement was 2.8 m s^{-1} and the corresponding estimated Ekman layer depth was 2.5 m. The stratification due to the surface

heating certainly reduces the depth of the surface shear layer but probably not as much as by an order of magnitude and we assume that the FT temperature is representative for the sea surface temperature.

Calculation of the root mean square difference

The SST products were compared with the FT temperature data. Using the ship track coordinates from satellite SST images the pixels covering the ship track were extracted. The average FT temperature was calculated for each pixel area. The number of FT temperature readings within a pixel varied between 50 and 300. The correspondence between FT data and four different MODIS SST products is shown in Fig. 4. The Terra products (Fig. 4a, b) differ more from the FT data than the Aqua products (Fig. 4c, d). As the SST and SST4 products are calculated using different algorithms, the differences in temperature that can be seen in Fig. 4c (ranges 90–100 km and 120–130 km) may be caused by the Aqua SST4 algorithm. For the evaluation of the coincidence of the MODIS SST products and FT temperature measurements the root mean square (RMS) difference (ΔT) of the satellite and FT temperature series was calculated as follows:

$$\Delta T = \sqrt{\sum \frac{(T_{\text{sat}} - T_{\text{ship}})^2}{n}},$$

where T_{sat} is the temperature from a MODIS product, T_{ship} is the pixel-averaged temperature of FT data, and n is the number of pixels on the ship track. The calculated RMS differences are presented in Table 1. For the MODIS Terra products the RMS differences are larger than for the Aqua products. The Aqua SST product has the smallest ΔT_1 and is the most compatible with the FT data (Fig. 3c). We also calculated the RMS differences for the ± 0.5 h time interval around the overflight of Aqua (Table 1). At the time of the Terra overflight there were no shipborne measurements. As expected, the RMS differences were smaller for the shorter time intervals.

Table 1. The RMS differences of all MODIS products and FT temperature calculated for the total length of the series (ΔT_1) and the RMS differences of the MODIS Aqua products and FT temperature series for the time interval ± 0.5 h around the overflight (ΔT_2)

MODIS product	ΔT_1	ΔT_2
Terra SST	0.753	–
Terra SST4	0.766	–
Aqua SST	0.572	0.312
Aqua SST4	0.578	0.524

– No relevant measurements made.

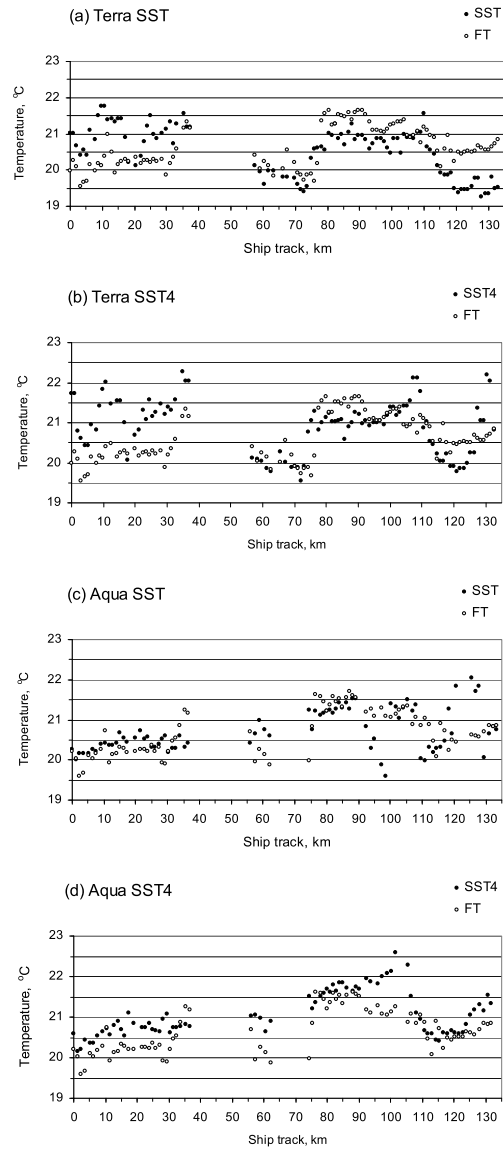


Fig. 4. Correspondence between FT temperature data (averaged over one pixel) and sea surface temperature products Terra SST (a), Terra SST4 (b), Aqua SST (c), and Aqua SST4 (d). The large gap (36–56 km) is due to the lack of FT measurements (see Fig. 1). The gap (c and d) near Osmussaar Island (62–74 km) is due to the accumulation of cyanobacteria.

CONCLUSIONS

Generally the Aqua products show a better correspondence with the FT temperature data than the Terra products. The correspondence between the ship-borne data and satellite data is the best in the case of the Aqua SST product. The RMS difference in the case of 1 h interval around the satellite overflight time was $\sim 0.4^{\circ}\text{C}$. Therefore it is assumed that the criterion of 0.4°C temperature differences can serve for detecting upwelling regions. Finding a criterion for spatial variability needs to be studied.

Comparison of the images showed that massive surface accumulation of cyanobacteria can cause a local increase of the sea surface temperature on the SST images for low wind speed.

ACKNOWLEDGEMENTS

This work was supported by the Estonian Science Foundation (grant No. 5596). We thank Jaan Laanemets, Urmas Raudsepp, and Aleksander Toompuu for providing valuable guidelines to improve the quality of the manuscript.

REFERENCES

- Bricaud, A., Bosc, E. & Antoine, D. 2002. Algal biomass and sea surface temperature in the Mediterranean Basin. Intercomparison of data from various satellite sensors, and implications for primary production estimates. *Remote Sens. Environ.*, **81**, 163–178.
- Borzelli, G., Manzella, G., Marullo, S. & Santoleri, R. 1999. Observations of coastal filaments in the Adriatic Sea. *J. Mar. Syst.*, **20**, 187–203.
- Csanady, G. T. 1982. *Circulation in the Coastal Ocean*. D. Reidel Publishing Company, Dordrecht, Holland.
- Gidhagen, L. 1987. Coastal upwelling in the Baltic Sea – satellite and in situ measurements of sea-surface temperatures indicating coastal upwelling. *Estuarine Coastal Shelf Sci.*, **24**, 449–462.
- Johannessen, O. M., Sandven, S., Jenkins, A. D., Durand, D., Pettersson, L. H., Espedal, H., Evensen, G. & Hamre, T. 2000. Satellite earth observation in operational oceanography. *Coastal Eng.*, **41**, 155–176.
- Kahru, M., Leppänen, J. M. & Rud, O. 1993. Cyanobacterial blooms cause heating of the sea surface. *Mar. Ecol. Prog. Ser.*, **101**, 1–7.
- Kartushinskaya, V. A. 2000. Time–space structure and variability of surface temperature frontal zones in the ocean (based on AVHRR satellite data). *Adv. Space Res.*, **25**, 1107–1110.
- Laanemets, J., Kononen, K., Pavelson, J. & Poutanen, E.-L. 2004. Vertical location of seasonal nutriclines in the western Gulf of Finland. *J. Mar. Syst.*, **52**, 1–13.
- Sur, H. I. & Ilyin, Y. P. 1997. Evolution of satellite derived mesoscale thermal patterns in the Black Sea. *Progr. Oceanogr.*, **39**, 109–151.
- Tang, D., Kester, D. R., Ni, I., Kawamura, H. & Hong, H. 2002. Upwelling in the Taiwan Strait during the summer monsoon detected by satellite and shipboard measurements. *Remote Sens. Environ.*, **83**, 457–471.
- Vahtera, E., Laanemets, J., Pavelson, J., Huttunen, M. & Kononen, K. 2005. Effect of upwelling on the pelagic environment and bloom-forming cyanobacteria in the western Gulf of Finland, Baltic Sea. *J. Mar. Syst.*, **58**, 67–82.

Satelliidi merepinna temperatuuri võrdlus alusmõõtmistega

Rivo Uiboupin ja Liis Sipelgas

29. juulil 2002 teostati Soome lahe läänepoolses regioonis merepinna temperatuuri mõõtmised, kasutades läbivoolusüsteemi. Saadud andmeid võrreldi MODIS-elt nelja erineva merepinna temperatuuri (SST) produktiga (Terra SST, Terra SST4, Aqua SST ja Aqua SST4). Kokkulangevuse uurimisel hinnati satelliidipiltide erinevusi. Võrreldi läbivoolusüsteemiga mõõdetud merepinna temperatuuri ja satelliidi merepinna temperatuuri produkte (Terra SST, Terra SST4, Aqua SST ja Aqua SST4) graafiliselt ning arvutati ruutkeskmised hälbed. Saadud tulemused näitasid, et Aqua merepinna temperatuuri produktid (Aqua SST ja Aqua SST4) on läbivoolusüsteemiga mõõdetud pinnakihi temperatuuridega paremas vastavuses kui Terra merepinna temperatuuri produktid (Terra SST ja Terra SST4). Läbivoolusüsteemiga mõõdetud temperatuuri ja satelliidi merepinna temperatuuri andmete kokkulangevus oli kõige parem satelliidi produkti Aqua SST korral. Ruutkeskmine hälve ajavahemiku jaoks 30 minutit enne ja pärast satelliidi ülelendu oli $0,312^{\circ}\text{C}$. Saadud tulemusi arvestades võib eeldada, et nii temperatuuri kui ka temperatuuri muutuste määramiseks tõusuhoovuse piirkonnas võib kasutada kriteeriumi $0,5^{\circ}\text{C}$.

Paper IV

Uiboupin, R., Laanemets, J. 2009. Observation of mesoscale eddies by using SAR data complemented with optical remote sensing and in situ measurements. In: Proceedings of International Geoscience and Remote Sensing Symposium: Geoscience and Remote Sensing Symposium, 2009 IEEE International, Cape Town, 12-17 July 2009 . IEEE, 2009, (1), 224 - 227.

OBSERVATION OF MESOSCALE EDDIES BY USING SAR DATA COMPLEMENTED WITH OPTICAL REMOTE SENSING AND IN SITU MEASUREMENTS

Rivo Uiboupin^{1,2} and Jaan Laanemets¹

¹ Marine Systems Institute at TUT, Akadeemia Rd 21B, Tallinn 12618, Estonia

² ESA/ESRIN, Via Galileo Galilei, 00044 Frascati RM, Italy

ABSTRACT

Mesoscale eddies were observed in the Baltic Sea using optical remote sensing, SAR imagery and high resolution in situ measurement from an autonomous system on a passenger ferry. Comparison between SAR data and in situ measurements was carried out to analyze the manifestation of sea surface temperature differences and biological surface slicks on SAR imagery. Correlation between radar backscatter and biological parameters (chlorophyll a and turbidity) was observed. Locations of upwelling related cold eddies and low temperature areas were clearly detectable on radar imagery as well. Therefore, SAR data complemented with in situ measurements enables to observe the evolution of mesoscale eddies in case there is no optical remote sensing data available (i.e. under cloud cover).

Index Terms— SAR, Mesoscale eddy, SST, chlorophyll a, Baltic Sea

1. INTRODUCTION

The summer coastal upwelling is an important physical process typically bringing cold and nutrient-rich deeper water to the surface layer. Offshore transport of upwelled water is mostly caused by mesoscale structures – filaments and eddies that are formed due to the instability of alongshore baroclinic jet and related thermohaline front [9]. Satellite sea surface temperature (SST) images allow determining upwelling characteristics and related mesoscale structures over the large sea areas. SST images in the Baltic Sea region have been analyzed by [3], [6] and [7] to determine upwelling parameters. However, due to the high cloudiness level in the Baltic Sea region relatively small fraction (10%-50%) of useful SST images is suitable for processing [4]. Since SAR data is not influenced by sun illumination and atmosphere it provides additional information as it enables to monitor the sea surface in cloudy conditions and during the night time. Therefore the use of SAR data for investigating dynamics of the whole upwelling cycle including related filaments and eddies should be considered.

The aim of current study was to examine how temperature differences and structures of natural film affect the

manifestation of cold mesoscale eddies on SAR images by using complementary multi-sensor data. Three types of sensors/data (SAR, optical remote sensing and in situ measurements) were used to observe the upwelling related mesoscale eddies in the western Gulf of Finland (Baltic Sea) in September 2008.

2. DATA

For detection of cold upwelling related eddies from SAR images additional information about sea surface temperature and chlorophyll a field for the region is needed. MODIS (Moderate Resolution Imaging Spectroradiometer) data (SST and ocean color) and in situ measurements of surface layer temperature, turbidity and chlorophyll a concentration along transect between Travemünde-Helsinki were used.

2.1. SAR

Two ASAR (Advanced Synthetic Aperture Radar) wide swath images from the Baltic Sea region were acquired at 09.04 (UTC time is used in this study) on 24 September and at 20.00 on 25 September 2008. The pixel spacing of SAR data was ~75 m. The images were co-registered after the sigma nought (σ^0) values were calculated from intensity. For speckle reduction a 3 by 3 pixel mean filter was applied on the images.

2.2. MODIS

MODIS data (with spatial resolution of ~1 km) from satellites Terra and Aqua were used in this study to describe the SST field in the north-eastern Baltic Sea. Three standard MODIS SST products with acquisition times at 10.05 and 11.55 of 23 September and at 11.00 of 24 September were available.

Chlorophyll a concentration data from MODIS imagery were also used for interpretation of SAR data. Although the standard MODIS ocean color product (OC3) strongly overestimates chlorophyll a concentration in case 2 waters (the Baltic Sea) it can be used to estimate the relative concentration differences.

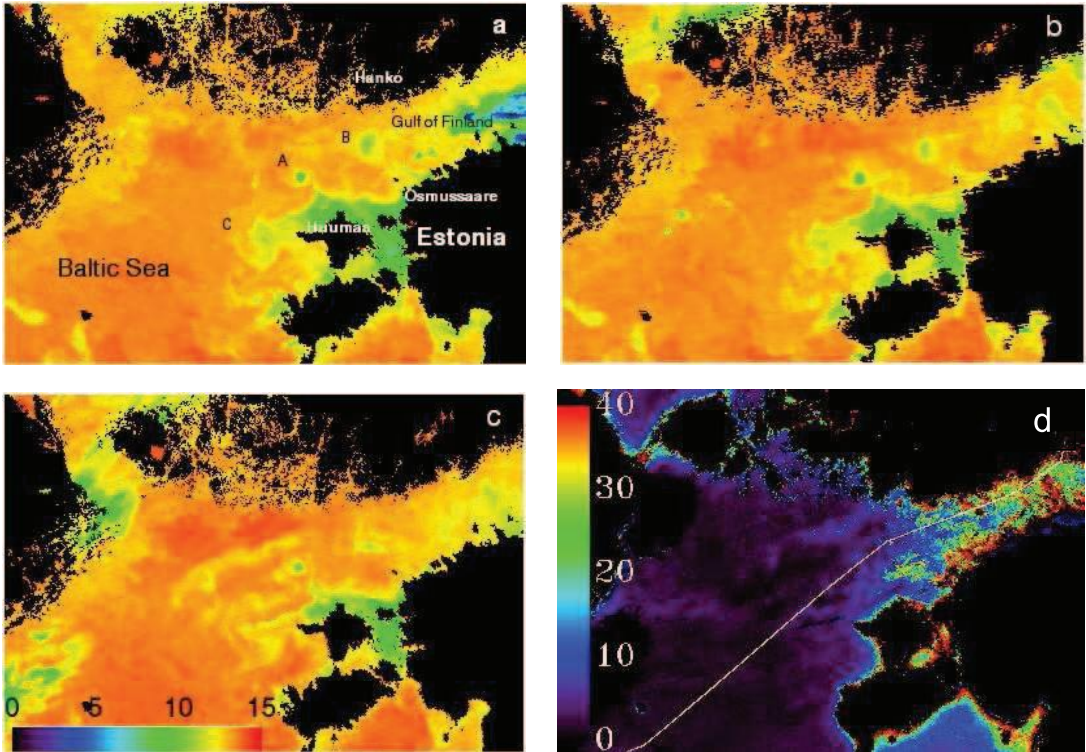


Figure X1. Modis SST images on 23 September at 10.05 (a), 23 September at 11.55 (b) and 24 September 2008 at 11.00 (c). Modis chlorophyll a concentration product (OC3) on 24 September to illustrate the relative concentration differences (d). Transect of in situ measurements is marked as white line (d).

2.3. In situ measurements

In situ temperature, chlorophyll a and turbidity data collected unattended on passenger ferry (Alg@line project) passing the region on route Travemünde-Helsinki were used to examine remote sensing data [5]. The data recording interval was 20 s, giving the horizontal resolution in a range from 150 to 200 m. Thus, Alg@line and SAR data have approximately the same spatial resolution. Time window of analyzed part of measurements along the transect (crossing the area under investigation on SAR scene) was from 15.30 on 24 September to 00.30 on 25 September.

3. METHODS

In order to analyze the manifestation of temperature and chlorophyll a differences on SAR images remote sensing data was compared with in situ measurements. SAR and MODIS data values that coincided with the measurement point along the transect were extracted for comparison.

Due to the lower incidence angle values (masks the signal from phenomena on sea surface) the data in the western part of SAR image (latitude and longitude higher than 59.5 N and 22.5 E) on 24 September were excluded and the area under investigation ranged from 58.2° to 59.5° N and from 19.8° to 23.5° E. On the SAR image from 25 September the area under investigation ranged from 58.2° to 59.5° N and from 19.8° to 24.0° E. Correlation coefficients were calculated to characterize the relation between SAR and in situ measured data along transect. Before the correlation coefficients were found the locations of spikes (eddies and low temperature areas corresponding to the low σ^0 values) were determined from both graphs to detect the difference caused by discrepancy in recording times.

4. RESULTS AND DISCUSSION

An upwelling can be seen along the northern coast of Hiiu Island on MODIS SST images (Figure 1). Wind data from the meteorological station on the NW coast of Estonia (59.25° N, 23.66° E) showed that upwelling

favorable wind blew from 20 to 23 September. As a result three upwelling related eddies (marked as A, B, and C) can be detected on SST images on 23 September (Figure 1a). The minimum temperature values in the center of eddy (A) were 9.6 °C at 10.05 and 9.5 °C at 11.55 on 23 September. On 24 September at 11.00 the corresponding temperature was 10.0 °C. The surrounding water had temperature value around 13.5 °C on all three images. Another eddy (C) can be seen on the line between Osmussaari Island and Hanko peninsula (Figure 1). The minimum temperature values in the eddy centre were 10.3, 11.0 and 11.2 °C on three consecutive images. The temperature of surrounding water was ~13.4 °C. On MODIS SST image from 23 September a weak eddy (B) can be seen (Figure 1a, Figure 1b). By 24 September the eddy has started to decay (Figure 1c). However, colder water was still present in the eddy region. The minimum temperature values in the eddy centre increased in time. On 23 September the values were 10.3 and 10.8 °C, while on 24 September the temperature reached 11.5 °C. The surrounding water temperature was 13.5 °C. In addition to temperature the chlorophyll a concentration differences were analyzed from MODIS imagery (Figure 1d). Comparison of MODIS chlorophyll a (Figure 1d) with in situ chlorophyll a measurements (Figure 3b) confirmed that MODIS ocean color product (OC3) is overestimating the chlorophyll a concentration values. Chlorophyll a concentration front can be detected at the entrance of the Gulf of Finland from in situ measurements and MODIS data. Two of the three eddies (A and C) were captured on SAR images on 24 and 25 September at the entrance of the Gulf of Finland (Figure 2a, Figure 2b). Also the areas that are covered with upwelling water (region of eddy B) are detected as low backscatter regions. The scale of the eddy (A) detected on SAR images on 24 September was about 25 km. The backscatter difference between eddy centre and surrounding water was ~12 db while on the following day (25 September) the difference was ~11 db. Since wind conditions were similar (wind speed was ~3 m/s) during the acquisition of the SAR images then it can be expected that backscatter differences from image to image were not caused by wind field differences. On 24 September the eddy C appeared as stretched in E-W direction and the scale in that direction was ~27 km. The scale of the eddy in the N-W direction was ~13 km. The difference of σ^0 value between eddy centre and surrounding area was ~10 db. Eddy that was marked as C was also detectable on 25 September when the difference between eddy centre and surrounding area was ~6 db. The scale of the eddy was ~13 km in NE-SW direction and ~10 km in NW-SE direction.

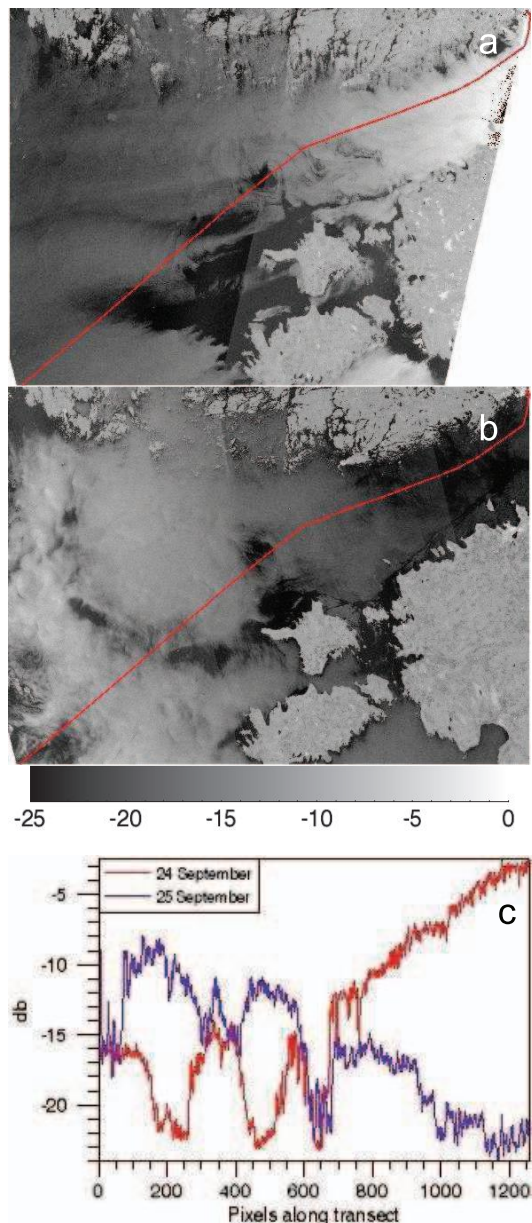


Figure 2. SAR images on 24 September at 09.04 (a) and 25 September at 20.00 (b). Transect is marked as red line on both images. σ^0 values along the transect (c).

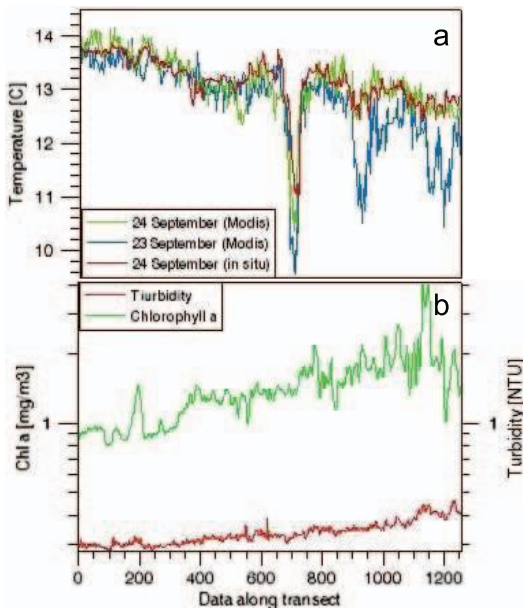


Figure 3. In situ measurements of temperature and MODIS SST values along the transect (from centre of Baltic Sea to Gulf of Finland) on 23 and 24 September (a). Chlorophyll a and turbidity data along transect on 24 September (b). Logarithmic scale.

Comparison of data sets showed accordance between SAR and in situ data. The low backscatter areas on SAR images are well correlated with chlorophyll a, temperature and turbidity data. The maximum and minimum values are at the same locations on SAR and in situ temperature images (Figure 2, Figure 3c). The correlation coefficient between these two datasets on 24 September was 0.19 and between the in situ temperature on 24 September and SAR backscatter on 25 September the value was 0.52. SAR data along the transect correlated better with chlorophyll a and turbidity measurements. For the SAR image from 24 September the corresponding correlations coefficients were 0.65 and 0.63. For radar image that was acquired on 25 September the values were 0.70 and 0.73.

[2] and [8] have shown that changes in SST field affect the radar backscatter through changes in air-sea boundary layer stability. This effect was also observed on remote sensing images from the 24 September (Figure 1c, Figure 2a). On the other hand [1] showed that in case the presence of surface slicks (i.e. high chlorophyll concentration) the effect of temperature is secondary. This could explain why SAR data correlated better with measurements of biological parameters than with temperature data.

5. CONCLUSIONS

SAR data complemented with operational high resolution in situ data provides a good basis for monitoring the evolution of mesoscale eddies in regions where cloud cover limits the use of optical remote sensing images. Current study showed that the upwelling related cold eddies can be detected from radar imagery. The comparison of remote sensing data and in situ measurements showed that the correlation coefficient between SAR data and biological parameters in low/moderate wind conditions can reach up to ~0.7 which exceeds the corresponding value between SAR backscatter and SST.

ACKNOWLEDGEMENTS

The study was supported by Estonian Science Foundation grants ETF7467 and ETF7581. ASAR data was provided by European Space Agency (ESA) and Alg@line data was provided by Finnish Environment Institute (SYKE).

REFERENCES

- [1] Clemente-Colon P., Yan X-H. „Observations of East Coast upwelling conditions in synthetic aperture radar imagery”, *IEEE Transactions on Geoscience and Remote Sensing*, Vol. 37(1), 239–248, 1999. Digital Object Identifier 10.1109/36.789620
- [2] C. A. Friehe, W. J. Shaw, D. P. Rogers, K. L. Davidson, W. G. Large, S. A. Stage, G. H. Crescenti, S. J. S. Khalsa, G. H. Greenhunt, and F. Li, “Air-sea fluxes and surface layer turbulence around a sea surface temperature front”, *J. Geophys. Res.*, vol. 96, 8593–8609, 1991.
- [3] M. Kahru, B. Hakansson, O. Rud, “Distribution of the sea-surface temperature fronts in the Baltic Sea as derived from satellite imagery”, *Cont. Shelf Res.*, Vol 15, 663-679, 1995
- [4] A. Krężel, M. Ostrowski, M. Szymelfenig, “Sea surface temperature distribution during upwelling along the Polish Baltic coast”, *Oceanologia*, Vol. 47, 415-432, 2005
- [5] J. Pulliainen, J. Vepsäläinen, S. Kaitala, M. Hallikainen, K. Kallio, V. Fleming and P. Maunula, „Regional water quality mapping through the assimilation of spaceborne remote sensing data to ship-based transect observations”. *J. Geophys. Res.*, Vol 109, C12009, 2004. doi: 10.1029/2003JC002167.
- [6] H. Siegel, M. Gerth, R. Rudloff, G. Tschersich G, “Dynamic features in the western Baltic Sea investigated using NOAA-AVHRR data”, *Dt. hydrogr. Z.*, Vol. 46, 191-209, 1994
- [7] R. Uiboupin, J. Laanemets, “Upwelling characteristics derived from satellite sea surface temperature data in the Gulf of Finland, Baltic Sea”, *Boreal Env. Res.* Vol 14(2), 297-304, 2009
- [8] Q. Zheng, X.-H. Yan, N. E. Huang, V. Klemas, and J. Pan, “The effect of water temperature on radar scattering from the water surface: An X-band laboratory study,” *The Global Atmos. Ocean Syst.*, Vol. 5, 273–294, 1997.
- [9] V. Zhurbas, J. Laanemets, E. Vahtera, “Modeling of the mesoscale structure of coupled upwelling/downwelling events and the related input of nutrients to the upper mixed layer in the Gulf of Finland, Baltic Sea”, *J. Geophys Res.*, Vol. 113, 1–8, 2008.

ABSTRACT

The sea surface temperature (SST) and chlorophyll *a* (Chl *a*) fields during series of upwelling events in the Gulf of Finland were investigated using remote sensing imagery from optical, infra-red, and radar sensors. Upwelling caused by the along-shore wind forcing typically brings cold and nutrient-rich deeper water to the surface layer, which may promote phytoplankton (cyanobacteria) blooms. The combined use of remote sensing imagery complemented with in situ and wind data provides information about SST fields and upwelling-related blooms as well as the locations and scales of upwelling fronts, filaments, and eddies.

The remote sensing data used in the current study originated from the following sensors: Moderate Resolution Imaging Spectroradiometer (MODIS), Medium Resolution Imaging Spectrometer (MERIS), and Advanced Synthetic Aperture Radar (ASAR). In order to estimate the suitability of remote sensing data for monitoring SST and Chl *a* fields in dynamic conditions, the satellite imagery was compared with in situ measurements. Comparison between MODIS SST retrieval and flow-through (FT) temperature showed a good correlation ($R > 0.96$), with an root mean square difference of $0.46\text{ }^{\circ}\text{C}$. A warm bias of $0.24\text{ }^{\circ}\text{C}$ was observed between the remote sensing SST and the FT temperature. It was shown that FT temperature measurements from a depth of 4 m could be used for validation of SST data in cases when the wind speed was over 5 m s^{-1} as the bias is reduced significantly compared to the low wind conditions. The Chl *a* concentration obtained from MERIS data using the FUB Case 2 waters processor was well correlated with in situ Chl *a* ($r^2 = 0.67$), but was underestimated on average by 25%.

The upwelling characteristics in the Gulf of Finland observed from MODIS SST imagery (June–September, 2000–2006) showed that upwelling events occurred more often along the northern coast of the Gulf and covered larger areas (19% of the Gulf area) compared to the southern Gulf (13%). Upwelling events were more extensive in the western part of the Gulf than in the eastern part. During the extreme upwelling, nearly 40% of the Gulf area was covered by upwelling water. Temperature differences between upwelling water and surrounding water were up to $15\text{ }^{\circ}\text{C}$. Due to the different cumulative wind stress and different topographies of the northern and southern coasts of the Gulf, the upwelling characteristics differed in the following way: (1) the upwelling events off the northern coast were more extensive and the upwelling water covered larger areas of the coastal sea, and (2) the upwelling filaments were predominantly observed off the northern coast.

Synthetic Aperture Radar (SAR) data (September 2008) allowed the diameter of the eddy core and the diameter of the eddy rotation field to be estimated. The study showed that the SST differences of $2\text{--}3.5\text{ }^{\circ}\text{C}$ resulted in attenuation of NRCS (normalized radar cross section) in a range of $10\text{--}12\text{ dB}$ in the region of the upwelling-related eddy.

Spatio-temporal variability of Chl *a* caused by a sequence of upwelling events in July (along the northern coast) and August (along the southern coast) of 2006 in the Gulf was investigated using MERIS, MODIS, and in situ data. The spatio-temporal variability of Chl *a* showed the evident influence of coupled upwelling and downwelling events and related filaments. The variability of Chl *a* was largest in the western and central parts of the Gulf, where mesoscale activity was the highest. Upwelling events had only a minor influence in the eastern part of the Gulf, where Chl *a* concentrations were relatively high and persistent throughout the study period. The highest Chl *a* concentrations (up to 14 mg m⁻³) along the northern coast were observed about two weeks after the upwelling peak. Comparison of the upwelling areas on the SST images and post-upwelling high Chl *a* areas on MERIS images showed structural similarities. The upwelling area along the northern coast (4879 km²) and the high Chl *a* area (5526 km²) about two weeks later were roughly coincident. The high Chl *a* values were likely induced by (1) growth of phytoplankton promoted by nutrient input, and (2) the northward Ekman transport of surface waters caused by easterly wind-forcing at the beginning of August.

RESÜMEE

Käesolevas töös uuriti apvellingutega seotud merepinna temperatuuri ja klorofüllü kontsentratsiooni muutusi Soome lahes, kasutades kaugseire andmeid. Piki kallast puhuvast tuulest põhjustatud apvelling toob veesamba sügavamatest kihtidest pinnakihti külma ja toitainerikast vett, mis on üheks eelduseks fütoplanktoni (sinivetikate) õitsenguks. Kaugseire andmete, kontaktmõõtmiste ja tuule andmete kooskasutamine võimaldab saada informatsiooni nii merepinna temperatuuri (SST) väljade, apvellingutega seotud fütoplanktoni õitsengute kui ka apvellinguga seotud keeriste ja filamentide mastaapide kohta.

Antud töös kasutati kaugseire andmeid, mis pärinevad järgmistelt satelliitsensoritelt: MODIS, Envisat/MERIS ja Envisat/ASAR. Hindamaks kaugseire andmete sobivust apvellingutega seotud merepinna temperatuuri ja klorofüllü kontsentratsiooni muutlikkuse jälgimiseks teostati võrdlev analüüs satelliidi andmete ja kontaktmõõtmiste vahel. MODIS-e SST andmed ja läbivoolusüsteemiga mõõdetud temperatuuri andmed olid heas korrelatsioonis ($R > 0,96$) ning ruutkeskmine hälve oli $0,46\text{ }^{\circ}\text{C}$. Võrdlusest selgus, et MODIS ülehindas süstemaatiliselt $0,24\text{ }^{\circ}\text{C}$ võrra merepinna temperatuuri väärtusi. Ka näitasid võrdluse tulemused, et 4 m sügavuselt läbivoolu süsteemiga kogutud temperatuuri andmeid saab kasutada kaugseire andmete valideerimiseks vaid juhul, kui tuule kiirus on üle 5 m s^{-1} , sest siis vähenes ruutkeskmine hälve kahe erineva mõõtmismeetodiga saadud temperatuuri ridade vahel. Klorofüllü kontsentratsiooni hinnangud, mis saadi kasutades Free University of Berlin poolt välja töötatud algoritmi optiliselt komplekssete vete jaoks, olid küll heas korrelatsioonis kontaktmõõtmistega ($r^2 > 0,96$), kuid alahindas kontsentratsiooni väärtusi keskmiselt 25%.

SAR andmete analüüs võimaldas määrata apvellinguga seotud keerise külma tuuma ja keerise kiirusvälja mõõtmeid. Samuti on näidatud, et merepinna temperatuuri kontrast $2\text{--}3,5\text{ }^{\circ}\text{C}$ apvellingu piirkonnas põhjustab NRCS (*normalized radar cross section*) nõrgenemise $10\text{--}12\text{ dB}$.

Merepinna temperatuuri piltide pealt määratud apvellingu parameetrite kohaselt esinesid apvellingu sündmused tihedamini Soome lahe põhjakaldal, kus nad katsid keskmiselt 19% lahe pindalast. Keskmine lõunakalda apvellingu veega kaetud pindala oli 13% lahe pindalast. Ekstreemsetel juhtumitel võib kuni 40% Soome lahe pindalast olla kaetud apvellingu veega. Apvellingud on ulatuslikumad Soome lahe lääne osas kui idapoolses lahe osas. Temperatuuri erinevused apvellingu poolt pinna kihti toodud vee ja seda ümbritseva vee vahel ulatus kuni $15\text{ }^{\circ}\text{C}$. Erineva atmosfääri mõju ning lahe põhja- ja lõunakalda topograafia iseärasuste tõttu erinesid apvellingu parameetrid järgnevalt: 1) apvellingud lahe Soome rannikumeres olid ulatuslikumad ja apvellingu vesi kattis suurema osa rannikumerest ja 2) apvellingu filamentid tekkisid põhiliselt Soome rannikumere apvellingute korral.

Apvellingute mõju klorofüllil välja ajalis-ruumilisele muutlikkusele Soome lahes uuriti 2006. a. suviste MERIS-e, MODIS-e ja välimõõtmiste andmete alusel. Juulis oli apvelling lahe põhjapoolses rannikumeres ja augustis lõunapoolses rannikumeres. MERIS-e klorofüllil kontsentratsiooni jaotuste analüüs näitas, et klorofüllil ajalis-ruumilises muutlikkuses kajastusid selgelt apvellingu ja daunvellingu sündmuste mõjud. Klorofüllil kontsentratsiooni muutlikkus oli suurim lahe lääne- ja keskosas, kus mesomastaapsete protsesside mõju oli suurim. Apvellingute mõju klorofüllil kontsentratsioonile oli väiksem lahe idapoolses osas, kus kontsentratsioonid olid püsivalt suhteliselt kõrged kogu vaadeldud perioodi vältel. Kõrgeimad klorofüllil kontsentratsiooni väärtused (kuni 14 mg m^{-3}) esinesid Soome lahe põhjapoolses rannikumeres kaks nädalat peale apvellingu sündmuse tippu. Kõrged klorofüllil kontsentratsioonid olid tekitatud (1) apvellinguga ülakihti toodud toitainete põhjustatud fütoplanktoni kasvust ja (2) augusti alguses esinenud idakaare tuulte poolt genereeritud põhjasuunalisest Ekmani transpordist. Apvellinguaegsete merepinna temperatuuri piltidel ja apvellingujärgsete klorofüllil kontsentratsiooni piltidel olid sarnased struktuurid ja ruumiline ulatus. Lahe põhjakalda apvellingu pindala (4879 km^2) ja kaks nädalat hiljem tekkinud kõrge klorofüllil kontsentratsiooniga ala (5526 km^2) olid ligikaudu võrdsed. Kõrge klorofüllil kontsentratsiooniga filamentide asukohad langesid kokku põhja kalda apvellingu külmade filamentide asukohtadega. Intensiivse Soome lahe lõunakalda apvellingu korral langesid madala klorofüllil kontsentratsiooniga alad kokku külma apvellingu veega kaetud piirkondadega (k.a. filamendid).

ELULOOKIRJELDUS

1. Isikuandmed

Ees- ja perekonnanimi Rivo Uiboupin
Sünniaeg ja -koht 12.05.1982, Järvakandi
Kodakondsus Eesti

2. Kontaktandmed

Address Akadeemia tee 15a, 12618 Tallinn, Estonia
E-posti aadress rivo.uiboupin@msi.ttu.ee

3. Hariduskäik

Õppeasutus	Lõpetamise aeg	Haridus (eriala/kraad)
Tallinna Tehnikaülikool	2008	Tehniline füüsika/ magistri kraad

4. Keelteoskus (alg-, kesk- või kõrgtase)

Keel	Tase
Eesti	Emakeel
Inglise	Kõrgtase
Vene	Algtase

5. Täiendusõpe

Õppimise aeg	Täiendusõppe läbiviija nimetus

6. Teenistuskäik

Töötamise aeg	Tööandja nimetus	Ametikoht
2005–...	Tallinna Tehnikaülikooli Meresüsteemide instituut	Insener
2009	ESA/ESRIN, Kaugseire teadus ja rakendus osakond	Stažöör

7. Teadustegevus-publikatsioonid Eesti Teadusinfosüsteemi klassifikaatori järgi

1.1

-Uiboupin, R., Laanemets, J., Sipelgas, L., Raag, L., Lips, I. and Buhhalko, N. 2012. Monitoring the effect of upwelling on the chlorophyll a distribution in the Gulf of Finland (Baltic Sea) using remote sensing and in situ data .*Oceanologia*, 54(3), 395 - 419.

-Uiboupin, R. and Laanemets, J. 2009. Upwelling characteristics derived from satellite sea surface temperature data in the Gulf of Finland, Baltic Sea. *Boreal Environment Research*, 14(2), 297–304.

-Myrberg, K., Lehmann, A., Raudsepp, U., Szymelfenig, M., Lips, I.; Lips, U., Matciak, M., Kowalewski, M., Krężel, A., Burska, D., Szymanek, L., Ameryk, A., Bielecka, L., Bradtke, K., Gałkowska, A., Gromisz, S., Jędrasik, J., Kaluźny, M., Kozłowski, Ł., Krajewska-Sołtys, A., Ołdakowski, B., Ostrowski, M., Zalewski, M., Andrejev, O., Suomi, I., Zhurbas, V., Kauppinen, O-K., Soosaar, E., Laanemets, J., Uiboupin, R., Talpsepp, L., Golenko, M.; Golenko, N., Vahtera, E. (2008). Upwelling events, coastal offshore exchange, links to biogeochemical processes – Highlights from the Baltic Sea Science Congress, March 19–22, 2007 at Rostock University. *Oceanologia*, 50(1), 95–113.

1.2

-Sipelgas, L., Raudsepp, U. and Uiboupin, R. 2008. Optical and physical properties of coastal water and their relations to radar (ASAR) data – case study of Muuga Bay in the Gulf of Finland. *Estonian Journal of Ecology*, 185–197.

-Uiboupin, R. and Sipelgas, L. (2007). Comparison of satellite sea surface temperature with in situ surface layer temperature. *Proceedings of the Estonian Academy of Sciences. Biology, Ecology*, 56(1), 47–56.

3.1

- Uiboupin, R. and Arino, O. 2010. Study of snowmelt impact on SST and TSM fields in the coastal zone of Barents Sea. In: *Proceedings of International Geoscience and Remote Sensing Symposium: Geoscience and Remote Sensing Symposium, 2009 IEEE International, Honolulu, 25–30 July 2010. IEEE, 2010, 4212–4215.*

-Sipelgas, L., Uiboupin, R. and Raudsepp, U. 2010. Monitoring environmental conditions in Muuga harbor using Envisat MERIS and ASAR data. *Geoscience and Remote Sensing Symposium (IGARSS), USA, 2010, 2010, 409–412.*

-Uiboupin, R., Axell, L., Raudsepp, U. and Sipelgas L. 2010. Comparison of operational ice charts with satellite based ice concentration products in the Baltic Sea. In: *IEEE Xplore: 4th IEES/OES Baltic Symposium, Riga, Latvia, August 25–27, 2010. IEEE-Inst Electrical Electronics Engineers Inc, 2010, 1–8.*

-Haran, G., Raudsepp, U., Alari, V., Uiboupin, R., Sipelgas, L. and Erm, A. 2010. Operational observations methods during offshore sand mining – case study in Tallinn Bay, the southern Gulf of Finland. IEEE/OES Baltic 2010 International Symposium Integrated Oceanographic Observation Systems and Data Bases for Climate Change Research, August 25–27, 2010, Riga, Latvia (1–11).

-Anderson, S., Raudsepp, U. and Uiboupin, R. 2010. Oil Spill statistics from SAR images in the North Eastern Baltic Sea ship route in 2007–2009. In: Geoscience and Remote Sensing Symposium (IGARSS), 2010 IEEE International: IGARSS 210, Hawaii 25.07–30.07.2010. IEEE Geoscience and Remote Sensing Society, 2010, 1883–1886.

-Anderson, S., Uiboupin, R., Verjovkina, S. and Raudsepp, U. (2010). SAR imagery and Seatrack Web as Decision making tools for illegal oil spill combating – a case study. 4th IEEE/OES Baltic Symposium Riga, Latvia, August 25–27, 2010. IEEE Geoscience and Remote Sensing Society, 2010, 1–6.

- Uiboupin, R. and Laanemets, J. 2009. Observation of mesoscale eddies by using SAR data complemented with optical remote sensing and in situ measurements. In: Proceedings of International Geoscience and Remote Sensing Symposium: Geoscience and Remote Sensing Symposium, 2009 IEEE International, Cape Town, 12–17 July 2009 . IEEE, 2009, (1), 224–227.

- Uiboupin, R., Sipelgas, L. and Raudsepp, U. 2009. Sea ice concentration and type analysis from dual pol Radarsat-2 and Modis images in the Baltic Sea. In: IEEE Proceedings of International Geoscience and Remote Sensing Symposium: International Geoscience and Remote Sensing Symposium. IEEE, 2009, (2), 590–593.

-Uiboupin, R., Raudsepp, U. and Sipelgas, L. 2008. Detection of oil spills on SAR images, identification of polluters and forecast of the slicks trajectory. US/EU-Baltic Symposium "Ocean Observations, Ecosystem-Based Management & Forecasting", Tallinn, 27–29 May, 2008. IEEE-Inst Electrical Electronics Engineers Inc, 2008, 270–274.

-Sipelgas, L. and Uiboupin, R. 2007. Elimination of oil spill like structures from radar image using MODIS data. In: Proceedings of Geoscience and Remote Sensing Symposium, 2007. IGARSS 2007. IEEE International. 23–28 July 2007: IGARSS 2007, 23–28 July 2007, Barcelona. IEEE, 2007, 429–431.

3.2

-Uiboupin, R. and Raudsepp, U. 2008. Õlireostuse tuvastamine SAR kujutiselt. Väljataga, K.; Kaukver, K. (Toim.). Kaugseire Eestis (195–204). Tallinn: Keskkonnaministeeriumi Info- ja Tehnokeskus.

8. Kaitstud lõputööd

Magistrikraad, 2008, Satelliidi merepinna temperatuuri andmetest määratud apvellingu parameetrid Soome lahes, Tallinna Tehnikaülikool, Meresüsteemide Instituut

9. Teadustöö põhisuunad

Mere kaugseire, apvellingud ja apvellingutega seotud mesomastaapsed protsessid.

10. Uurimisprojektid

Eesti teadusfondi grantid

- Apvellingud Soome lahes ja nendega seotud toitainete transport, 2008-2011.
- Jää karakteristikute sünoptiline muutlikkus Soome lahes kasutades kaugseire ja numbrilise modelleerimise meetodeid, 2008-2011.
- Lainetuse tekitatud hoovused ja meretaseme tõus rannikumeres, 2011-2014.

Siseriiklikud projektid

- Mere õlireostuse varase avastamise ja leviku prognoosi tehnoloogia, 2006-2008 (EAS).

Rahvusvahelised projektid

- GMES merealaste tuumteenuste arendamine ja pre-operatiivne valideerimine (MyOcean), 2009-2012 (EU/FP7).
- Süvendustööde keskkonnamõju seire sadamates, 2011-2012 (ESA- European Space Agency).
- Innovaatiline lainetuse prognoosisüsteem laevade ohutuks navigatsiooniks, 2011-2014 (EU/EUROSTARS programm).
- Liivi laht kui tuuleenergia ressurss, 2010-2012 (EU/INTERREG/EST-LAT programme).
- Nafta jääs – HIROMB'i ja STW prognooside parandamine, 2008 (SIDA).

CURRICULUM VITAE

1. Personal data

Name Rivo Uiboupin
Date and place of birth 12 May 1982, Järvakandi

2. Contact information

Address Akadeemia tee 15a, 12618 Tallinn, Estonia
E-mail rivo.uiboupin@msi.ttu.ee

3. Education

Educational institution	Graduation year	Education (field of study/degree)
Tallinn University of Technology	2008	Engineering Physics/MSc

4. Language competence/skills (fluent; average, basic skills)

Language	Level
Estonian	Native
English	Fluent
Russian	Basic skills

5. Special courses

Period	Educational or other organisation

6. Professional employment

Period	Organisation	Position
2005–to date	Marine Systems Institute at Tallinn University of Technology	Engineer
2009	ESA/ESRIN, Earth Observation Science and Applications Department	Trainee

7. Scientific work – Publications according to Estonian Research Information System.

1.1 (Articles indexed by the ISI WEB of Science)

-Uiboupin, R., Laanemets, J., Sipelgas, L., Raag, L., Lips, I. and Buhhalko, N. 2012. Monitoring the effect of upwelling on the chlorophyll a distribution in the Gulf of Finland (Baltic Sea) using remote sensing and in situ data .*Oceanologia*, 54(3), 395 - 419.

-Uiboupin, R. and Laanemets, J. 2009. Upwelling characteristics derived from satellite sea surface temperature data in the Gulf of Finland, Baltic Sea. *Boreal Environment Research*, 14(2), 297 - 304.

-Myrberg, K., Lehmann, A., Raudsepp, U., Szymelfenig, M., Lips, I.; Lips, U., Matciak, M., Kowalewski, M., Krężel, A., Burska, D., Szymanek, L., Ameryk, A., Bielecka, L., Bradtke, K., Gałkowska, A., Gromisz, S., Jędrasik, J., Kaluźny, M., Kozłowski, Ł., Krajewska-Sołtys, A., Ołdakowski, B., Ostrowski, M., Zalewski, M., Andrejev, O., Suomi, I., Zhurbas, V., Kauppinen, O-K., Soosaar, E., Laanemets, J., Uiboupin, R., Talpsepp, L., Golenko, M.; Golenko, N., Vahtera, E. (2008). Upwelling events, coastal offshore exchange, links to biogeochemical processes – Highlights from the Baltic Sea Science Congress, March 19 – 22, 2007 at Rostock University. *Oceanologia*, 50(1), 95 - 113.

1.2 (Pre-reviewed articles in other international research journals)

-Sipelgas, L., Raudsepp, U. and Uiboupin, R. 2008. Optical and physical properties of coastal water and their relations to radar (ASAR) data- case study of Muuga Bay in the Gulf of Finland. *Estonian Journal of Ecology*, 185 - 197.

-Uiboupin, R. and Sipelgas, L. (2007). Comparison of satellite sea surface temperature with in situ surface layer temperature. *Proceedings of the Estonian Academy of Sciences. Biology, Ecology*, 56(1), 47 - 56.

3.1 (Articles in proceedings indexed by the ISI WEB of Science)

- Uiboupin, R. and Arino, O. 2010. Study of snowmelt impact on SST and TSM fields in the coastal zone of Barents Sea. In: *Proceedings of International Geoscience and Remote Sensing Symposium: Geoscience and Remote Sensing Symposium, 2009 IEEE International, Honolulu, 25-30 July 2010. IEEE, 2010*, 4212 - 4215.

-Sipelgas, L., Uiboupin, R. and Raudsepp, U. 2010. Monitoring environmental conditions in Muuga harbor using Envisat MERIS and ASAR data. *Geoscience and Remote Sensing Symposium (IGARSS), USA, 2010*, 409 - 412.

-Uiboupin, R., Axell, L., Raudsepp, U. and Sipelgas L. 2010. Comparison of operational ice charts with satellite based ice concentration products in the Baltic

Sea. In: IEEE Xplore: 4th IEES/OES Baltic Symposium, Riga, Latvia, August 25-27, 2010. IEEE-Inst Electrical Electronics Engineers Inc, 2010, 1-8.

- Haran, G., Raudsepp, U., Alari, V., Uiboupin, R., Sipelgas, L. and Erm, A. 2010. Operational observations methods during offshore sand mining – case study in Tallinn Bay, the southern Gulf of Finland. IEEE/OES Baltic 2010 International Symposium Integrated Oceanographic Observation Systems and Data Bases for Climate Change Research, August 25–27, 2010, Riga, Latvia (1–11).

-Anderson, S., Raudsepp, U. and Uiboupin, R. 2010. Oil Spill statistics from SAR images in the North Eastern Baltic Sea ship route in 2007- 2009. In: Geoscience and Remote Sensing Symposium (IGARSS), 2010 IEEE International: IGARSS 210, Hawaii 25.07-30.07.2010. IEEE Geoscience and Remote Sensing Society, 2010, 1883 - 1886.

-Anderson, S., Uiboupin, R., Verjovkina, S. and Raudsepp, U. (2010). SAR imagery and Seatrack Web as Decision making tools for illegal oil spill combating- a case study. 4th IEEE/OES Baltic Symposium Riga, Latvia, August 25-27 2010. IEEE Geoscience and Remote Sensing Society, 2010, 1 - 6.

- Uiboupin, R. and Laanemets, J. 2009. Observation of mesoscale eddies by using SAR data complemented with optical remote sensing and in situ measurements . In: Proceedings of International Geoscience and Remote Sensing Symposium: Geoscience and Remote Sensing Symposium, 2009 IEEE International, Cape Town, 12-17 July 2009. IEEE, 2009, (1), 224 - 227.

- Uiboupin, R., Sipelgas, L. and Raudsepp, U. 2009. Sea ice concentration and type analysis from dual pol Radarsat-2 and Modis images in the Baltic Sea. In: IEEE Proceedings of International Geoscience and Remote Sensing Symposium: International Geoscience and Remote Sensing Symposium. IEEE, 2009, (2), 590 - 593.

-Uiboupin, R., Raudsepp, U. and Sipelgas, L. 2008. Detection of oil spills on SAR images, identification of polluters and forecast of the slicks trajectory. US/EU-Baltic Symposium "Ocean Observations, Ecosystem-Based Management & Forecasting", Tallinn, 27-29 May, 2008. IEEE-Inst Electrical Electronics Engineers Inc, 2008, 270 - 274.

-Sipelgas, L. and Uiboupin, R. 2007. Elimination of oil spill like structures from radar image using MODIS data. In: Proceedings of Geoscience and Remote Sensing Symposium, 2007. IGARSS 2007. IEEE International. 23-28 July 2007: IGARSS 2007, 23-28 July 2007, Barcelona, IEEE, 2007, 429 - 431.

3.2

-Uiboupin, R. and Raudsepp, U. 2008. Õlireostuse tuvastamin SAR kujutiselt. Väljataga, K.; Kaukver, K. (Editor). Kaugseire Eestis (195 - 204). Tallinn: Keskkonnaministeeriumi Info- ja Tehnokeskus.

8. Defended theses

Master's thesis, 2008, Upwelling characteristics derived from satellite sea surface temperature data in the Gulf of Finland, Tallinn University of Technology, Marine Systems Institute.

9. Main areas of scientific work/Current research topics

Marine remote sensing, upwelling, mesoscale physical processes.

10. Research projects

Estonian Science Foundation Grants

- Upwelling events and the related nutrient transport in the Gulf of Finland, 2008-2011.
- Synoptic-scale variations of ice characteristics in the Gulf of Finland using remote sensing and numerical modelling, 2008-2011.
- Wave induced currents and sea level setup in the coastal sea, 2011-2014.

National engineering projects

- Early detection and drift forecast of marine oil pollution, 2006-2008 (EAS).

International research projects

- Development and pre-operational validation of upgraded GMES Marine Core Services and capabilities (MyOcean), 2009-2012 (EU/FP7).
- Environmental monitoring of harbor dredging, 2011-2012 (ESA-European Space Agency).
- Advanced wave forecast for safe navigation of small vessels, 2011-2014 (EU/EUROSTARS programme).
- Gulf of Riga as a Resource for Wind Energy, 2010-2012 (EU/INTERREG EST-LAT programme).
- Oil in ice - improved forecasts in HIROMB and STW, 2008 (SIDA).

**DISSERTATIONS DEFENDED AT
TALLINN UNIVERSITY OF TECHNOLOGY ON
NATURAL AND EXACT SCIENCES**

1. **Olav Kongas**. Nonlinear Dynamics in Modeling Cardiac Arrhythmias. 1998.
2. **Kalju Vanatalu**. Optimization of Processes of Microbial Biosynthesis of Isotopically Labeled Biomolecules and Their Complexes. 1999.
3. **Ahto Buldas**. An Algebraic Approach to the Structure of Graphs. 1999.
4. **Monika Drews**. A Metabolic Study of Insect Cells in Batch and Continuous Culture: Application of Chemostat and Turbidostat to the Production of Recombinant Proteins. 1999.
5. **Eola Valdre**. Endothelial-Specific Regulation of Vessel Formation: Role of Receptor Tyrosine Kinases. 2000.
6. **Kalju Lott**. Doping and Defect Thermodynamic Equilibrium in ZnS. 2000.
7. **Reet Koljak**. Novel Fatty Acid Dioxygenases from the Corals *Plexaura homomalla* and *Gersemia fruticosa*. 2001.
8. **Anne Paju**. Asymmetric oxidation of Prochiral and Racemic Ketones by Using Sharpless Catalyst. 2001.
9. **Marko Vendelin**. Cardiac Mechanoenergetics *in silico*. 2001.
10. **Pearu Peterson**. Multi-Soliton Interactions and the Inverse Problem of Wave Crest. 2001.
11. **Anne Menert**. Microcalorimetry of Anaerobic Digestion. 2001.
12. **Toomas Tiivel**. The Role of the Mitochondrial Outer Membrane in *in vivo* Regulation of Respiration in Normal Heart and Skeletal Muscle Cell. 2002.
13. **Olle Hints**. Ordovician Scolecodonts of Estonia and Neighbouring Areas: Taxonomy, Distribution, Palaeoecology, and Application. 2002.
14. **Jaak Nõlvak**. Chitinozoan Biostratigraphy in the Ordovician of Baltoscandia. 2002.
15. **Liivi Kluge**. On Algebraic Structure of Pre-Operad. 2002.
16. **Jaanus Lass**. Biosignal Interpretation: Study of Cardiac Arrhythmias and Electromagnetic Field Effects on Human Nervous System. 2002.
17. **Janek Peterson**. Synthesis, Structural Characterization and Modification of PAMAM Dendrimers. 2002.
18. **Merike Vaher**. Room Temperature Ionic Liquids as Background Electrolyte Additives in Capillary Electrophoresis. 2002.
19. **Valdek Mikli**. Electron Microscopy and Image Analysis Study of Powdered Hardmetal Materials and Optoelectronic Thin Films. 2003.
20. **Mart Viljus**. The Microstructure and Properties of Fine-Grained Cermets. 2003.
21. **Signe Kask**. Identification and Characterization of Dairy-Related *Lactobacillus*. 2003

22. **Tiiu-Mai Laht.** Influence of Microstructure of the Curd on Enzymatic and Microbiological Processes in Swiss-Type Cheese. 2003.
23. **Anne Kuusksalu.** 2–5A Synthetase in the Marine Sponge *Geodia cydonium*. 2003.
24. **Sergei Bereznev.** Solar Cells Based on Polycrystalline Copper-Indium Chalcogenides and Conductive Polymers. 2003.
25. **Kadri Kriis.** Asymmetric Synthesis of C₂-Symmetric Bimorpholines and Their Application as Chiral Ligands in the Transfer Hydrogenation of Aromatic Ketones. 2004.
26. **Jekaterina Reut.** Polypyrrole Coatings on Conducting and Insulating Substrates. 2004.
27. **Sven Nõmm.** Realization and Identification of Discrete-Time Nonlinear Systems. 2004.
28. **Olga Kijatkina.** Deposition of Copper Indium Disulphide Films by Chemical Spray Pyrolysis. 2004.
29. **Gert Tamberg.** On Sampling Operators Defined by Rogosinski, Hann and Blackman Windows. 2004.
30. **Monika Übner.** Interaction of Humic Substances with Metal Cations. 2004.
31. **Kaarel Adamberg.** Growth Characteristics of Non-Starter Lactic Acid Bacteria from Cheese. 2004.
32. **Imre Vallikivi.** Lipase-Catalysed Reactions of Prostaglandins. 2004.
33. **Merike Peld.** Substituted Apatites as Sorbents for Heavy Metals. 2005.
34. **Vitali Syritski.** Study of Synthesis and Redox Switching of Polypyrrole and Poly(3,4-ethylenedioxythiophene) by Using *in-situ* Techniques. 2004.
35. **Lee Põllumaa.** Evaluation of Ecotoxicological Effects Related to Oil Shale Industry. 2004.
36. **Riina Aav.** Synthesis of 9,11-Secosterols Intermediates. 2005.
37. **Andres Braunbrück.** Wave Interaction in Weakly Inhomogeneous Materials. 2005.
38. **Robert Kitt.** Generalised Scale-Invariance in Financial Time Series. 2005.
39. **Juss Pavelson.** Mesoscale Physical Processes and the Related Impact on the Summer Nutrient Fields and Phytoplankton Blooms in the Western Gulf of Finland. 2005.
40. **Olari Ilison.** Solitons and Solitary Waves in Media with Higher Order Dispersive and Nonlinear Effects. 2005.
41. **Maksim Säkki.** Intermittency and Long-Range Structurization of Heart Rate. 2005.
42. **Enli Kiipli.** Modelling Seawater Chemistry of the East Baltic Basin in the Late Ordovician–Early Silurian. 2005.

43. **Igor Golovtsov**. Modification of Conductive Properties and Processability of Polyparaphenylene, Polypyrrole and polyaniline. 2005.
44. **Katrin Laos**. Interaction Between Furcellaran and the Globular Proteins (Bovine Serum Albumin β -Lactoglobulin). 2005.
45. **Arvo Mere**. Structural and Electrical Properties of Spray Deposited Copper Indium Disulphide Films for Solar Cells. 2006.
46. **Sille Ehala**. Development and Application of Various On- and Off-Line Analytical Methods for the Analysis of Bioactive Compounds. 2006.
47. **Maria Kulp**. Capillary Electrophoretic Monitoring of Biochemical Reaction Kinetics. 2006.
48. **Anu Aaspõllu**. Proteinases from *Vipera lebetina* Snake Venom Affecting Hemostasis. 2006.
49. **Lyudmila Chekulayeva**. Photosensitized Inactivation of Tumor Cells by Porphyrins and Chlorins. 2006.
50. **Merle Uudsemaa**. Quantum-Chemical Modeling of Solvated First Row Transition Metal Ions. 2006.
51. **Tagli Pitsi**. Nutrition Situation of Pre-School Children in Estonia from 1995 to 2004. 2006.
52. **Angela Ivask**. Luminescent Recombinant Sensor Bacteria for the Analysis of Bioavailable Heavy Metals. 2006.
53. **Tiina Lõugas**. Study on Physico-Chemical Properties and Some Bioactive Compounds of Sea Buckthorn (*Hippophae rhamnoides* L.). 2006.
54. **Kaja Kasemets**. Effect of Changing Environmental Conditions on the Fermentative Growth of *Saccharomyces cerevisiae* S288C: Auxo-accelerostat Study. 2006.
55. **Ildar Nisamedtinov**. Application of ^{13}C and Fluorescence Labeling in Metabolic Studies of *Saccharomyces* spp. 2006.
56. **Alar Leibak**. On Additive Generalisation of Voronoi's Theory of Perfect Forms over Algebraic Number Fields. 2006.
57. **Andri Jagomägi**. Photoluminescence of Chalcopyrite Tellurides. 2006.
58. **Tõnu Martma**. Application of Carbon Isotopes to the Study of the Ordovician and Silurian of the Baltic. 2006.
59. **Marit Kauk**. Chemical Composition of CuInSe_2 Monograin Powders for Solar Cell Application. 2006.
60. **Julia Kois**. Electrochemical Deposition of CuInSe_2 Thin Films for Photovoltaic Applications. 2006.
61. **Ilona Oja Açıık**. Sol-Gel Deposition of Titanium Dioxide Films. 2007.
62. **Tiia Anmann**. Integrated and Organized Cellular Bioenergetic Systems in Heart and Brain. 2007.

63. **Katrin Trummal.** Purification, Characterization and Specificity Studies of Metalloproteinases from *Vipera lebetina* Snake Venom. 2007.
64. **Gennadi Lessin.** Biochemical Definition of Coastal Zone Using Numerical Modeling and Measurement Data. 2007.
65. **Enno Pais.** Inverse problems to determine non-homogeneous degenerate memory kernels in heat flow. 2007.
66. **Maria Borissova.** Capillary Electrophoresis on Alkylimidazolium Salts. 2007.
67. **Karin Valmsen.** Prostaglandin Synthesis in the Coral *Plexaura homomalla*: Control of Prostaglandin Stereochemistry at Carbon 15 by Cyclooxygenases. 2007.
68. **Kristjan Piirimäe.** Long-Term Changes of Nutrient Fluxes in the Drainage Basin of the Gulf of Finland – Application of the PolFlow Model. 2007.
69. **Tatjana Dedova.** Chemical Spray Pyrolysis Deposition of Zinc Sulfide Thin Films and Zinc Oxide Nanostructured Layers. 2007.
70. **Katrin Tomson.** Production of Labelled Recombinant Proteins in Fed-Batch Systems in *Escherichia coli*. 2007.
71. **Cecilia Sarmiento.** Suppressors of RNA Silencing in Plants. 2008.
72. **Vilja Mardla.** Inhibition of Platelet Aggregation with Combination of Antiplatelet Agents. 2008.
73. **Maie Bachmann.** Effect of Modulated Microwave Radiation on Human Resting Electroencephalographic Signal. 2008.
74. **Dan Hüvonen.** Terahertz Spectroscopy of Low-Dimensional Spin Systems. 2008.
75. **Ly Villo.** Stereoselective Chemoenzymatic Synthesis of Deoxy Sugar Esters Involving *Candida antarctica* Lipase B. 2008.
76. **Johan Anton.** Technology of Integrated Photoelasticity for Residual Stress Measurement in Glass Articles of Axisymmetric Shape. 2008.
77. **Olga Volobujeva.** SEM Study of Selenization of Different Thin Metallic Films. 2008.
78. **Artur Jõgi.** Synthesis of 4'-Substituted 2,3'-dideoxynucleoside Analogues. 2008.
79. **Mario Kadastik.** Doubly Charged Higgs Boson Decays and Implications on Neutrino Physics. 2008.
80. **Fernando Pérez-Caballero.** Carbon Aerogels from 5-Methylresorcinol-Formaldehyde Gels. 2008.
81. **Sirje Vaask.** The Comparability, Reproducibility and Validity of Estonian Food Consumption Surveys. 2008.
82. **Anna Menaker.** Electrosynthesized Conducting Polymers, Polypyrrole and Poly(3,4-ethylenedioxythiophene), for Molecular Imprinting. 2009.
83. **Lauri Ilison.** Solitons and Solitary Waves in Hierarchical Korteweg-de Vries Type Systems. 2009.

84. **Kaia Ernits.** Study of In₂S₃ and ZnS Thin Films Deposited by Ultrasonic Spray Pyrolysis and Chemical Deposition. 2009.
85. **Veljo Sinivee.** Portable Spectrometer for Ionizing Radiation “Gammamapper”. 2009.
86. **Jüri Virkepu.** On Lagrange Formalism for Lie Theory and Operadic Harmonic Oscillator in Low Dimensions. 2009.
87. **Marko Piirsoo.** Deciphering Molecular Basis of Schwann Cell Development. 2009.
88. **Kati Helmja.** Determination of Phenolic Compounds and Their Antioxidative Capability in Plant Extracts. 2010.
89. **Merike Sõmera.** Sobemoviruses: Genomic Organization, Potential for Recombination and Necessity of P1 in Systemic Infection. 2010.
90. **Kristjan Laes.** Preparation and Impedance Spectroscopy of Hybrid Structures Based on CuIn₃Se₅ Photoabsorber. 2010.
91. **Kristin Lippur.** Asymmetric Synthesis of 2,2'-Bimorpholine and its 5,5'-Substituted Derivatives. 2010.
92. **Merike Luman.** Dialysis Dose and Nutrition Assessment by an Optical Method. 2010.
93. **Mihhail Berezovski.** Numerical Simulation of Wave Propagation in Heterogeneous and Microstructured Materials. 2010.
94. **Tamara Aid-Pavlidis.** Structure and Regulation of BDNF Gene. 2010.
95. **Olga Bragina.** The Role of Sonic Hedgehog Pathway in Neuro- and Tumorigenesis. 2010.
96. **Merle Randrüüt.** Wave Propagation in Microstructured Solids: Solitary and Periodic Waves. 2010.
97. **Marju Laars.** Asymmetric Organocatalytic Michael and Aldol Reactions Mediated by Cyclic Amines. 2010.
98. **Maarja Grossberg.** Optical Properties of Multinary Semiconductor Compounds for Photovoltaic Applications. 2010.
99. **Alla Maloverjan.** Vertebrate Homologues of Drosophila Fused Kinase and Their Role in Sonic Hedgehog Signalling Pathway. 2010.
100. **Priit Pruunsild.** Neuronal Activity-Dependent Transcription Factors and Regulation of Human *BDNF* Gene. 2010.
101. **Tatjana Knjazeva.** New Approaches in Capillary Electrophoresis for Separation and Study of Proteins. 2011.
102. **Atanas Katerski.** Chemical Composition of Sprayed Copper Indium Disulfide Films for Nanostructured Solar Cells. 2011.
103. **Kristi Timmo.** Formation of Properties of CuInSe₂ and Cu₂ZnSn(S,Se)₄ Monograin Powders Synthesized in Molten KI. 2011.

104. **Kert Tamm.** Wave Propagation and Interaction in Mindlin-Type Microstructured Solids: Numerical Simulation. 2011.
105. **Adrian Popp.** Ordovician Proetid Trilobites in Baltoscandia and Germany. 2011.
106. **Ove Pärn.** Sea Ice Deformation Events in the Gulf of Finland and This Impact on Shipping. 2011.
107. **Germa Väli.** Numerical Experiments on Matter Transport in the Baltic Sea. 2011.
108. **Andrus Seiman.** Point-of-Care Analyser Based on Capillary Electrophoresis. 2011.
109. **Olga Katargina.** Tick-Borne Pathogens Circulating in Estonia (Tick-Borne Encephalitis Virus, *Anaplasma phagocytophilum*, *Babesia* Species): Their Prevalence and Genetic Characterization. 2011.
110. **Ingrid Sumeri.** The Study of Probiotic Bacteria in Human Gastrointestinal Tract Simulator. 2011.
111. **Kairit Zovo.** Functional Characterization of Cellular Copper Proteome. 2011.
112. **Natalja Makarytsheva.** Analysis of Organic Species in Sediments and Soil by High Performance Separation Methods. 2011.
113. **Monika Mortimer.** Evaluation of the Biological Effects of Engineered Nanoparticles on Unicellular Pro- and Eukaryotic Organisms. 2011.
114. **Kersti Tepp.** Molecular System Bioenergetics of Cardiac Cells: Quantitative Analysis of Structure-Function Relationship. 2011.
115. **Anna-Liisa Peikolainen.** Organic Aerogels Based on 5-Methylresorcinol. 2011.
116. **Leeli Amon.** Palaeoecological Reconstruction of Late-Glacial Vegetation Dynamics in Eastern Baltic Area: A View Based on Plant Macrofossil Analysis. 2011.
117. **Tanel Peets.** Dispersion Analysis of Wave Motion in Microstructured Solids. 2011.
118. **Liina Kaupmees.** Selenization of Molybdenum as Contact Material in Solar Cells. 2011.
119. **Allan Olsper.** Properties of VPg and Coat Protein of Sobemoviruses. 2011.
120. **Kadri Koppel.** Food Category Appraisal Using Sensory Methods. 2011.
121. **Jelena Gorbatšova.** Development of Methods for CE Analysis of Plant Phenolics and Vitamins. 2011.
122. **Karin Viipsi.** Impact of EDTA and Humic Substances on the Removal of Cd and Zn from Aqueous Solutions by Apatite. 2012.
123. **David Schryer.** Metabolic Flux Analysis of Compartmentalized Systems Using Dynamic Isotopologue Modeling. 2012.
124. **Ardo Illaste.** Analysis of Molecular Movements in Cardiac Myocytes. 2012.
125. **Indrek Reile.** 3-Alkylcyclopentane-1,2-Diones in Asymmetric Oxidation and Alkylation Reactions. 2012.
126. **Tatjana Tamberg.** Some Classes of Finite 2-Groups and Their Endomorphism Semigroups. 2012.
127. **Taavi Liblik.** Variability of Thermohaline Structure in the Gulf of Finland in Summer. 2012.

128. **Priidik Lagemaa**. Operational Forecasting in Estonian Marine Waters. 2012.
129. **Andrei Errapart**. Photoelastic Tomography in Linear and Non-linear Approximation. 2012.
130. **Külliki Krabbi**. Biochemical Diagnosis of Classical Galactosemia and Mucopolysaccharidoses in Estonia. 2012.
131. **Kristel Kaseleht**. Identification of Aroma Compounds in Food using SPME-GC/MS and GC-Olfactometry. 2012.
132. **Kristel Kodar**. Immunoglobulin G Glycosylation Profiling in Patients with Gastric Cancer. 2012.
133. **Kai Rosin**. Solar Radiation and Wind as Agents of the Formation of the Radiation Regime in Water Bodies. 2012.
134. **Ann Tiiman**. Interactions of Alzheimer's Amyloid-Beta Peptides with Zn(II) and Cu(II) Ions. 2012.
135. **Olga Gavrilova**. Application and Elaboration of Accounting Approaches for Sustainable Development. 2012.
136. **Olesja Bondarenko**. Development of Bacterial Biosensors and Human Stem Cell-Based *In Vitro* Assays for the Toxicological Profiling of Synthetic Nanoparticles. 2012.
137. **Katri Muska**. Study of Composition and Thermal Treatments of Quaternary Compounds for Monocrystalline Solar Cells. 2012.
138. **Ranno Nahku**. Validation of Critical Factors for the Quantitative Characterization of Bacterial Physiology in Accelerostat Cultures. 2012.
139. **Petri-Jaan Lahtvee**. Quantitative Omics-level Analysis of Growth Rate Dependent Energy Metabolism in *Lactococcus lactis*. 2012.
140. **Kerti Orumets**. Molecular Mechanisms Controlling Intracellular Glutathione Levels in Baker's Yeast *Saccharomyces cerevisiae* and its Random Mutagenized Glutathione Over-Accumulating Isolate. 2012.
141. **Loreida Timberg**. Spice-Cured Sprats Ripening, Sensory Parameters Development, and Quality Indicators. 2012.
142. **Anna Mihhalevski**. Rye Sourdough Fermentation and Bread Stability. 2012.
143. **Liisa Arike**. Quantitative Proteomics of *Escherichia coli*: From Relative to Absolute Scale. 2012.
144. **Kairi Otto**. Deposition of In₂S₃ Thin Films by Chemical Spray Pyrolysis. 2012.
145. **Mari Sepp**. Functions of the Basic Helix-Loop-Helix Transcription Factor TCF4 in Health and Disease. 2012.
146. **Anna Suhhova**. Detection of the Effect of Weak Stressors on Human Resting Electroencephalographic Signal. 2012.
147. **Aram Kazarjan**. Development and Production of Extruded Food and Feed Products Containing Probiotic Microorganisms. 2012.